ANTI-VEGF THERAPY MODULATES IMMUNE CELL INFILTRATION

AND FUNCTION IN MULTIPLE BREAST CANCER MODELS

APPROVED BY SUPERVISORY COMMITTEE

_____

Rolf A. Brekken, PhD (mentor)

_____

Philip E. Thorpe, PhD (chairman)

_____

Jerry Y. Niederkorn, PhD

_____

Philipp E. Scherer, PhD

Dedicated to

Mom, Dad, Kyle, Danny, Ma'Cray, and Twister

ANTI-VEGF THERAPY MODULATES IMMUNE CELL INFILTRATION AND FUNCTION IN MULTIPLE BREAST CANCER MODELS

by

KRISTI DAWN LYNN

DISSERTATION

Presented to the Faculty of the Graduate School of Biomedical Sciences

The University of Texas Southwestern Medical Center at Dallas

In Partial Fulfillment of the Requirements

For the Degree of

DOCTOR OF PHILOSOPHY

The University of Texas Southwestern Medical Center at Dallas

Dallas, Texas

July, 2011

ACKNOWLEDGEMENTS

I would like to express my sincere gratitude to the many people who have made this research and my training possible. First, I would like to thank my mentor Dr. Rolf Brekken, whose patience, insight, and humor has guided me in this journey. I would also like to acknowledge my committee members Drs. Philip Thorpe, Jerry Niederkorn, and Philipp Scherer for challenging and supporting me along the way.

This study could not have been accomplished without the collaboration and support of my friends and lab mates. I would especially like to acknowledge Drs. Christina Roland and Sean Dineen who worked with me to publish a number of manuscripts. I would also like to acknowledge Laura Sullivan, Juliet Carbon, and Dr. Marie Burdine for thoughtful scientific discussion as well as "girl talk" at lunch when I needed a brief get away.

Finally I would like to acknowledge my family for their constant support, love, and encouragement throughout this process. My parents, Roger and Chonda Williams, have overcome the challenges of life with strength, perseverance, and determination and have instilled these virtues in me. I would like to acknowledge my husband Danny for his support and most of all patience with the graduate

school process. Most of all I would like to acknowledge my children, Ma'Cray and Twister Lynn. They are my inspiration and although they may not be old enough to realize it yet, all of this hard work was for them.

ANTI-VEGF THERAPY MODULATES IMMUNE CELL INILTRATION AND FUNCTION IN MULTIPLE BREAST CANCER MODELS

Publication No.

Kristi Dawn Lynn, Ph.D

The University of Texas Southwestern Medical Center at Dallas, 2011

Supervising Professor: Rolf A. Brekken, Ph.D

Breast cancer is the most frequently diagnosed malignancy in women in North America. Advancements in standard treatment regimens have improved the overall outlook for breast cancer patients in recent years; however, 40,000 women a year succumb to this disease. Breast cancer is initiated when mammary epithelial cells acquire mutations in genes that regulate cell proliferation, survival, polarity, and differentiation. However, a growing body of evidence indicates that the stromal cell response to these malignant cells participates in tumorigenesis and is required for the tumor to advance past the hyperplastic stage.

Angiogenesis, or expansion of the existing vascular network, is required for the growth of solid tumors. For this reason, tumor angiogenesis is an attractive target for tumor therapy. Many of the current anti-angiogenic therapies target vascular endothelial growth factor-A (VEGF). VEGF binds to and activates two

primary VEGF receptors, VEGFR1 and VEGFR2. VEGFR2 is the primary angiogenic receptor, while the function of VEGFR1 is less defined. It is important to note that the VEGFRs are expressed on endothelial cells, tumor cells and on many host immune cells. Therefore, to better understand the biology of anti-VEGF therapy it is important to consider the effects of VEGF on all VEGFR-positive cells in the tumor microenvironment.

In the present study, immune cell infiltration and function were analyzed following anti-VEGF therapy. Inhibition of VEGF:VEGFR2 signaling with r84 or mouse-chimeric (mcr84) decreases tumor-associated myeloid-derived suppressor cells and increases mature dendritic cells in multiple models of breast cancer. In contrast to other immunosuppressive cell types, an increase in anti-inflammatory macrophage infiltration was observed following treatment with mcr84, corresponding to an increase in the cytokine pleiotrophin (PTN). Once expressed, PTN stimulates the phosphorylation of anaplastic lymphoma kinase on tumor associated macrophages. These macrophages promote anti-inflammation, angiogenesis, immune tolerance, and metastasis. Importantly, these phenomena can be inhibited using the receptor tyrosine kinase inhibitor crizotinib, Furthermore, the combination of mcr84 and crizotinib decreased metastatic burden in animals with already disseminated disease.

These findings suggest that mcr84 is a valid clinical candidate in breast cancer and its combination with crizotinib has the potential to reduce metastastic burden in patients with already disseminated disease.

TABLE OF CONTENTS

PRIOR PUBLICATIONS

Dineen, S.P., **Lynn, K**.D., Holloway, S.E., Miller, A.F., Shames, D.S., Sullivan, J.P., Beck, A.W., Barnett, C.C., Fleming, J.B., and Brekken, R.A. Valscular endothelial growth factor receptor 2 mediates macrophage infiltration into orthotopic pancreatic tumor in mice. Cancer Res 2008;68:4340-4346.

Roland, C.L.,* Dineen, S.P.,* **Lynn, K.D**.,* Sullivan, L.A., Dellinger, M.T., Sadegh, L., Sullivan, J.P., Shames, D.S., and Brekken, R.A. Inhibition of VEGF reduces angiogenesis and modulates immune cell infiltration of orthotopic breast cancer xenografts. Mol Can Ther 2009;8: 1761-1771. *denotes equal contributing author.

Roland, C.L., **Lynn, K.D.,** Toombs, J.E., Dineen, S.P., Udugamasooriya, D.G., and Brekken, R.A. Changes in cytokine levels following anti-VEGF therapy modulates immune cell infiltration in pre-clinical models of breast cancer. PLoS One 2009;4: e7669.

Lynn, K.D, Udugamasooriya, D.G.**,** Roland, C.L., Castrillon, D.H., Kodadek, T., and Brekken, R.A. GU81, a VEGFR2 antagonist peptoid, enhances the anti-tumor activity of doxorubicin in the murine MMTV-PyMT transgenic model of breast cancer. BMC Cancer 2010; 10:397.

Lynn, K.D., Roland, C.L., Brekken, R.A. VEGF and pleiotrophin modulate the immune profile of breast cancer. Cancers 2010; 2: 970-988.

LIST OF FIGURES AND TABLES

LIST OF ABBREVIATIONS

VEGF – vascular endothelial growth factor

PlGF – placental growth factor

VEGFR – vascular endothelial growth factor receptor

HER2 – human epidermal growth factor receptor 2

FDA – Food and Drug Administration

PDGFR – platlet-derived growth factor receptor

FGF – fibroblast growth factor

FGFR – fibroblast growth factor receptor

PLC – phospholipase C

ERK – extracellular signal regulated kinase

NSCLC – non-small cell lung cancer

Ang – angiopoietin

SDF – stromal-derived factor

HSC – hematopoietic stem cell

EC – endothelial cell\

MDSC – myeloid-derived suppressor cell

MMP – matrix metalloproteinase

EG-VEGFR – endocrine gland-derived vascular endothelial growth factor receptor

PKR – prokineticin receptor

IL – interleukin

CXCL – chemokine (C-X-C motif) ligand

G-CSF – granulocyte colony stimulating factor

DC – dendritic cell

CD – cluster of differentiation

NF-κB - nuclear factor kappa-light-chain-enhancer of activated B cells

T reg – regulatory T-cell

FoxP3 – forkhead box P3

TGFβ – transforming growth factor beta

CSF-1 – colony-stimulating factor 1

CSF-1R – colony-stimulating factor 1 receptor

INF – interferon

LPS – lipopolysaccharide

RBP - recombining binding protein

TNF – tumor necrosis factor

CCR – chemokine (C-C motif) receptor

TAM – tumor associated macrophage

Mip – macrophage inflammatory protein

IRF – interferon regulator factor

Arg – arginase

ADAM – a disintegrin and metalloproteinase domain

ITGB7- intergrin beta 7

ITGA6 – intergrin alpha 6

STAB – stabilin

ECM – exctracellular matrix protein

CXCR - chemokine (C-X-C motif) receptor

ETS – E26 transforming specific

CTS – cathepsin

MARCO – macrophage receptor with collagenous structure

CCL – chemokine (C-C motif) ligand

PTN – pleiotrophin

RPTP – receptor tyrosine phosphatase

ALK – anaplastic lymphoma kinase

MMTV – mouse mammary tumor virus

PyMT – polyoma middle-T antigen

EMT – epithelial to mesenchymal transition

SFM – serum-free media

ALCL – anaplastic large cell lymphoma

NPM – nucleophosmin

MAPK – mitogen activated protein kinase

PI3K – phosphoinositide-3 kinase

JAK – janus kinase

STAT – signal transducer and activator of transcription

cMet – epithelial to mesenchymal transition factor

FAE – fatal adverse event

Ctrl – control

RTKi – receptor tyrosine kinase inhibitor

Tie – tyrosine kinase with immunoglobulin-like and EGF-like domains

MVD – microvessel density

TCI – tumor cell injection

SEM – standard error mean

HDMEC – human dermal endothelial cells

Flt – fms-related tyrosine kinase

Dll4 – delta-like ligand 4

Hes1 – hairy and enhancer of split 1

ICC – imunocytochemistry

IHC – immunohistochemistry

RT – reverse transcription

qPCR – quantitative polymerase chain reaction

iNOS – inducible nitric oxide synthase

MCP – macrophage chemotactic protein

MIG – monokine induced by interferon gamma

mcr84 – mouse chimeric r84

criz – crizotinib

GM-CSF – granulocyte monocyte colony stimulating factor

CHAPTER ONE

ANTI-VEGF THERAPY, IMMUNE CELLS, AND THE TUMOR MICROENVIRONMENT

1.1 Introduction to VEGF and anti-VEGF therapy in breast cancer

Breast cancer is the most frequently diagnosed malignancy in women in North America. Advancements in standard treatment regimens have improved the overall outlook for breast cancer patients in recent years; however, 40,000 women a year succumb to this disease (2009). Breast cancer is initiated when mammary epithelial cells acquire mutations in genes that regulate cell proliferation, survival, polarity, and differentiation (reviewed in (Tysnes and Bjerkvig 2007)). However, a growing body of evidence indicates that the stromal cell response to these malignant cells participates in tumorigenesis and is required for the tumor to advance past the hyperplastic stage (reviewed in (DeNardo and Coussens 2007; Tysnes and Bjerkvig 2007)). The tumor stroma consists of fibroblasts, endothelial cells, and immune cells.

The vascular endothelial growth factor (VEGF) family consists of five family members: VEGF-A (referred to as VEGF), VEGF-B, VEGF-C, VEGF-D, and

placental growth factor (PlGF). VEGF family members interact with VEGF receptors (VEGFR1,2 or 3), as well as the non-enzymatic co-receptors Neuropilin-1 and Neuropilin-2 (Ferrara 2004; Hoeben et al. 2004). VEGF induces endothelial cell proliferation, survival, and migration (Ferrara and Henzel 1989; Alon et al. 1995; Gerber et al. 1998) and is a potent vascular permeability factor (Senger et al. 1990). VEGF-induced angiogenesis, or blood vessel sprouting from an existing vascular network, is relatively rare in most adult tissues and occurs normally only during wound healing and menstruation (Ferrara 2004).

Angiogenesis is required for the growth of solid tumors (Folkman 1971). For this reason, tumor angiogenesis is an attractive target for tumor therapy. Many of the current anti-angiogenic therapies target VEGF (Dvorak 2002). VEGF binds to and activates two primary VEGF receptors, VEGFR1 and VEGFR2. VEGFR2 is the primary angiogenic receptor, while the function of VEGFR1 is less defined (reviewed in (Pradeep et al. 2005)). VEGFR1, however, has been implicated in macrophage chemotaxis (Sawano et al. 2001), tumor cell survival (Lee et al. 2007) and invasion (Yang et al. 2006). It is important to note that the VEGFRs are expressed on endothelial cells, tumor cells and on many host immune cells. Therefore, to better understand the biology of anti-VEGF therapy it is important to consider the effects of VEGF on all VEGFR-positive cells in the tumor microenvironment.

1.1.1 VEGF as a target for breast cancer therapy

Bevacizumab (Avastin®, Genentech), a humanized monoclonal antibody that binds human VEGF and prevents VEGF-induced activation VEGFR1 and VEGFR2, was first successful in the clinic for the treatment of metastatic colon cancer in combination with chemotherapy in 2004 (Hurwitz et al. 2004). Bevacizumab was approved for the treatment of metastatic HER2/NEU-negative breast cancer in 2007, but this approval was revoked in 2010 (Miller et al. 2007; Miles et al. 2010; Robert et al. 2011). The most relevant evidence for the efficacy of bevacizumab in the treatment of metastatic breast cancer comes from two large phase III clinical trials. In the first study, patients treated with the combination of capecitabine plus bevacizumab demonstrated increased overall response rate compared to capecitabine alone (Miller et al. 2005). The next major phase III clinical trial prior to the FDA approval of bevacizumab was the ECOG 2100 trial (Miller et al. 2007). Patients treated with paclitaxel plus bevacizumab had prolonged progression-free survival as compared to those treated with paclitaxel alone (11.8 *versus* 5.9 months). However, there were no differences in overall survival between the two groups. Sub-group analysis revealed that patients with the *VEGF-2578 AA* genotype or *VEGF-1154 A* allele had prolonged overall survival in the combination arm compared with the alternate genotypes.

Additionally, expression of the genotypes *VEGF-634 CC* and *VEGF-1498 TT* were associated with significantly less grade 3 or 4 hypertension compared with the alternate genotypes (Schneider et al. 2008), demonstrating the need for molecular characterization of tumors to maximize therapeutic benefit of anti-VEGF therapy.

FDA approval for the use of bevacizumab to treat metastatic HER2/NEU-negative breast cancer was revoked in 2010 following the completion of two additional Phase III randomized trials (Miles et al. 2010; Robert et al. 2011). In the AVADO trial, patients in the combination arm (docetaxel plus bevacizumab) had a modest improvement in progression free survival compared to those who received docetaxel alone (8.2 *versus* 9.0 months), however there was no improvement in overall survival (Miles et al. 2010). In the second trial (RIBBON), patients were randomized to receive chemotherapy alone (anthracycline, taxane-based, or capecitibane) or in combination with bevacizumab. These results confirm that bevacizumab provides only a modest increase in progression free survival (1.2 months *versus* anthracycline or taxane-based therapy) and (2.9 months *versus* capecitibane) and no increase in overall survival (Robert et al. 2011). The FDA weighed these small benefits against the risks associated with bevacizumab therapy (hypertension, proteinura, and hemorrhage) and made the decision to revoke bevacizumab's approval for metastatic HER2/NEU-negative breast cancer. Despite this major setback, the

future for anti-VEGF therapy in breast cancer may still hold promise, according to clinicaltrials.gov there are still a great number of open trials examining VEGF inhibition in breast cancer (Table 1.1).

Drug	Class	Targets	Company	Active Trials	Phase
Bevacizumab	Humanized mAb	VEGF-A	Genentec	96	I, II, II, IV
VEGF-trap	Fusion Protein	VEGF-A	Regeneron	1	III
Pazopanib	RTKi	VEGFR1,2,3 PDGFRα/β, cKit	GlaxoSmithKline	9	I, II, III
PTC 299	Small molecule inhibitor of post-transcriptional VEGF mRNA processing	VEGF mRNA	PTC Therapeutics	1	I
Sorafenib	RTKi	VEGFR2,3 PDGFRα/β, cKit, Raf	Bayer	16	I, II, III
Vatalanib (PTK787)	RTKi	VEGFR1,2,3 PDGFRα/β, cKit	Bayer-Schering, Novartis	1	I
Motesanib (AMG706)	RTKi	VEGFR1,2,3 PDGFRα/β, cKit	Amgen	3	I, II
Sunitinib	RTKi	VEGFR1,2,3 PDGFRα/β, cKit	Pfizer	24	I, II, III
E-3810	RTKi	VEGFR1,2,3 FGFR1, 2	Ethical Oncology Science	1	I

Table 1.1. Active trials investigating anti-VEGF agents in breast cancer. Source: clinicaltrials.gov accessed on May 18, 2011.

1.1.2 Introduction to r84

In our laboratory, we have characterized 2C3, a monoclonal antibody to human VEGF that, in contrast to bevacizumab, blocks VEGF interaction with VEGFR2 only (Brekken et al. 1998; Brekken et al. 2000). We have previously

shown 2C3 to be effective in controlling the growth of breast and pancreatic cancer in animal models (Holloway et al. 2006; Whitehurst et al. 2007; Dineen et al. 2008; Roland et al. 2009). The pre-clinical success of 2C3 led to the development of a fully human monoclonal antibody that retains the binding characteristics of 2C3. A number of human single chain fragments were screened for ability to inhibit the VEGF:VEGFR2 interaction, compete with 2C3 for VEGF-binding, and bind multiple VEGF isoforms (Sullivan et al. 2010). The single chain fragments with the most desirable characteristics were cloned into a full length human antibody expression vector and subsequent antibodies were tested for efficacy in subcutaneous A673 rhabdomyosarcoma xenografts (Carbon 2007; Sullivan et al. 2010). The antibody with the most sought-after characteristics, termed r84, binds both human and mouse VEGF and specifically prevents VEGF from interacting with VEGFR2 (Figure 1.1) (Sullivan et al. 2010).

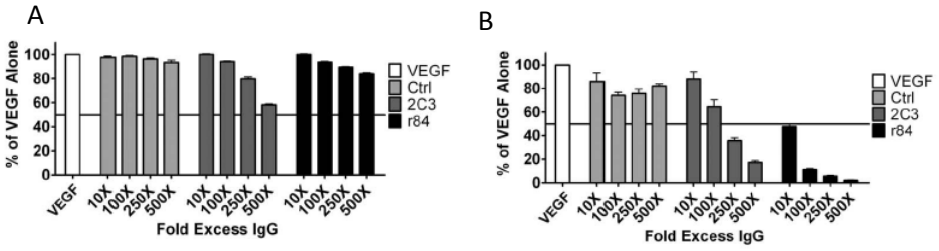

Figure 1.1. r84 binds VEGF and specifically inhibits binding the VEGFR2. VEGFR1(A) and VEGFR2 (B, left panel) coated at 1 mg/mL were incubated with 4.76 nM or 2.38 nM biotinylated VEGF, respectively, +/- the indicated fold excesses of antibody (Control IgG, 2C3, r84). **Adopted from (Sullivan et al. 2010).**

In vitro studies verify that r84 specifically inhibits VEGF:VEGFR2 signaling in endothelial cells as confirmed by reduction of VEGF-induced VEGFR2, p38, PLCγ, and ERK1/2 phosphorylation. Furthermore, r84 was unable to reduce VEGF-induced VEGFR1 phosphorylation (Sullivan et al. 2010).

The *in vivo* efficacy of r84 has been examined in multiple pre-clinical lung and breast cancer models, where it reduces tumor growth and microvessel density (MVD). In a number of these studies, r84 was directly compared with the clinically approved anti-VEGF antibody bevacizumab and was either as effective or more effective than this standard in the anti-VEGF field (Roland et al. 2009; Roland et al. 2009; Sullivan et al. 2010).

Bevacizumab, in contrast to r84, inhibits VEGF from binding and activating VEGFR1 and VEGFR2. Although bevacizumab is beneficial and FDA approved for patients with metastatic colorectal (Hurwitz et al. 2004), non-small cell lung cancer (NSCLC) (Sandler et al. 2006), glioblastoma (Norden et al. 2008; Friedman et al. 2009), and metastatic renal cell carcinoma (RCC) (Rini et al. 2008), this benefit does not come without risks. A recent meta-analysis of 10,217 patients who received bevacizumab revealed that the likelihood a given patient would experience a fatal adverse event (FAE) was 2.5% (Ranpura et al. 2011). Furthermore, patients receiving bevacizumab in combination with chemotherapy were significantly more likely to experience a FAE than those receiving

chemotherapy alone (relative risk = 1.46; incidence 2.5% vs. 1.7%) (Ranpura et al. 2011). The most common causes of FAEs in this study were hemorrhage (23.5%), neutropenia (12.2%), and gastrointenstinal tract perforation (7.1%) (Ranpura et al. 2011).

These statistics suggest that r84 may also have an extensive toxicity profile, however, extensive long term dosing studies in the mouse suggest this may not be true. Long-term dosing with either r84 or mouse chimeric-r84 (mcr84) had no significant impact on kidney function, liver function, or blood pressure in either immunocompromised or immunocompetent animals (Sullivan et al. 2010). In contrast, a similar experiment completed using bevacizumab and other high affinity anti-VEGF antibodies in a mouse expressing a humanized form of VEGF did reveal significant kidney and liver toxicity (Gerber et al. 2007). These data indicate that specific inhibition of VEGF:VEGFR2 signaling with r84 could provide an clinical anti-VEGF agent with similar efficacy to bevacizumab and a reduced toxicity profile.

1.2 Immune modulation following Anti-VEGF therapy

The theory surrounding the development of anti-VEGF of therapy was based on the known effects of VEGF on endothelial cell proliferation, migration, and survival (Ferrara and Henzel 1989; Alon et al. 1995; Gerber et al. 1998). It was thought that by targeting endothelial cells, which are genetically stable

compared to genetically instable tumor cells, we would be able to eradicate tumors by cutting off the supply of oxygen and nutrients, however, the modest clinically efficacy of anti-VEGF therapy reveals that there is much left to understand. At best we are able to improve overall survival but patients are not cured using anti-VEGF therapy either alone or in combination with chemotherapy (Hurwitz et al. 2004; Sandler et al. 2006; Norden et al. 2008; Rini et al. 2008; Friedman et al. 2009; Miles et al. 2010; Robert et al. 2011).

The majority of human mammary tumors are either innately resistant or will acquire resistance to anti-VEGF therapy (Ellis and Hicklin 2008), suggesting that these tumors activate alternate angiogenesis pathways. The alternate angiogenic factors fibroblast growth factor (FGF 1 and 2), ephrin A1 and 2, angiopoietin (Ang-1 and 2), placental growth factor (PlGF), stromal cell-derived factor 1 alpha (SDF-1α), and others, have been implicated in resistance to anti-VEGF therapy (reviewed in (Grepin and Pages 2010)). Furthermore, many of these affect immune cell infiltration and function (Kitayama et al. 1994; Berardi et al. 1995; Zhao et al. 1995; Byrd et al. 1999; Ribatti et al. 1999; Takagi et al. 2000; Selvaraj et al. 2003; Burger and Kipps 2006; Lewis et al. 2007; Lewis and Hughes 2007; Lin et al. 2007; Nakayama et al. 2007; Schulz et al. 2009). It is important to note that the VEGFRs are expressed on endothelial cells, tumor cells, and many host immune cells. Therefore, to better understand the effects of anti-

VEGF therapy it is important to consider the effects of VEGF on all cells in the tumor microenvironment.

1.2.1 VEGF and the bone marrow

Bone marrow consists of a diverse population of cells including hematopoietic stem cells (HSCs), endothelial cells (ECs), chondroblasts, osteoblasts, and other stromal cells. VEGF is expressed by a number of cells in bone marrow, including HSCs, and serves a variety of functions (Robertson et al. 1999; Gerber et al. 2002). Interestingly, VEGF-deficient HSCs and bone marrow mononuclear cells are unable to form colonies *in vitro* or repopulate lethally irradiated hosts, suggesting that VEGF regulates HSC survival (Robertson et al. 1999). Further studies indicate that VEGF maintains HSC pluripotency and regulates survival through an internal autocrine loop (Gerber et al. 2002). Receptor tyrosine kinase inhibitors, such as sunitinib (Sutent®, Pfizer) and sorafenib (Nexavar®,Bayer), can cross the cell membrane and inhibit this autocrine survival loop, however this loop is not accessed or inhibited by anti-VEGF antibodies (Gerber et al. 2002). Clinical data further support the importance of the internal autocrine VEGF loop in HSC survival, as both sunitinib (Demetri et al. 2006; Motzer et al. 2007) and sorafenib (2009) are myelosuppressive as monotherapies, whereas bevacizumab is not. Interestingly, mice treated *in vivo* with VEGF-Trap or an antibody directed against VEGFR2

experience significantly delayed hematopoietic recovery following treatment with sublethal irradiation (Hooper et al. 2009; Kopp et al. 2009). This lag in hematopoietic reconstitution is not due to direct effects on HSC survival but rather is attributed to delayed regeneration of sinusoidal endothelial cells in the bone marrow, which is required for HSC self-renewal, survival, and differentiation (Hooper et al. 2009; Kopp et al. 2009).

VEGF secretion effectively mobilizes mononuclear myeloid cell from the bone marrow. These cells home to target organs, position themselves in perivascular regions, and promote angiogenesis through secretion of angiogenic cytokines (Grunewald et al. 2006). Recent work also specifies an important function for HSCs in tumor metastasis. Circulating HSCs home to sites of future metastasis, where they secrete proteases and growth factors, effectively preparing the "soil" for the metastasizing tumor cells. Homing to the pre-metastatic niche is purported to require VEGFR1 signaling, as treatment with anti-VEGFR1 antibodies can prevent HSC homing and subsequent metastasis (Kaplan et al. 2005). In summary, VEGF signaling is important in the maintenance and survival of HSCs and promotes their mobilization from the bone marrow and homing to target organs (Table 1.2).

1.2.2 VEGF and Myeloid Derived Suppressor Cells

Myeloid derived suppressor cells (MDSCs) are an immature and heterogeneous population of cells described as $CD11b^{+}Gr1^{+}CD14^{-}$. MDSCs expand during tumorigenesis, inflammation, and infection and suppress the adaptive immune system through inhibition of T-cell function. MDSC induced T-cell anomalies in tumors include antigen-specific T-cell tolerance, nonspecific suppression of T-cell function, and induction of T-cell apoptosis (Nagaraj and Gabrilovich 2008). MDSCs exert these effects through the secretion of arginase, reactive oxygen, and reactive nitrogen species. MDSCs also secrete MMP-9, which regulates the bioavailability of VEGF in the tumor microenvironment, thus MDSCs increase VEGF bioavailability and indirectly increase tumor angiogenesis (Yang et al. 2004). Furthermore, VEGF increases the number of MDSCs by preventing the differentiation of these cells into neutrophils, macrophages, and dendritic cells (Gabrilovich et al. 1998).

$CD11b^{+}Gr1^{+}$ cells can mediate refractoriness to anti-VEGF therapy through secretion of the alternative angiogenic factor Bv8. Bv8 binds to and signals through two G-protein coupled receptors termed EG-VEGFR/PKR-1 and EG-VEGFR/PKR-2. Strikingly, refractoriness to anti-VEGF therapy is alleviated when mice are treated with a combination of anti-VEGF and anti-Bv8 therapy (Shojaei et al. 2007; Shojaei et al. 2007). Following these studies, the effects of

acute and long term anti-VEGF therapy on MDSC number and function has become a topic of significant interest. We examined these effects using different of anti-VEGF strategies and three separate pre-clinical mouse models (Roland et al. 2009). Our results indicate the effects of anti-VEGF therapy on MDSC infiltration are model dependent (Table 1.2). In MDA-MB-231 xenografts and MMTV-PyMT transgenic tumors simultaneous blockade of both VEGFR1 and VEGFR2 increased MDSC infiltration, however, this did not hold true in 4T1 syngenic tumors, where all anti-VEGF strategies reduced MDSC accumulation (Roland et al. 2009). A potential explanation of this phenomenon is the level of intra-tumoral cytokine levels. IL-1β levels are changed following anti-VEGF therapy and regulate MDSC infiltration in a bimodal manner. We found low levels of IL-1β (<5pg/mg/protein) correlate with increased MDSC infiltration in the MDA-MB-231 and MMTV-PyMT models while elevated levels of IL-1β (>50 pg/mg/protein) following anti-VEGF therapy in the 4T1 model correlated with reduced MDSC infiltration (Roland et al. 2009).

1.2.3 VEGF and Neutrophils

While many studies have focused on the function of tumor-associated macrophages in tumor progression, the function of tumor associated neutrophils has not been studied in detail. However, recent evidence indicates that neutrophils also participate actively in tumorigenesis through a number of mechanisms

including the secretion of angiogenic growth factors (*i.e.*, VEGF) and matrix-metalloproteinases, such as MMP-9 (Bergers et al. 2000; Scapini et al. 2004; Nozawa et al. 2006). In fact, neutrophil derived MMP-9 mediates the angiogenic switch in a mouse model of pancreatic cancer (Bergers et al. 2000; Nozawa et al. 2006). Neutrophils respond to chemotactic agents including CXCL8 (IL-8), G-CSF, and VEGF. Neutrophil migration toward VEGF is mediated by VEGFR1 activation (Ancelin et al. 2004). Anti-VEGF therapy modulates neutrophil infiltration in an agent dependent manner, whereby agents that specifically block activation of VEGFR2 increase neutrophil infiltration. In contrast those that block activation of both VEGFR1 and VEGFR2 decrease neutrophil infiltration, indicating that VEGFR1 is the primary receptor involved in VEGF-induced neutrophil chemotaxis into tumors (Table 1.2) (Roland et al. 2009; Roland et al. 2009). It is important to note, that the differentiation of MDSCs into neutrophils following VEGFR2-specific therapy may also contribute to neutrophil accumulation in this model. Alternatively, recent evidence indicates that macrophages can reduce neutrophil infiltration by inhibiting CXCL8-dependent chemotaxis (Pahler et al. 2008). Therefore, macrophage numbers often correlate inversely with neutrophil levels. We have found that in general anti-VEGF strategies reduce macrophage infiltration; however only selective inhibition of VEGF-activation of VEGFR2 by receptor specific agents resulted in marked accumulation of neutrophils (Pahler et al. 2008; Roland et al. 2009). Interestingly,

neutrophil numbers in the blood are an independent prognostic indicator of response to anti-VEGF therapy in patients with renal cell carcinoma, whereby increased neutrophil number correlates with a decreased overall survival following anti-VEGF therapy (Heng et al. 2009).

1.2.4 VEGF and Dendritic Cells

Dendritic cells (DC) are the most potent antigen presenting cells and are crucial for induction and maintenance of anti-tumor responses. Defects in antigen presentation by DCs related to abnormal differentiation and activation are regulated by many soluble factors in the tumor microenvironment (Gabrilovich 2004). VEGF was the first described tumor-derived factor shown to inhibit DC differentiation (Gabrilovich et al. 1996). During physiologic DC differentiation, variations in VEGFR expression regulate maturation of DC from bone marrow progenitor cells to immature DC in peripheral blood and to mature antigen presenting DCs in secondary lymphoid organs (Gabrilovich et al. 1998; Oyama et al. 1998; Huang et al. 2007). VEGF activation of VEGFR1 on $CD34^{+}$ early progenitor cells blocks activation of NF-κB, resulting in inhibition of HSC differentiation along the DC lineage (Gabrilovich et al. 1998; Oyama et al. 1998). However, inhibition of DC function, via impaired antigen presentation and blunted T-cell stimulation and proliferation result from VEGFR2 activation (Huang et al. 2007; Mimura et al. 2007).

The effects of VEGF and VEGF-targeted therapies on tumors extend beyond the effects on angiogenesis. Previously, using MDA-MB-231 xenografts, we found an increase in mature DC in animals treated with r84, an anti-VEGF antibody that selectively inhibits VEGF binding to VEGFR2, but not bevacizumab, an antibody that inhibits VEGF from binding VEGFR1 and VEGFR2 (Roland et al. 2009). Using the 4T1 model in immunocompetent animals, we found a similar effect after only one week of therapy, where inhibition of VEGF binding to VEGFR2 with mouse chimeric r84 reduced the number of total DC, but increased the mature fraction of these cells (Table 1.2) (Roland et al. 2009).

Clinical data support that VEGF can induce DC defects in cancer patients. First, in cancer patients, elevated systemic VEGF levels correlate with low DC frequencies (Osada et al. 2008). Furthermore, patients with metastatic cancer have an increased proportion of immature DC, a population of cells not capable of stimulating T-cell responses (Osada et al. 2008). Additionally, in certain types of cancer, DC differentiation has been shown to be negatively affected by VEGF, as demonstrated in pre-clinical models (Fricke et al. 2007). Despite this wealth of pre-clinical data the majority of anti-VEGF agents have minimal effect on DC activity in human patients (Fricke et al. 2007; van Cruijsen et al. 2007; Hipp et al. 2008). However, this is not true in all cases. Select anti-VEGF agents (renal cell cancer/sorafenib and colorectal cancer/bevacizumab) can reverse deficits in DC

maturation (Osada et al. 2008). These data highlight the importance of VEGF in DC maturation in cancer patients and support the further investigation of the anti-VEGF therapy on DC subsets.

1.2.5 VEGF and Regulatory T-cells

Regulatory T-cells (T_{reg}) are a specialized immunosuppressive population of T-cells defined by the expression of CD25 and FoxP3. T_{regs} are produced by the immune system to control self-tolerance and prevent autoimmunity and exert these effects through the secretion of anti-inflammatory cytokines such as TGFβ and IL-10 (Dieckmann et al. 2001). Tumors take advantage of this regulatory mechanism to prevent anti-tumor responses. They recruit and expand naturally occurring T_{reg} populations and induce the formation of new T_{reg} cohorts, which specifically recognize tumor-associated antigens. In fact, high FoxP3 expression is associated with increased TGFβ and VEGF levels, invasiveness, and metastasis in infiltrating breast carcinoma, indicating that FoxP3 expression can be used as a prognostic indicator (Gupta et al. 2007). TGFβ is reported to increase VEGF expression, explaining the correlation in these two parameters (Donovan et al. 1997). We have examined the effects of anti-VEGF therapy on T_{reg} accumulation in two immunocompetent mouse models and have found that the effects are model dependent.

In MMTV-PyMT tumors, anti-VEGF therapy that specifically inhibits VEGFR2 signaling decreases T_{reg} accumulation, whereas blockade of both VEGFR1 and VEGFR2 signaling actually increases T_{reg} infiltration. In contrast, all anti-VEGF therapies inhibit T_{reg} accumulation in 4T1 tumors (Table 1.2) (Roland et al. 2009).

1.2.6 VEGF and Macrophages

Inflammatory cells comprise a major portion of the overall tumor mass and of these, macrophages represent an abundant and important cell type (Pollard 2004). In fact, macrophages have been shown to regulate the angiogenic switch in MMTV-PyMT tumors (Lin et al. 2006).

VEGF stimulates macrophage chemotaxis (Sawano et al. 2001) into the tumor microenvironment, and we and others have shown that anti-VEGF therapy can reduce macrophage infiltration in pre-clinical tumor models (Table 1.2) (Salnikov et al. 2006; Whitehurst et al. 2007; Dineen et al. 2008; Roland et al. 2009; Roland et al. 2009). We found that macrophages harvested from a tumor-bearing animal express both VEGFR1 and VEGFR2, whereas those harvested from non-tumor bearing mice are $VEGFR1^{+}$ but deficient in VEGFR2. Furthermore, when VEGFR2 is expressed, it becomes the dominant receptor driving VEGF-induced chemotaxis and specific blockade of VEGF:VEGFR2 interaction is sufficient to inhibit chemotaxis (Dineen et al. 2008; Roland et al.

2009). Interestingly, analysis of human peripheral blood from cancer patients and healthy volunteers revealed a population of $VEGFR2^{+}/CD45^{bright}/CD14^{+}$ monocytes; this population was significantly more prominent in blood from cancer patients compared to that of healthy volunteers, confirming our pre-clinical findings (Vroling et al. 2007).

Cell Type	VEGF Effects	Pre-Clinical Anti-VEGF	Clinical Anti-VEGF
Hematopoietic stem cells (HSCs)	Regulates pluripotency, survival, and mobilization from the bone marrow [25,26]	Anti-VEGFR2 inhibits reconstitution following sublethal irradiation [30,31] Anti-VEGFR1 prevents mobilization and recruitment to pre-metastatic niche in a Lewis lung carcinoma model [33]	Sunitinib and sorafenib result in myelosuppression as monotherapies [27–29]
Macrophages	Macrophage chemotaxis [7]	Reduces macrophage infiltration in multiple breast cancer and other cancer models [48–52]	Unknown
Myeloid derived suppressor cells (MDSCs)	Promotes differentiation into neutrophils, macrophages, and dendritic cells [59]	VEGFR2 specific inhibition decreases MDSC in MDA-MB-231 xenograft and MMTV-PyMT transgenic models [50] Inhibition of both VEGFR1 and VEGFR2 increases MDSC number in the tumor in MDA-MB-231 xenograft and MMTV-PyMT transgenic models [50]	Sunitinib decreases MDSCs in in patients with renal cell carcinoma (RCC) [91] Bevacizumab decreases MDSCs in patients with a variety of cancers [77]
Neutrophils	Neutrophil chemotaxis [65]	VEGFR2 specific inhibition increases neutrophil infiltration into tumors in multiple breast cancer models [49,50] Inhibition of both VEGFR1 and VEGFR2 decrease neutrophil infiltration into tumors in multiple breast cancer models [49,50]	Unknown
Dendritic cells (DCs)	VEGF:VEGFR1 activation inhibits the differentiation of HSCs down the DC lineage [71,72] VEGF:VEGFR2 activation inhibits DC antigen presenting cell functions [73,74]	Specific inhibition of VEGF: VEGFR2 activation increases the number of mature dendritic cells in the MDA-MB-231 xenograft and 4T1 syngeneic breast cancer models [49,50]	Sorafenib reverses defects in DC maturation in patients with RCC [78] Bevacizumab reverses defects in DC maturation in colorectal cancer patients [78]
Regulatory T-cells (Tregs)	VEGF expression can be correlated to high FoxP3 expression in breast carcinoma [83]	VEGFR2 specific inhibition decreases Tregs MMTV-PyMT transgenic model [50] Inhibition of both VEGFR1 and VEGFR2 increases Tregs in the MMTV-PyMT transgenic model [50]	Sunitinib decreased Tregs in patients with RCC [91]

Table 1.2. Summary of the effects of VEGF, pre-clinical and clinical anti-VEGF therapy on the immune profile. **Adopted from (Lynn 2010)**.

1.3 **Macrophages in the metastatic cascade**

Metastatic spread requires cells to invade into the vasculature, survive in circulation, and extravasate, survive, and prosper at the metastatic site (Chambers et al. 2002). This process, however, is inefficient. Cancer patients release thousands of tumor cells into circulation everyday but only a few will ever form distant metastatic lesions (Qian and Pollard 2010). The fate of most circulating tumor cells is death, suggesting extravasation and the formation of micrometastases as the rate limiting steps (Joyce and Pollard 2009).

A growing body of clinical evidence suggests that macrophage infiltration promotes tumor progression. One meta-analysis confirms that in clinical studies that examine macrophage infiltration, 80% found that macrophage infiltration conferred a worse prognosis (Bingle et al. 2002). In breast cancer specifically, an increase in macrophage hotspots correlates with decreased relapse-free and overall survival (Leek et al. 1996; Leek and Harris 2002).

Experimental evidence for the tumor promoting capabilities of macrophages in pre-clinical models of breast cancer is equally compelling. Genetic ablation of colony stimulating factor-1 (CSF-1) in the MMTV-PyMT transgenic breast cancer model results in delayed tumor progression and potent metastasis inhibition (Lin et al. 2001). Anti-sense nucleotides and antibodies targeting CSF-1 or its receptor (CSF-1R) have also been used in transgenic and

xenograft breast cancer models to inhibit macrophage infiltration, resulting in delayed tumor progression and reduced metastasis (Aharinejad et al. 2009; Abraham et al. 2010). Recent studies also suggest that a distinct macrophage population assists in metastasis by facilitating tumor cell intravasation and extravasation (Figure 1.2) (Wyckoff et al. 2007; Qian et al. 2009).

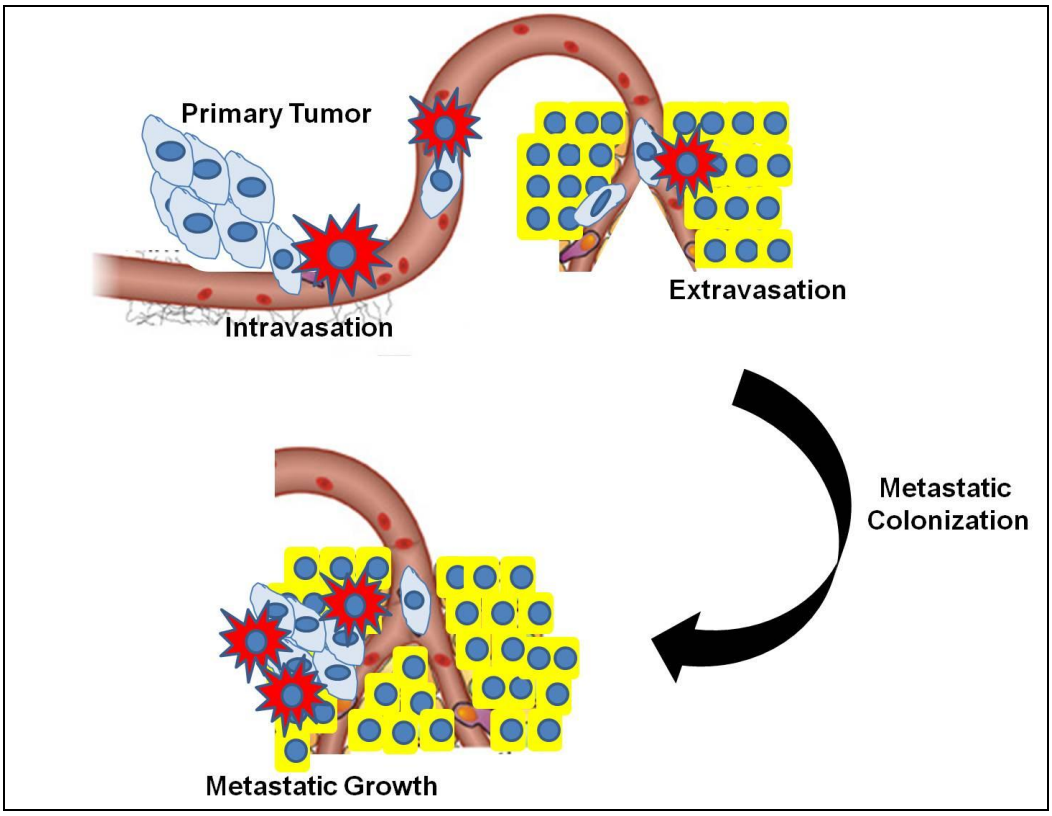

Figure 1.2. Macrophage involvement in the metastatic cascade. In order for tumors cells to metastasize to a distant organ, they must first intravasate into the vasculature, survive in circulation, extravasate, and colonize and grow at the metastatic site. Macrophages (red) assist tumor cells (blue) at each stage in the metastatic cascade.

1.3.1 Classification of macrophages into pro-inflammatory (anti-tumor) and anti-inflammatory (pro-tumor) subpopulations

For simplicity macrophages can be grouped into to two basic categories: classically activated and alternatively activated. These have been previously described as M1 and M2, respectively, but this classification system seems to be falling from favor. Classically activated macrophages are stimulated by INFγ and microbial products (LPS) and have an increased ability to endocytose and destroy pathogens (Ezekowitz and Gordon 1984; Adams 1989; Mosser and Handman 1992). Recent publications also suggest the Notch pathway as a critical mediator in the classical activation of macrophages (Outtz et al. 2010; Wang et al. 2010). In fact, macrophages deficient for the Notch pathway regulated transcription factor RBP-J display an anti-inflammatory cytokine profile despite stimulation with pro-inflammatory activators (INFγ and LPS) (Wang et al. 2010). Classically activated macrophages are potent effector cells that produce pro-inflammatory cytokines (IL-6, IL-12, TNFα) and are capable of killing tumor cells (Figure 1.3).

Alternatively activated macrophages can be stimulated by a diverse array of molecules including IL-4, IL-13, IL-10, TGFβ, and glucocortocoids (Mantovani et al. 2002; Gordon 2003). The physiological functions of alternatively activated macrophages are to promote collagen deposition, angiogenesis, and tissue repair (Hesse et al. 2001; Szekanecz and Koch 2001; Rosenkilde and Schwartz 2004; Strieter et al. 2005; Strieter et al. 2005). In the context of tumor biology, alternatively

activated macrophages secrete angiogenic and anti-inflammatory cytokines (IL-10, TGFβ, and VEGF) and therefore suppress the immune system and promote tumor progression (Figure 1.3) (reviewed in (Allavena et al. 2008)). Macrophage depletion inhibits tumor growth and metastasis in many pre-clinical breast cancer models, suggesting the majority of macrophages in the tumor microenvironment display an anti-inflammatory phenotype (Lin et al. 2006; Zeisberger et al. 2006).

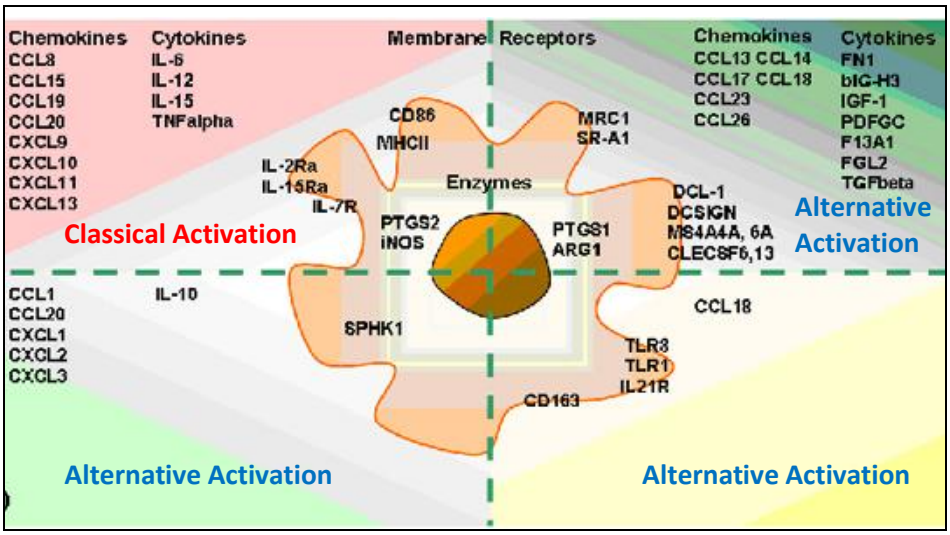

Figure 1.3. Macrophage gene signatures associated with classical (red) or alternative (blue) activation and polarization. **Adapted from (Martinez et al. 2008)**.

1.3.2 Macrophage functions in the metastatic cascade

Macrophages assist tumor cells in every step of the metastatic cascade. Multiphoton microscopy has allowed for the direct visualization of tumor cell intravasation in the MMTV-PyMT transgenic breast cancer model; interestingly tumor cell intravasation occurs in direct association with perivascular

macrophages (Wyckoff et al. 2007). More specifically, tumor cell intravasation occurs through clusters of macrophages located at the abluminal side of vessels, suggesting that macrophages promote tumor cell chemotaxis to the vessel then promote intravasation through remodeling of the local microenvironment (Wyckoff et al. 2007; Pollard 2008). Furthermore, genetic depletion of macrophages significantly reduces tumor cell ability to invade into the vasculature (Wyckoff et al. 2007).

Macrophages are also mediators of tumor cell extravasation, seeding, and growth at the metastatic site in animal models of breast cancer metastatsis (Qian et al. 2009). More specifically, intravital imaging confirms that tumor cell extravasation into the lung occurs in direct cell-cell contact with macrophages following i.v. injection of tumor cells (Qian et al. 2009). Perivascular macrophages at the metastatic site recognize extravasating tumor cells, interact with them, and assist their invasion into the lung, perhaps through the secretion of proteases and motility factors (Qian et al. 2009). This distinct macrophage population can be described as $F480^{+}CD11b^{+}Gr1^{-}CCR2^{hi}CX3CR1^{hi}$ and $VEGFR1^{hi}$. Macrophage depletion using genetic or chemical means significantly reduces tumor cell seeding of the metastatic site, suggesting that macrophage involvement in this process is critical (Qian et al. 2009). Most compelling and interesting is the evidence that genetic or chemical depletion of macrophages even after initial seeding has occurred is still able to reduce total metastatic burden

(Qian et al. 2009). Following extravasation, tumor cells may continue to influence macrophage differentiation into a subpopulation that can further enhance tumor cell survival and growth at the metastatic site (Qian et al. 2009). The shear abundance of clinical and pre-clinical data linking macrophages to disease progression and metastasis in breast cancer makes these cells an attractive therapeutic target. Even more exciting is the pre-clinical data suggesting that macrophage inhibition has the potential to prevent metastasis and significantly reduce metastatic burden in those with already disseminated disease.

1.3.3 Characteristics of macrophages involved in metastatsis

Macrophages serve vastly different functions under normal physiological conditions and tumor progression. For this reason, it is reasonable to infer that tumor-associated macrophages (TAMs) will have a different gene expression profile compared to normal macrophages. In fact, high density gene expression analysis of macrophages from mouse mammary tumors reveals that the expression of genes involved in immune regulation (MIP1a, IL-18, IRF4, ARG), cell adhesion (ITGB7, ITGA6), matrix degradation (ADAM8, MMP-12), and angiogenesis (VEGF, STAB1, CXCL4, ECM1) were significantly increased in TAMs (Ojalvo et al. 2009).

Jeff Pollard's group has extensively characterized five subpopulations of TAMs [reviewed in (Qian and Pollard 2010)]. These populations are grouped into

those involved in intravasation, angiogenesis, tumor cell invasion, immune regulation, and seeding at distant sites. Macrophages involved in tumor cell intravasation are found on the abluminal side of the vessel and are phagocytic (Wyckoff et al. 2007; Qian and Pollard 2010). Angiogenic macrophages are characterized by the expression of VEGFR1, VEGF, CXCR4, Tie2, Cathepsin (CTS) B&S, and ETS2 (Leek and Harris 2002; De Palma et al. 2005; Lin et al. 2006; Lin et al. 2007; Qian and Pollard 2010; Zabuawala et al. 2010). Macrophages involved in tumor cell invasion express EGF, CTS B&S, and have enhanced activation of the Wnt pathway (Wyckoff et al. 2004; Hagemann et al. 2005; Pukrop et al. 2006; Wyckoff et al. 2007; Ojalvo et al. 2010; Qian and Pollard 2010). Another subpopulation of macrophages is programmed by the tumor to inhibit anti-tumor immune response; these are characterized by the expression of arginase, MARCO, IL-10, and CCL22 and can stimulate the recruitment and expansion of regulatory T-cells in the tumor microenvironment (Curiel et al. 2004; Biswas et al. 2006; Perruche et al. 2008; Kuang et al. 2009; Ojalvo et al. 2009; Qin 2009; Qian and Pollard 2010). Macrophages responsible for tumor cell seeding, so called metastatic macrophages, express VEGFR1, CCR2, and CXCR4, however, this subpopulation is negative for Tie2 expression (Qian et al. 2009; Qian and Pollard 2010). Given this complex view of TAM classification and the extensive involvement macrophages have at every stage of

tumor progression, an enhanced understanding of macrophage phenotypic regulation is needed.

1.4 Pleiotrophin

Pleiotrophin (PTN) is expressed extensively during development, but expression in adult tissues is restricted except during times of inflammation and remodeling (Rauvala 1989; Vanderwinden et al. 1992; Silos-Santiago et al. 1996; Yeh et al. 1998). PTN signals through receptor protein tyrosine phosphatase (RPTP)β/ζ and downstream effectors including anaplastic lymphoma kinase (ALK), β-catenin, β-adducin and others to promote cell proliferation, migration, differentiation, and transformation (Milner et al. 1989; Courty et al. 1991; Fang et al. 1992; Laaroubi et al. 1994; Perez-Pinera et al. 2006). PTN is an important angiogenic cytokine in many models of breast cancer (Perez-Pinera et al. 2007) and is expressed highly by approximately 60% of primary breast tumors (Fang et al. 1992; Riegel and Wellstein 1994).

1.4.1 Pleiotrophin: Structure, Expression, and Signaling Pathway

PTN is an 18 kDa, 136 amino acid, heparin binding cytokine. Structurally PTN consists of a 32 amino acid signal sequence and two lysine-rich domains, one at each the N and C-terminal of the protein. Between these two lysine-rich domains are two thrombospondin type I domains. These domains are responsible

for PTN's ability to bind heparin and its receptor RPTPβ/ζ (Meng et al. 2000; Perez-Pinera et al. 2008).

PTN is expressed extensively during development, although its expression is temporally regulated. PTN is expressed in the developing central and peripheral nervous system, salivary glands, lung, kidney, digestive system, sense organs, and skeletal system (Mitsiadis et al. 1995). Expression levels are highest in the postnatal brain during glial and neuron differentiation (Rauvala 1989). In adult tissues, PTN is expressed constitutively in testicular Leydig cells, the uterus, and a subpopulation of glia and neurons (Milner et al. 1989; Vanderwinden et al. 1992; Silos-Santiago et al. 1996). Furthermore, PTN expression can be reactivated during certain physiological and pathological processes such as ischemic brain injury and would healing (Yeh et al. 1998; Deuel et al. 2002) and cancer (Perez-Pinera et al. 2007) (Fang et al. 1992; Riegel and Wellstein 1994).

PTN signals through a receptor protein phosphatase known as RPTPβ/ζ (Meng et al. 2000). There is some controversy as to whether PTN may also bind toALK, but the evidence that ALK phosphorylation is controlled indirectly by RPTPβ/ζ is substantial (Perez-Pinera et al. 2007). RPTPβ/ζ maintains steady-state phosphorylation levels of a number of substrates including ALK, β-catenin, β-adducin and others under normal cellular conditions. When bound by PTN, RPTPβ/ζ is inactive and can no longer keep substrate phosphorylation in check.

The result is a net increase in substrate phosphorylation following PTN stimulation resulting in changes in cellular phenotype (Milner et al. 1989; Courty et al. 1991; Fang et al. 1992; Laaroubi et al. 1994; Perez-Pinera et al. 2006).

PTN knockout mice have been generated and are viable and fertile. To date there are no published studies examining tumor progression in these animals. Instead studies have focused on the function of PTN in the nervous system. PTN knockout mice display deficits in spatial learning compared to their wild-type counterparts (Amet et al. 2001; Pavlov et al. 2002). Furthermore, PTN deficient mice exhibit increased drug seeking behavior and amphetamine-induced neurotoxicity when expose to amphetamines (Gramage and Herradon 2010; Gramage et al. 2010; Gramage et al. 2010). Another study reports decreased bone formation and osteopenia in PTN deficient animals (Imai et al. 2009).

1.4.2 Pleiotrophin in the tumor microenvironment

PTN is an important angiogenic cytokine in many models of breast cancer (Perez-Pinera et al. 2007) and is expressed highly by approximately 60% of primary breast tumors (Fang et al. 1992; Riegel and Wellstein 1994). When MCF-7 human breast cancer cells were engineered to express high levels of PTN, tumor progression and angiogenesis was enhanced (Choudhuri et al. 1997). Additionally, expression of a dominant negative PTN by MDA-MB-231 human breast cancer cells abrogated angiogenesis and progression to malignancy (Zhang

et al. 1997). Finally, when PTN was over-expressed in the mammary fat pad of MMTV-PyMT transgenic mice, angiogenesis and tumor progression was accelerated significantly (Chang et al. 2007). PTN functions as an angiogenic factor and promotes remodeling of the tumor microenvironment and epithelial-mesenchymal transition (EMT) (Perez-Pinera et al. 2006; Chang et al. 2007). These studies suggest that PTN is an attractive therapeutic target in breast cancer; however, more information is needed concerning the effects of PTN on the tumor microenvironment including recruitment and activation of immune cells.

1.4.3 Pleiotrophin and immune cells

PTN is expressed in the adult bone marrow where it stimulates osteogenic differentiation at low concentrations (Tare et al. 2002). PTN is crucial for the differentiation of many stem cell types including human embryonic stem cells (Vazin et al. 2009), neural stem cells, late retinal progenitor cells (Roger et al. 2006), and myoblasts (Caruelle et al. 2004). PTN also promotes nitric oxide (NO)-dependent mobilization and migration of endothelial progenitor cells (Heiss et al. 2008). These studies suggest that PTN functions primarily as a stem cell differentiation factor, but it is unknown what specific effects PTN has on HSC survival and differentiation. There are very few studies examining the effects of PTN other immune cell populations, however, there is some evidence that PTN can function as a neutrophil chemotactic agent (Ochiai et al. 2004).

In contrast to other immune cell populations there are a number of studies examining the effects of PTN on monocyte/macrophage populations. PTN induces the expression of VEGFR2 on macrophages and is reported to promote the transdifferentiation of macrophages into functional endothelial cells *in vitro* (Sharifi et al. 2006; Dineen et al. 2008; Chen et al. 2009). More specifically, proliferating macrophages (RAW 264.7 cells on chamber slides) were exposed to recombinant PTN and then probed for VEGFR2 expression. These studies demonstrate that recombinant PTN protein can promote VEGFR2 on macrophages *in vitro* (Figure 1.4 (A)).

To further characterize this phenomenon, we analyzed the effect of conditioned media from MDA-MB-231 and MCF-7 cell lines on VEGFR2 expression by macrophages *in vitro*. we chose these cell lines based on microarrary data demonstrating that MDA-MB-231 cells express PTN but MCF-7 cells do not and other published results indicating the same (Choudhuri et al. 1997; Chang et al. 2007). Exposure of RAW cells to conditioned media from MDA-MB-231 cells for 12 hours induced VEGFR2 expression, whereas MCF-7 conditioned media did not (Figure 1.4(B)). Furthermore, we analyzed frozen sections of MCF-7 tumors and demonstrated that despite the lack of tumor cell production of PTN, there was PTN in the tumor microenvironment, as well as VEGFR2+ macrophages (Figure 1.4(C&D)). This data suggests PTN in the tumor microenvironment is not entirely tumor-cell derived.

When VEGFR2 is expressed, it becomes the dominant receptor driving VEGF-induced macrophage chemotaxis and specific blockade of VEGF:VEGFR2 interaction is sufficient to inhibit chemotaxis (Dineen et al. 2008; Roland et al. 2009). To confirm the functional significance of VEGFR2 expression by macrophages, we analyzed VEGF-induced migration of RAW cells *in vitro*. RAW cells (VEGFR1+ VEGFR2-) show a slight increase in migration towards VEGF (Figure 1.5(A)). This stimulation is not affected by the addition of 2C3 to the bottom of the transwell chamber. However, when VEGFR2 is induced by stimulation with PTN (Figure 1.4(A)), RAW cells show a significant migration toward VEGF (Figure 1.5(B)). Importantly, this effect is blocked by the addition of 2C3, demonstrating VEGFR2 dependence.

Furthermore, PTN may promote an angiogenic (anti-inflammatory) macrophage phenotype *in vitro* (Collino et al. 2009). This suggests that while anti-VEGF therapy reduces macrophage infiltration into the tumor, compensating expression of PTN can promote an anti-inflammatory phenotype in those macrophages that are either (1) in the tumor prior to therapy or (2) migrate into the tumor in response to a non-VEGF cytokine.

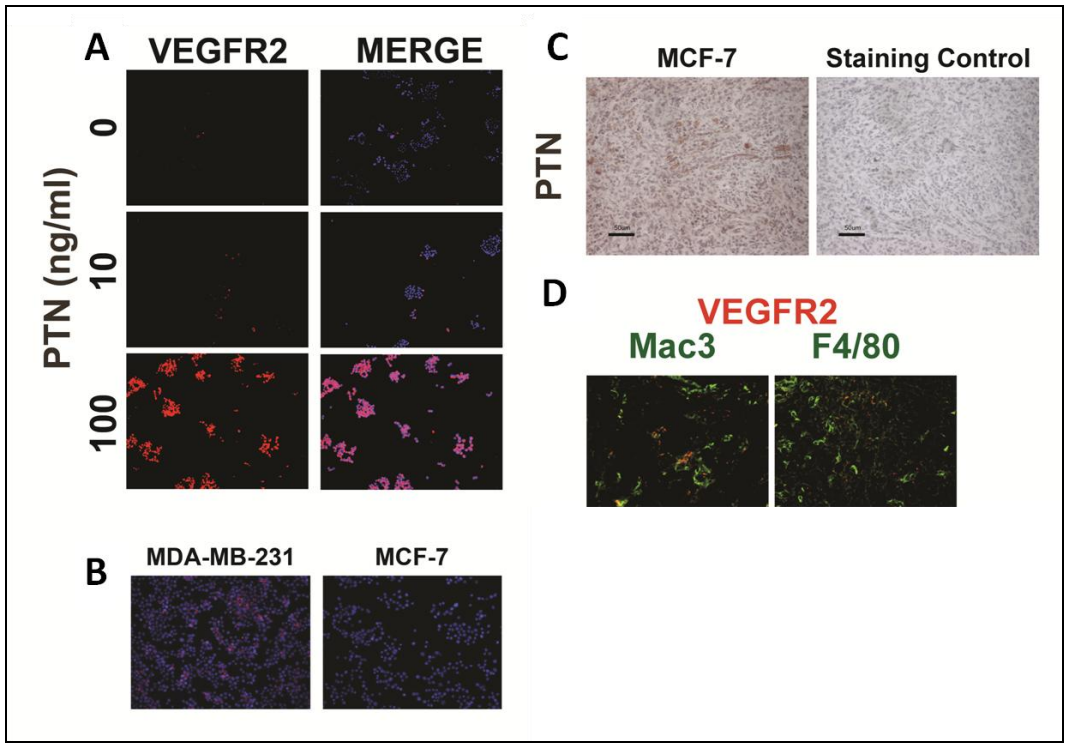

Figure 1.4 PTN induces the expression of VEGFR2 on macrophages *in vitro.* (A&B) RAW 264.7 (RAW) cells were incubated for 12 hours in chamber slides in the presence or absence of PTN (10 or 100 ng/ml) or TCM from MDA-MB-231 or MCF-7 cells. Immunocytochemistry showed an increase in VEGFR2 expression after PTN and MDA-MB-231 TCM stimulation. Representative images from three independent experiments are shown (total magnification, 200X) The tumor microenvironment of MCF-7 breast tumors contains PTN and $VEGFR2^{+}$ macrophages. (C) Frozen sections of MCF-7 mammary fat pad tumors demonstrate PTN is present in the tumor microenvironment despite the fact that the cell line itself does not produce significant PTN. (D) Immunohistochemistry for Mac-3 and F4/80 demonstrate the presence of $VEGFR2^{+}$ macrophages within these tumors. Total magnification, 200X. **Adopted from (Dineen et al. 2008)**.

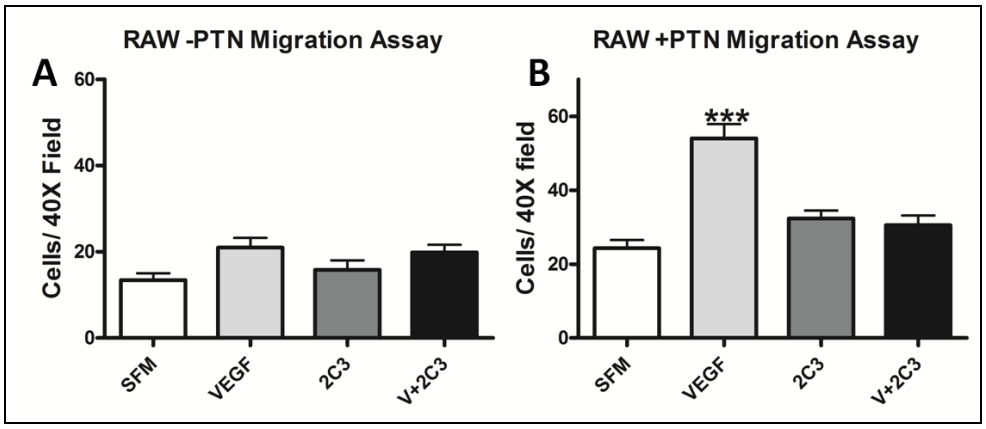

Figure 1.5. VEGFR2 is the dominant receptor mediating VEGF-induced macrophage chemotaxis. The effect of 2C3 on VEGF-induced macrophage migration was assessed by the use modified Boyden chamber assays. (A) Unstimulated RAW cells migrate only minimally to VEGF (40 ng/ml) compared to serum free media (SFM). And this is unaffected by the presence of 2C3. (B) RAW cells stimulated with PTN (100 ng/mL) migrate significantly more toward VEGF and this process is blocked by 2C3. **Adopted from (Dineen et al. 2008).**

Interestingly, conditioned media from the ovarian cancer cell line SKOV3 is unable to induce the differentiation of monocytes into $CD14^+/VEGFR2^+$ cells, until these cells are forced to undergo epithelial to mesenchymal transition (EMT) (Collino et al. 2009). Conditioned media from SKOV3 cells with a mesenchymal phenotype contains increased levels of PTN and induces the differentiation of monocytes into $CD14^+/VEGFR2^+$ cells (Collino et al. 2009). These $CD14^+/VEGFR2^+$ angiogenic monocytes are able to increase *in vitro* tube formation when co-cultured with endothelial cells and induce endothelial cell migration, indicating that $VEGFR2^+$ monocytes may represent a sub-type of anti-inflammatory macrophages (Collino et al. 2009). Furthermore, addition of an anti-PTN blocking antibody to mesenchymal SKOV3 CM prevented the

differentiation of primary monocytes into $CD14^{+}/VEGFR2^{+}$ angiogenic monocytes (Collino et al. 2009).

1.4.4 Drugs targeting the PTN- RPTPβ/ζ-ALK signaling axis

Anaplastic Lymphoma Kinase (ALK) was first discovered in the context of the oncogenic (NPM)-ALK fusion protein in anaplastic large cell lymphomas (ALCL). This fusion protein consists of the N-terminal portion of nucleophosmin (NPM) fused to the cytoplasmic domain of ALK and is constitutively active (Le Beau et al. 1989; Mason et al. 1990; Morris et al. 1994). ALK is expressed extensively in the developing central and peripheral nervous systems, but expression in the adult appears to be limited to a few neural cells, pericytes, and endothelial cells in the brain (Iwahara et al. 1997; Motegi et al. 2004; Pariser et al. 2005; Pariser et al. 2005; Tamura et al. 2006). I have found that ALK is also expressed and activated on a subpopulation of macrophages in the tumor microenvironment (discussed extensively in Chapter Three). ALK knockout mice have no significant abnormalities; however they do perform better on a number of neurological tests (Bilsland et al. 2008).

Receptor Protein Phosphatase β (RPTPβ/ζ) maintains steady-state phosphorylation levels ALK under normal cellular conditions. When bound by PTN, RPTPβ/ζ is inactive and can no longer keep ALK phosphorylation in check. Once de-repressed by the binding of PTN to RPTPβ/ζ , ALK signals through the

MAPK, PLCγ, PI3K/Akt, and JAK/STAT3 pathways to promote cell proliferation, survival, and differentiation (Figure 1.6) [reviewed in (Palmer et al. 2009)].

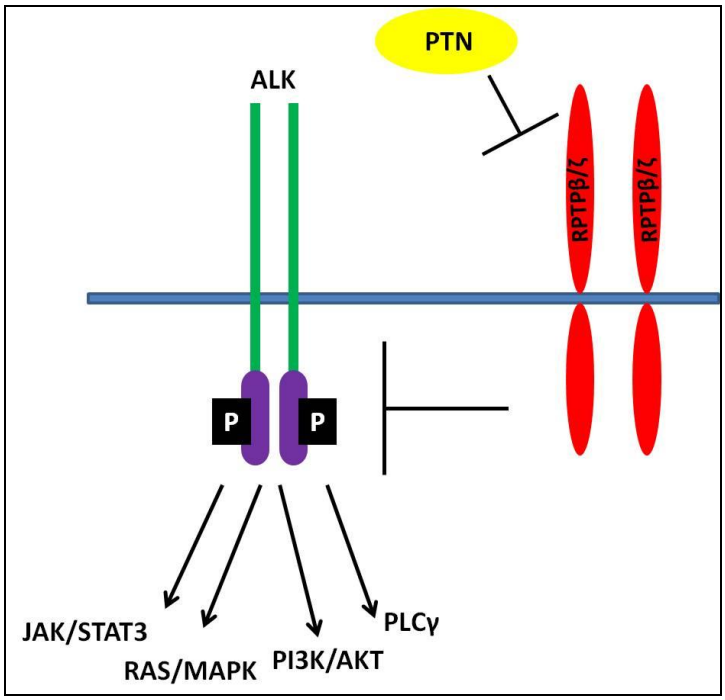

Figure 1.6. PTN indirectly modulates ALK activity through inactivation of RPTPβ/ζ. Under normal cellular conditions RPTPβ/ζ inactivates ALK. When PTN binds RPTPβ/ζ an inactive homodimer is formed, allowing ALK phosphorylation and downstream signaling to continue unchecked.

ALK has been implicated in the pathogenesis of a variety of human cancers [reviewed in (Webb et al. 2009)]. ALK fusion proteins have been identified in B-cell lymphomas (Chikatsu et al. 2003; De Paepe et al. 2003; Onciu et al. 2003; Reichard et al. 2007), inflammatory myofibroblastic tumors (Griffin et al. 1999), esophageal squamous cell carcinomas (Jazii et al. 2006; Du et al. 2007),

and non small cell lung carcinomas (Rikova et al. 2007; Soda et al. 2007; Inamura et al. 2008). Furthermore, ALK amplification (George et al. 2007), protein overexpression (Lamant et al. 2000), and activating mutations (George et al. 2008) have been extensively characterized in neuroblastoma. Finally, there is evidence suggesting a function for full length, wild-type ALK in glioblastoma (Powers et al. 2002; Grzelinski et al. 2005; Lu et al. 2005) and breast cancer (Dirks et al. 2002; Perez-Pinera et al. 2007; Perez-Pinera et al. 2007).

The involvement of ALK in the pathogenesis of this vast variety of cancer types has led to the development of a number of small molecule inhibitors, although none have currently achieved FDA approval. Crizotinib (Pfizer ©) was developed as a small molecule inhibitor of cMet but after extensive testing, it was discovered that crizotinib is 20-fold more selective for ALK and cMet than any of the other 120 kinases tested (Zou et al. 2007). Pre-clinical studies have confirmed crizotinib's efficacy in ALK-dependent ALCL (Christensen et al. 2007). Clinical trials are currently underway to determine the clinical efficacy of crizotinib in patients with ALCL and NSCLC. The success of crizotinib has led to the development of more potent and specific ALK inhibitors, including NVP-TAE684 (Galkin et al. 2007).

CHAPTER TWO

ANTI-VEGF THERAPY REDUCES ANGIOGENESIS AND MODULATES IMMUNE CELL INFILTRATION AND CYTOKINE LEVELS IN MULTIPLE PRE-CLINICAL BREAST CANCER MODELS

2.1 Introduction

Virchow first identified a link between inflammation and cancer in the late 1800s (Balkwill and Mantovani 2001). Since that time, the concept that chronic inflammation in the tumor microenvironment contributes to tumor progression has been validated in many types of cancer (Balkwill and Mantovani 2001; Coussens and Werb 2002; Vakkila and Lotze 2004). However, the underlying mechanisms for this connection remain unclear. Solid tumor malignancies consist of a diverse population of cells, including tumor cells, fibroblasts, endothelial cells and immune cells (Hanahan and Weinberg 2000; Pollard 2004). It is now clear that chronically activated immune cells can promote tumor growth and facilitate tumor survival. Macrophages typically are the main inflammatory component, but a variety of immune cells infiltrate tumors and can participate in tumor promotion (Murdoch et al. 2008). In general, these cells confer a worse prognosis in many types of cancer, including breast cancer (Bingle et al. 2002).

Vascular endothelial growth factor-A (VEGF) is a primary stimulant for tumor angiogenesis, making it a critical target for cancer therapy (Dvorak 2002). VEGF binds and activates VEGF receptor 1 (VEGFR1) and VEGFR2. Although the function of VEGFR2 in tumor angiogenesis has been characterized thoroughly, the function of VEGFR1 has not been well defined (Roskoski 2007). Clinically, elevated levels of VEGF correlate with increased lymph node metastases and a worse prognosis in breast cancer (Konecny et al. 2004). Bevacizumab (Avastin®, Genentech), a humanized monoclonal antibody that binds human VEGF and prevents VEGF from binding VEGFR1 and VEGFR2, was approved for the treatment of metastatic HER2/NEU-negative breast cancer in 2007, but this approval was revoked in 2010 (Miller et al. 2007; Miles et al. 2010; Robert et al. 2011). The perceived clinical success of bevacizumab has bolstered the development and testing of agents that directly target VEGF, selectively inhibit VEGFR1 or VEGFR2, or promiscuously block both VEGF receptors as well as other receptor tyrosine kinases (Lacouture et al. 2008; Wilhelm et al. 2008). Previously, we have shown that selective inhibition of VEGF binding to VEGFR2 with a fully human monoclonal antibody (r84) is sufficient for effective control of tumor growth in a preclinical model of breast cancer (Roland et al. 2009). However, few studies have compared directly the effectiveness of different anti-VEGF strategies in preclinical models.

The anti-tumor effect of angiogenesis inhibitors is due in part to reduction of VEGF-induced angiogenesis (Ellis and Hicklin 2008). Immune cells also express receptors for VEGF; however, the effect of anti-VEGF therapy on the infiltration of immune cells into tumors has not been fully characterized. VEGF is a major chemoattractant for inflammatory cells, including macrophages, neutrophils, dendritic cells (DCs), myeloid-derived suppressor cells (MDSCs) and T-cells (Ancelin et al. 2004; Huang et al. 2007; Dineen et al. 2008; Ko et al. 2009; Ozao-Choy et al. 2009; Shin et al. 2009). In tumor xenograft models, anti-VEGF therapy leads to a reduction in macrophage infiltration (Salnikov et al. 2006; Whitehurst et al. 2007; Dineen et al. 2008; Roland et al. 2009). Recently, we found that selective inhibition of VEGF from binding VEGFR2 with r84 resulted in decreased in MDSC infiltration and increased neutrophil and mature dendritic cell infiltration in MDA-MB-231 human breast cancer xenografts (Roland et al. 2009). Like macrophages, MDSCs ($CD11b^{+}Gr1^{+}$) are an important contributor to tumor progression whereby, these cells secrete immunosuppressive mediators and induce T-lymphocyte dysfunction (Gabrilovich et al. 2001; Serafini et al. 2004). MDSCs express VEGFR1 and VEGFR2 (Murdoch et al. 2008) and studies in non-tumor bearing animals demonstrate that activation of VEGFR2 promotes MDSC infiltration into the spleen (Huang et al. 2007). VEGF is also important for monocyte chemotaxis and is a key regulator of the differentiation and migration of dendritic cells (DCs) (Dikov et al. 2005; Huang et al. 2007). In non-tumor

bearing animals, VEGFR1 activation inhibits stem cell differentiation to the dendritic cell lineage whereas VEGFR2 activation decreases the number and function of mature dendritic cells in the spleen (Huang et al. 2007). Unlike other myeloid cell types, increased tumor-infiltrating DCs is associated with improved prognosis and specifically, the number of $CD83^+$ DCs has been shown to inversely correlate with lymph node metastasis and tissue expression of VEGF and TGFβ in human breast cancer specimens (Iwamoto et al. 2003). $CD4^+CD25^+FoxP3^+$ regulatory T cells (Treg) contribute to maintenance of immunologic self-tolerance. However, the function of Treg as natural immune suppressors may also contribute to the immune imbalance found in cancers (Linehan and Goedegebuure 2005). Blood from patients with breast or pancreatic cancer has an increased percentage of Treg compared to healthy individuals (Liyanage et al. 2002). Treg secrete immunosuppressive cytokines such as TGFβ and IL-10, but little IFN-γ (Liyanage et al. 2002). Though TGFβ can induce peripheral Treg, it is not required for the generation of a thymic-derived subset of these cells. Recently, IL-2, IFN-γ and TNF-α have been implicated in Treg generation (Chen et al. 2007; Zheng et al. 2007; Feng et al. 2008). However, the effect of anti-VEGF therapy on Treg infiltration is unknown.

In the present study, we use three distinct preclinical models of breast cancer to compare the effect of different anti-VEGF therapies on breast cancer growth, vascular parameters, immune cell infiltration and intra-tumoral cytokine

levels. We found that inhibition of VEGFR1 or VEGFR2 activation resulted in changes in intra-tumoral levels of IL-1β and CXCL1 that correlate with changes in immune cell infiltration. Furthermore, serum levels of IL-1β and IL-6 correlate with tumor response to anti-VEGF therapy and may be predictive clinical markers.

2.2 Results

2.2.1 Comparison of anti-VEGF strategies on MDA-MB-231 tumor growth and angiogenesis.

Anti-VEGF therapy has been validated clinically in many types of cancer, including breast cancer (Hurwitz et al. 2004; Miller et al. 2007). However, few studies have investigated whether differential blockade of the VEGF pathway results in differential effects on tumor growth and the tumor microenvironment in breast cancer. We studied the effect of selectively blocking the VEGF pathway using the agents listed in Table 2.1 in mice bearing established MDA-MB-231 human breast xenografts.

Agent	Class	Target	Target Species
r84	Human Ab	VEGF (blocks VEGFR2 only)	Mouse & Human
mcr84	Murine chimeric Ab	VEGF (blocks VEGFR2 only)	Mouse & Human
bevacizumab	Humanized Ab	VEGF (blocks VEGFR1 and VEGFR2)	Human
MF1	Rat Ab	VEGFR1	Mouse
RAFL-2	Rat Ab	VEGFR2	Mouse
GU81	Peptoid	VEGFR1/2	Mouse & Human
sunitinib	Small molecule	VEGFR1/2, cKit, PDGFRβ	Mouse & Human

Table 2.1. Anti-VEGF agents. Ab: antibody; VEGF: Vascular endothelial growth factor; VEGFR1: VEGF receptor 1; VEGFR2: VEGF receptor 2; PDGFRβ: Platelet-derived growth factor receptor β. **Adopted from (Roland et al. 2009).**

The effect of therapy with all six agents was evaluated after one and four weeks of drug exposure. After one week of therapy, only tumors from mice treated with r84 or bevacizumab were significantly smaller than control-treated tumors (Figure 2.1 (A)). After four weeks of therapy, selective blockade of VEGF binding to VEGFRs (r84; bevacizumab) and the RTKI (sunitinib) significantly limited tumor growth compared to control treatment (Figure 2.1 (A)). Tumors treated with agents that selectively block VEGFR1 (MF1), VEGFR2 (RAFL-2), or both receptors (GU81) did not control tumor growth compared to control IgG at the one and four week time points. Tumor volume increased an average of 393% from day 31 (week 1) to day 52 (week 4) post tumor cell injection (TCI)

time in mice receiving a control IgG. Treatment with r84, bevacizumab, RAFL-2, GU81, and sunitinib resulted in mean tumor volume increases of 102, 244, 239, 224, and 109%, respectively. Each of these inhibitors block VEGFR2 activity; in contrast, treatment with the anti-VEGFR1 antibody MF-1 resulted in an increase of 464% (Figure 2.1 (A)). These results support the concept that inhibition of VEGFR1 is not adequate to control the growth of human breast tumor xenografts.

To determine the effect of anti-VEGF therapy on angiogenesis, we assessed microvessel density (MVD; number of vessels/100X field) and vascular area (% positive fluorescent area/100X field) at the one and four week time points (Figure 2.1 (B)). Percent change (Δ) in MVD or vascular area was defined as week 4 MVD or vascular area/mean week 1 MVD or vascular area. After one week of therapy, only bevacizumab-treated tumors had significantly fewer vessels ($p<0.05$) compared to control-treated tumors (Figure 2.1 (B)). However, overall vascular area was decreased in tumors from animals treated with bevacizumab, r84 and sunitinib (Figure 2.1 (C)); indicating vessel size was decreased after anti-VEGF therapy. After four weeks of therapy (Figure 2.1 (B)), only r84 and bevacizumab reduced microvessel density compared to control IgG ($p<0.001$). Interestingly, r84 prevented an increase in MVD from week 1 to week 4 of therapy, while MVD increased in all other treatment conditions (Figure 2.1 (B); % Δ in MVD). However, tumors from all anti-VEGF therapies, except RAFL-2 had an increase in vascular area over the course of therapy (Figure 2.1 (C); % Δ in

vascular area). In comparing the anti-angiogenic activity of these agents, we found that selectively blocking VEGF from binding VEGFR2 (r84) was as or more effective than all other anti-VEGF strategies in decreasing MVD and vascular area in MDA-MB-231 orthotopic xenografts.

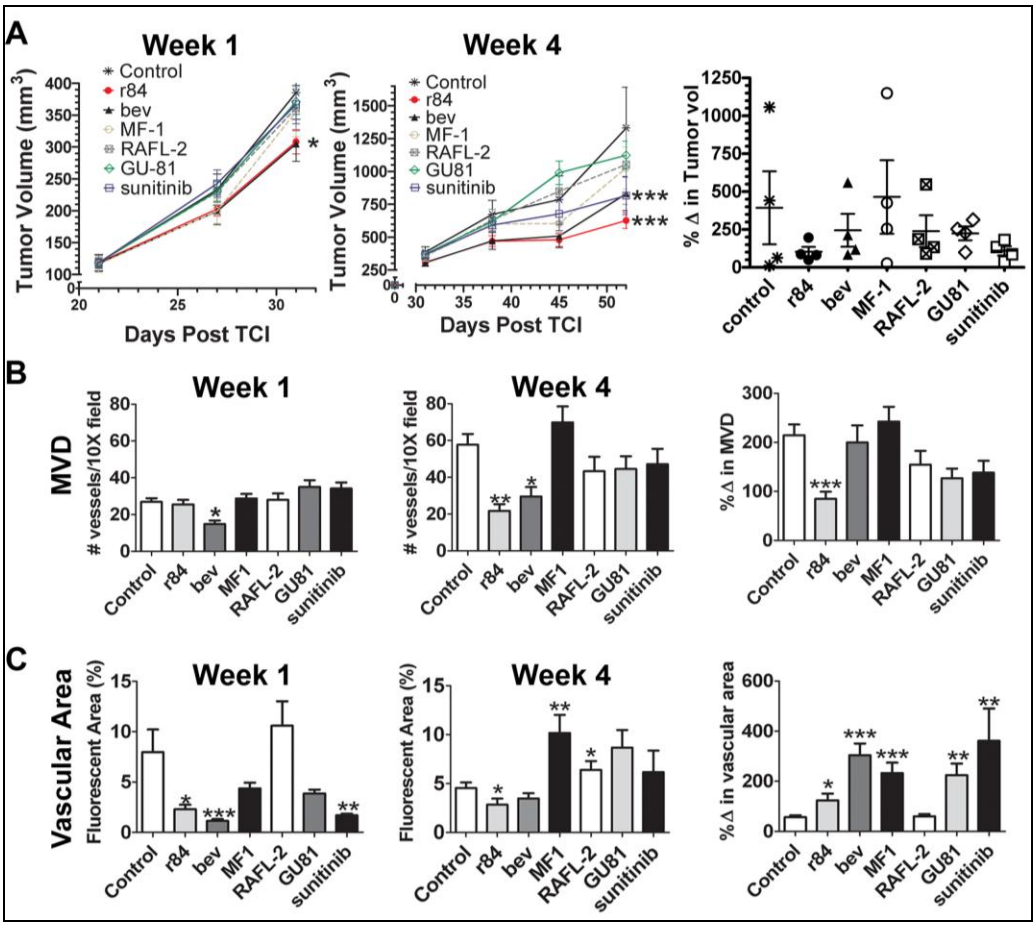

Figure 2.1. Anti-tumor and anti-vascular effects of VEGF pathway inhibition in MDA-MB-231 xenografts. MDA-MB-231 human breast cancer cells (5 x 10^6) were injected into the mammary fat pad of SCID mice. Treatment with control IgG, bevacizumab (bev), r84, MF1, or RAFL-2 (250 μg twice weekly), GU81 (120 μg daily), sunitinib (200 μg daily) was initiated in established tumors (~150 mm^3) on day 24 post tumor cell injection (TCI) and continued for 1 (Week 1) or 4 (Week 4) weeks. (A) Mean tumor volume after 1 (n=12/group) and 4 (n=4/group) weeks of therapy is displayed. The mean percent change in tumor volume from 1 to 4 weeks of therapy is displayed as a scatter plot and was determined by dividing the tumor volume from individual mice at after 4 weeks of therapy by the mean tumor volume of the group after 1 week of therapy (n=4/group/timepoint). (B-C) Tumor sections were analyzed by immunofluorescence using MECA-32, an endothelial cell marker for microvessel density (MVD, B) and vascular area (C). Data are displayed as mean ± SEM and represents 5 images (Total magnification, 100X) per tumor and three tumors per group. Images were analyzed using Elements software. *p=0.05, **p=0.01, ***p<0.001. **Adopted from (Roland et al. 2009)**.

To determine if the effect of r84, 2C3 (which also specifically prevents the VEGF:VEGFR2 interactions and decreases tumor growth in MDA-MB-231 xenografts (Brekken et al. 2000; Roland et al. 2009)), and bevacizumab on MDA-MB-231 tumor growth *in vivo* could be due to blocking VEGF activation of tumor cells directly, we evaluated tumor cell proliferation and migration *in vitro*. MDA-MB-231 *in vitro* proliferation was unaffected by VEGF, 2C3, bevacizumab, or r84 treatment (data not shown). However, we found that MDA-MB-231 cells migrated strongly toward VEGF, and this migration was blocked by the addition of 2C3, r84, or bevacizumab (Figure 2.2 ((A)). These results suggest that VEGF binding to VEGFR2 expressed by MDA-MB-231 cells induces cell migration.

The expression of VEGFR2 on MDA-MB-231 breast cancer cells has been controversial. Some groups have shown that minimal VEGFR2 is expressed on the cell surface (Lee et al. 2007), whereas others have demonstrated it is expressed at high levels following serum starvation (Liang et al. 2006). To examine VEGFR expression in MDA-MB-231 cells and tumors, we performed qRT-PCR for VEGF receptors on whole cell lysates from MDA-MB-231 cells and tumors. Human (HDMECs) and murine (bEnd.3) endothelial cells were used as positive and negative controls, respectively, for testing the species specificity of the primers. we found that MDA-MB-231 cells expressed a detectable level of VEGFR1, VEGFR2, NRP-1 and NRP-2 *in vitro* (Figure 2.2 (B)). Expression of each receptor *in vivo* was compared to the level of expression *in vitro*. We found a

2.7, 3.7, and 8-fold increase in expression of VEGFR1 in control, bevacizumab, and r84-treated tumors, respectively, compared to MDA-MD-231 cells *in vitro*. In contrast, the level of VEGFR2 message did not change *in vivo* in any of the treatment groups. The level of NRP-1 was elevated slightly (1.8-2.5-fold) *in vivo* while NRP-2 levels increased 6.9, 7.9, and 9.3-fold in tumors from mice treated with control, r84, and bevacizumab, respectively (Figure 2.2 (C)). These results demonstrate that *in vitro,* MDA-MB-231 cells express all VEGFRs however; levels of VEGFR1 and NRP-1 and NRP-2 are elevated when MDA-MB-231 cells are grown *in vivo*.

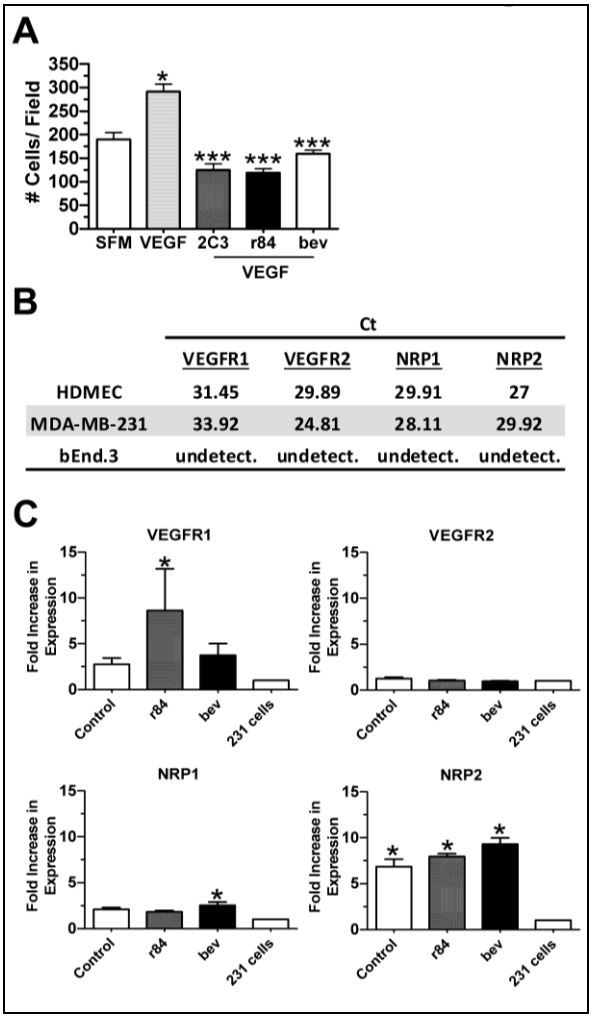

Figure 2.2. MDA-MB-231 cells express VEGF receptors and VEGFR2 mediates tumor cell migration. A) *In vitro* migration assays were performed using 24 well plates with 8 μm transwell inserts. MDA-MB-231 cells were allowed to migrate overnight towards serum free media (SFM), VEGF (40 ng/ml) or VEGF + the indicated IgG (40 μg/ml). MDA-MB-231 migrated significantly toward VEGF (VEGF vs. SFM, *, p<05). Migration was reduced in the presence of r84, 2C3 and bevacizumab. The mean number of cells per high-power field in each condition is shown. Six high power fields were counted per insert. Assays were done in triplicate. Anti-VEGF treatment vs. VEGF, ***, p<0.001. B) RNA isolated from human (HDMECs) and murine (bEnd.3) endothelial cells and MDA-MB-231 cells was used for qRT-PCR analysis of VEGFR1, VEGFR2, NRP1, and NRP2. The mean *Ct* (cycle threshold) value for each target is displayed. C) RNA was isolated from tumors at the time of sacrifice from control, bevacizumab and r84-treated animal and used for qRT-PCR. MDA-MB-231 cells express VEGFR1, VEGFR2, NRP-1 and NRP-2. The ratio of tumor cell expression *in vivo*/MDA-MB-231 cells *in vitro* is shown and is expressed as the fold increase in expression based on *Ct*. Data normalized to GAPDH. *, p<0.05 vs MDA-MB-231 cells *in vitro*. **Adopted from (Roland et al. 2009)**.

*2.2.2 VEGF is an important cytokine for immune cell infiltration in MDA-MB-231 human breast cancer xenografts***.**

We found that macrophages harvested from a tumor-bearing animal express both VEGFR1 and VEGFR2, whereas those harvested from non-tumor bearing mice are $VEGFR1^{+}$ but deficient in VEGFR2 in an orthotopic model of pancreatic cancer (Dineen et al. 2008). Furthermore, when VEGFR2 is expressed, it becomes the dominant receptor driving VEGF-induced chemotaxis and specific blockade of VEGF:VEGFR2 interaction is sufficient to inhibit chemotaxis (Dineen et al. 2008).To evaluate VEGFR2 expression on systemic macrophages in mice bearing MDA-MB-231 orthotopic breast tumors, we harvested peritoneal macrophages from tumor-bearing and non-tumor bearing animals and evaluated VEGFR2 expression by immunocytochemistry (Figure 2.3 (A)). Using two different anti-VEGFR2 antibodies, we show that peritoneal macrophages from tumor-bearing (TB) animals express significantly higher levels of VEGFR2 compared to peritoneal macrophages from non-tumor bearing animals (NTB). VEGFR1 expression demonstrated a similar expression pattern, whereby VEGFR1 mRNA was undetectable in NTB animals, but was detectable in peritoneal macrophages from tumor-bearing animals by RT-PCR (data not shown). To assess the functional significance of VEGFR2 expression on peritoneal macrophages, we analyzed VEGF-induced migration of peritoneal

macrophages *ex vivo*. Peritoneal macrophages from non–tumor-bearing animals ($VEGFR2^{-}$) show only minimal migration toward VEGF, which is unaffected by the presence of 2C3 or control antibody, where as peritoneal macrophages harvested from tumor-bearing animals ($VEGFR2^{+}$) migrate strongly toward VEGF, and this is abrogated by the addition of 2C3, indicating that this is a VEGF:VEGFR2 mediated event (Figure 2.3 (B)).

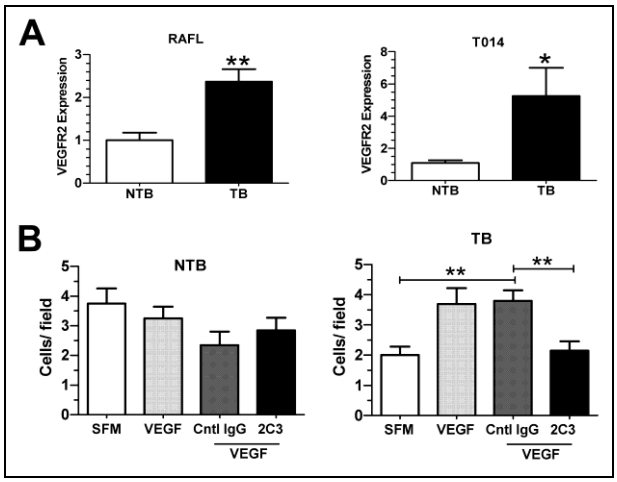

Figure 2.3. VEGFR2 is expressed on systemic macrophages in mice bearing MDA-MB-231 orthotopic tumors and is the dominant receptor mediating VEGF-induced macrophage chemotaxis. A) Macrophages from tumor-bearing (TB) and non–tumor-bearing (NTB) animals were isolated by peritoneal lavage, plated on chamber slides and evaluated for VEGFR2 expression by immunocytochemistry using two different anti-VEGFR2 antibodies (RAFL and T014). Peritoneal macrophages from tumor-bearing animals have a significant increase in VEGFR2 expression compared to NTB animals (*, $p<0.05$; **, $p<0.01$). B) Migration assays were performed with primary peritoneal macrophages from NTB or TB mice using 24 well plates with 3 μm transwell inserts. Peritoneal macrophages were allowed to migrate overnight towards serum-free media (SFM), VEGF (40 ng/ml), or VEGF + the indicated IgG (40 μg/ml). The mean (+/- SEM) number of cells per high-power field in each condition is shown. Four to five high power fields were counted per insert. Assays were done in duplicate or triplicate. Data shown is displayed as fold change in migration compared to SFM and is representative of at least three independent experiments and was analyzed with Kruskal-Wallis test. VEGF and VEGF + control IgG stimulated migration of macrophages from TB animals compared to control (**, $p<0.01$) and this was abrogated by treatment with 2C3 (**, $p<0.01$). **Adopted from (Roland et al. 2009)**.

Previously, we have shown a reduction in macrophage and MDSC infiltration and an increase in neutrophil infiltration into xenografts following anti-VEGF therapy (Whitehurst et al. 2007; Dineen et al. 2008; Roland et al. 2009). Surprisingly, after one week of therapy, selective blockade of VEGFR2 with RAFL-2 significantly induced macrophage infiltration into tumors compared with control treated animals (RAFL-2: 78.8 ± 10.5 vs control: 15.4 ± 4.5 cells/200X field; $p<0.01$; Figure 2.4 (A)). However, after four weeks of therapy, all anti-VEGF agents reduced macrophage infiltration (Figure 2.4 (A)). Neutrophil infiltration was examined using the anti-neutrophil antibody, 7/4. Acute selective inhibition of VEGFR1 (MF1) or VEGFR2 (RAFL-2) induced neutrophil accumulation into tumors (Figure 2.4 (B)). While chronic inhibition of VEGFR2 activation by r84 and RAFL-2, but not other strategies, resulted in increased neutrophil accumulation in tumors (Figure 2.4 (B)). Next, we investigated the effect of anti-VEGF therapy on MDSC infiltration ($CD11b^{+}Gr1^{+}$ cells) into tumors. Bevacizumab treatment resulted in MDSC accumulation after 1 and 4 weeks of therapy, although the increase was only significant after 1 week (Figure 2.4 (C)). Sunitinib on the other hand reduced the number of MDSC cells at both time points although again this was only significant after one week of therapy (Figure 2.4 (C)). GU81, which binds both VEGFR1 and VEGFR2 had little effect on MDSC numbers after 1 week of therapy; however at the 4 week time point, there was a significant increase in MDSC infiltration compared to

control-treated animals (Figure 2.4 ((C). r84, MF-1, and RAFL-2 had no discernable effect on MDSC numbers after one week of therapy although each reduced MDSC infiltration after 4 weeks of treatment (Figure 2.4 (C)). How VEGF governs MDSC recruitment into tumors is unclear. Our data suggests that blockade of VEGFR1 and VEGFR2 (e.g., bevacizumab and GU81) can induce an increase in MDSC infiltration, while selective blockade of one VEGF receptor limits MDSC accumulation in this xenograft model of breast cancer.

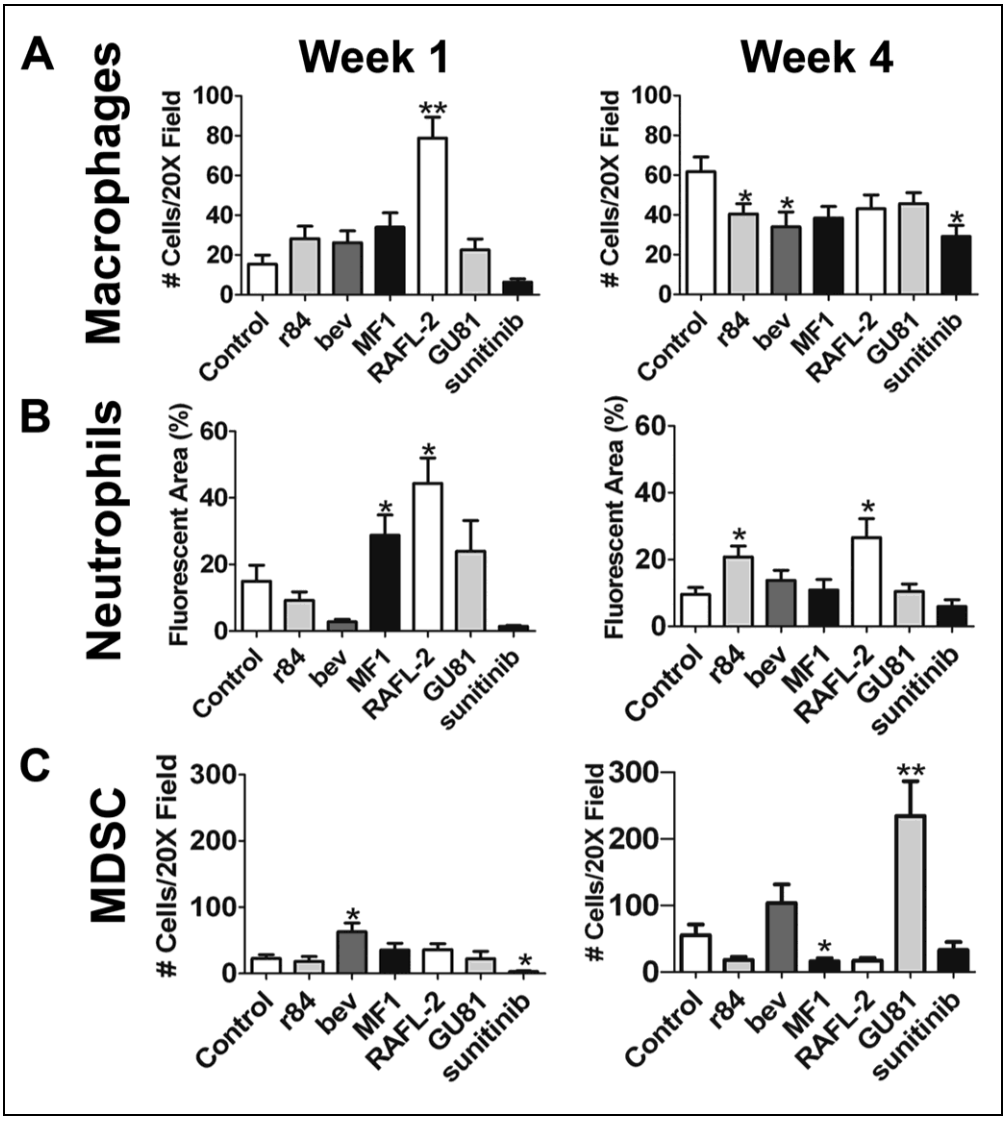

Figure 2.4. Inhibition of VEGF receptor activation utilizing different blocking strategies results in variations in immune cell infiltration in MDA-MB-231 human breast cancer xenografts. (A-C) Tumor sections were analyzed by immunofluorescence using F4/80, a macrophage marker, (A), and 7/4, a neutrophil marker (B). Tumor sections were evaluated by immunofluorescence for myeloid-derived suppressor cells (MDSCs, C) defined as the number of cells that express CD11b and Gr1 per 200X field. Data are displayed as mean ± SEM and represents 5 images (Total magnification, 200X) per tumor and three tumors per group. Images were overlayed and analyzed using Elements software. *p=0.05, **p=0.01. **Adopted from (Roland et al. 2009)**.

2.2.3 Mouse chimeric r84 delays tumor growth and improves the immune profile in inflammatory 4T1 breast tumors.

Growth of 4T1 tumors cells in the mammary fat pad of BALB/c mice is an inflammatory model of breast cancer in which immune cells comprise 40-50% of the overall tumor mass (DuPre and Hunter 2007; DuPre et al. 2007). To extend our previous observations, we performed similar experiments utilizing this immunocompetent model of breast cancer. By qRT-PCR, we demonstrate that 4T1 cells express VEGFR1 but not VEGFR2 *in vitro* (Table 2.2).

	bEND.3	**4T1**
VEGFR1	**25.981**	**31.034**
VEGFR2	**15.79**	**Undet.**
GAPDH	**14.104**	**15.19**

Table 2.2. 4T1 cells express VEGFR1 but not VEGFR2. RNA isolated from murine (bEnd.3) endothelial cells and 4T1 mouse breast cancer cells was used for qRT-PCR analysis of VEGFR1 and VEGFR2 and normalized to GAPDH. The mean *Ct* (cycle threshold) value for each target is displayed. **Adopted from (Roland et al. 2009)**.

For *in vivo* studies, mice with small but established tumors were treated for 1 or 3 weeks with a control IgG, a mouse chimeric version of r84 engineered to express the epitope binding region of r84 fused to mouse Fc (mcr84), GU81, or sunitinib (Table 2.1). As seen in the MDA-MB-231 model, after one and three weeks of therapy, inhibition of mouse VEGF binding to VEGFR2 (mcr84)

significantly reduced tumor growth compared to control IgG (Figure 2.5 (A)). Interestingly, GU81 controlled tumor growth after one and three weeks, while sunitinib had little effect on tumor volume or weight at either time point (Figure 2.5 (A)).

Though mcr84 and GU81 limited tumor growth after one week of therapy, tumors from GU81-treated animals had increased MVD and vascular area (Figure 2.5 (C&D), week 1). In contrast, after three weeks of therapy, tumors from all treatment groups had a reduction in MVD compared to control (Figure 2.5 (C), week 3; Figure 2.6 (A)). Unpredictably, tumors from animals treated with mcr84 had increased vascular area compared to control-treated tumors (4.37% ± 0.85 vs 1.67% ± 0.13, respectively; $p<0.05$) after three weeks of therapy (Figure 2.5 (D)). We hypothesize that this phenomenon is attributed to the increase in IL-1β, which can serve as alternate angiogenic factor (2.12 (C)). However, all three agents prevented an increase in MVD from week 1 to week 3 of therapy (Figure 2.5 (C); % Δ in MVD). These surprising vascular changes following mcr84 and GU81 therapy were validated using two additional endothelial cell markers, endomucin and CD31 (data not shown).

Similar to MDA-MB-231 tumors, inhibition of VEGF resulted in reduced macrophage infiltration ($CD68^+$ cells). This was evident with mcr84 at both time points. GU81 and sunitinib also reduced macrophage numbers after three weeks

of therapy although the changes did not reach reached statistical significance (Figure 2.6 (B), Figure 2.7 (A)). We also found that neutrophil infiltration ($7/4^+$ cells) was reduced significantly following chronic therapy with GU81 or sunitinib (Figure 2.6 (C), Figure 2.7 (B)).

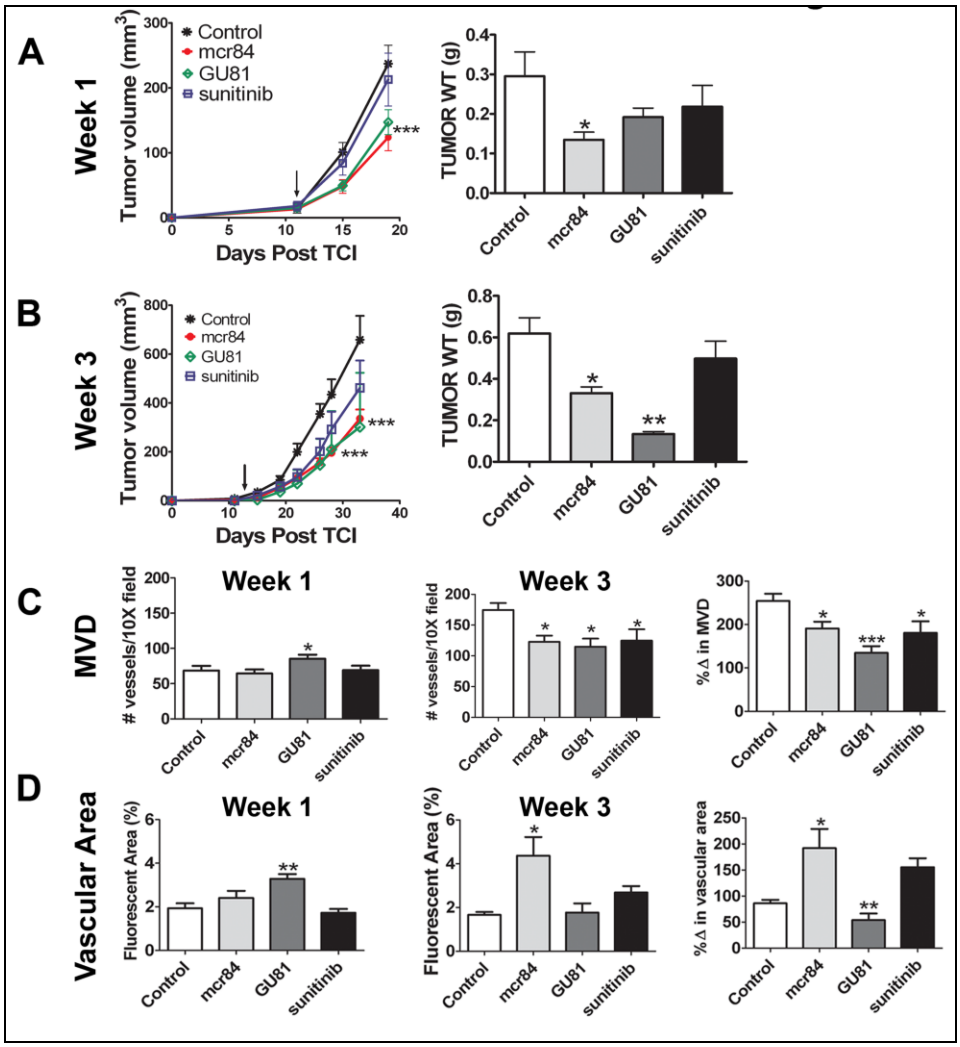

Figure 2.5. Anti-VEGF therapy delays tumor growth and reduces microvessel density in the inflammatory 4T1 breast cancer model. (A-B) 4T1 murine breast cancer cells were injected into the mammary fat pad of BALB/c mice. Treatment with 250 μg twice weekly of either control IgG or mcr84, 120 μg daily GU81 or 200 μg daily sunitinib was initiated in established tumors on day 12 post tumor cell injection (TCI; arrow) and continued for 1 (A) or 3 (B) weeks (n=4/group/timepoint). Tumor volumes were measured twice weekly and mean tumor volume +/- SEM is displayed. (C-D) Tumor sections were analyzed by immunofluorescence using MECA-32, an endothelial cell marker for microvessel density (MVD, C) and vascular area (D). Data are displayed as mean ± SEM and represents 5 images (Total magnification, 100X) per tumor and three tumors per group. Images were analyzed using Elements software. *p=0.05, **p=0.01, ***p<0.001. **Adopted from (Roland et al. 2009)**.

Tregs were identified by the co-expression of CD25 and FoxP3. Though we did not see any significant changes in Treg infiltration after one week of anti-VEGF therapy (Figure 2.7 (C)), chronic anti-VEGF therapy inhibited the infiltration of Treg into tumors compared to control IgG (Figure 2.6 (E), Figure 2.7 (C)). In the MDA-MB-231 model, we found a significant increase in MDSCs in tumors treated with chronic GU81 (Figure 2.4 (C)). However, in the 4T1 breast cancer model, we found a significant reduction in MDSC infiltration in all anti-VEGF groups at both time points (Figure 2.6 (F), Figure 2.7 (D)).

Previously, we identified an increase in $CD83^{+}CD11c^{+}$ mature dendritic cells in MDA-MB-231 tumors treated with r84 (Roland et al. 2009). We found a similar effect in the 4T1 model, whereby there was an overall decrease in $CD11c^{+}$ cells in all treatment groups after one week of therapy (Figure 2.7 (E)). Furthermore, when we looked at the number of $CD83^{+}CD11c^{+}$ mature dendritic cells (Figure 2.6 (D), Figure 2.7 (E)), tumors from animals treated with mcr84 had a significant increase in this population of cells compared to all other treatment groups. In addition, when we specifically analyzed the $CD11c^{+}$ population of cells, we found that approximately 48% of dendritic cells within mcr84 tumors expressed CD83, whereas only 14.8, 27.8 and 16.8% of dendritic cells in control, GU81 or sunitinib, respectively, expressed CD83 (Figure 2.7 (E); $p<0.001$).

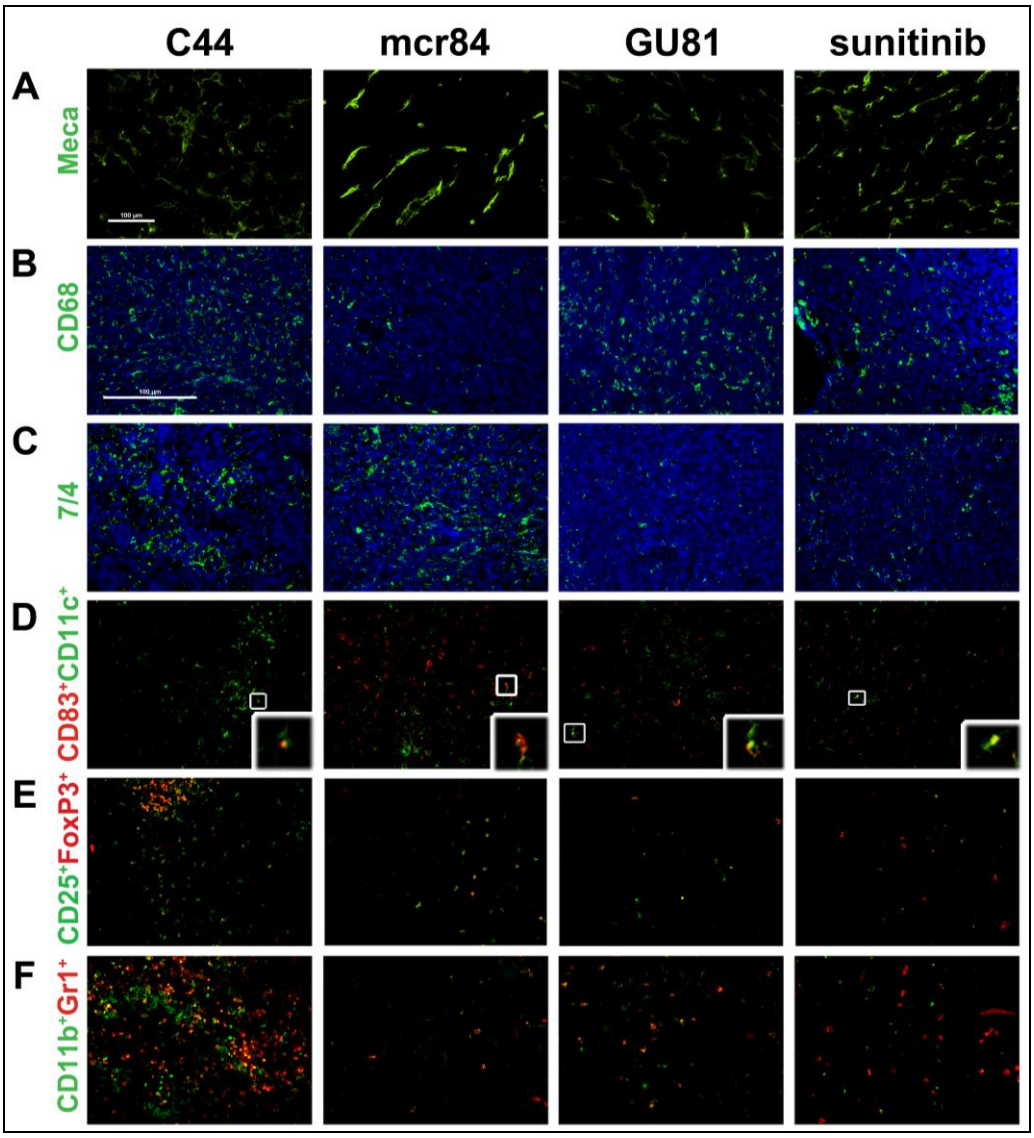

Figure 2.6. Representative immunofluorescence images of microvessel density and immune cell infiltration in the 4T1 model. Tumor sections from mice treated with the indicated anti-VEGF agent were analyzed by immunofluorescence using MECA-32, an endothelial cell marker (A), CD68, a macrophage marker (B), and 7/4, a neutrophil marker (C). Tumor sections were evaluated by immunofluorescence for mature dendritic cells by co-localization (box) of CD83 and CD11c (D); Treg by co-localization of $CD25^+$and $FoxP3^+$ cells (E); and myeloid-derived suppressor cells defined as the number of cells that express CD11b and Gr1 per 200X field (F). The inset on each picture in row D is a magnified view of co-localization of CD83 and CD11c. Representative pictures of control and anti-VEGF treated tumors are displayed. Total magnification, 200X; except for Meca-32 staining (100X), scale bar, 100 μm. Images were overlayed and analyzed using Elements software. Quantitation of signal intensity is shown in Figures 2.5 and 2.7. **Adopted from (Roland et al. 2009)**.

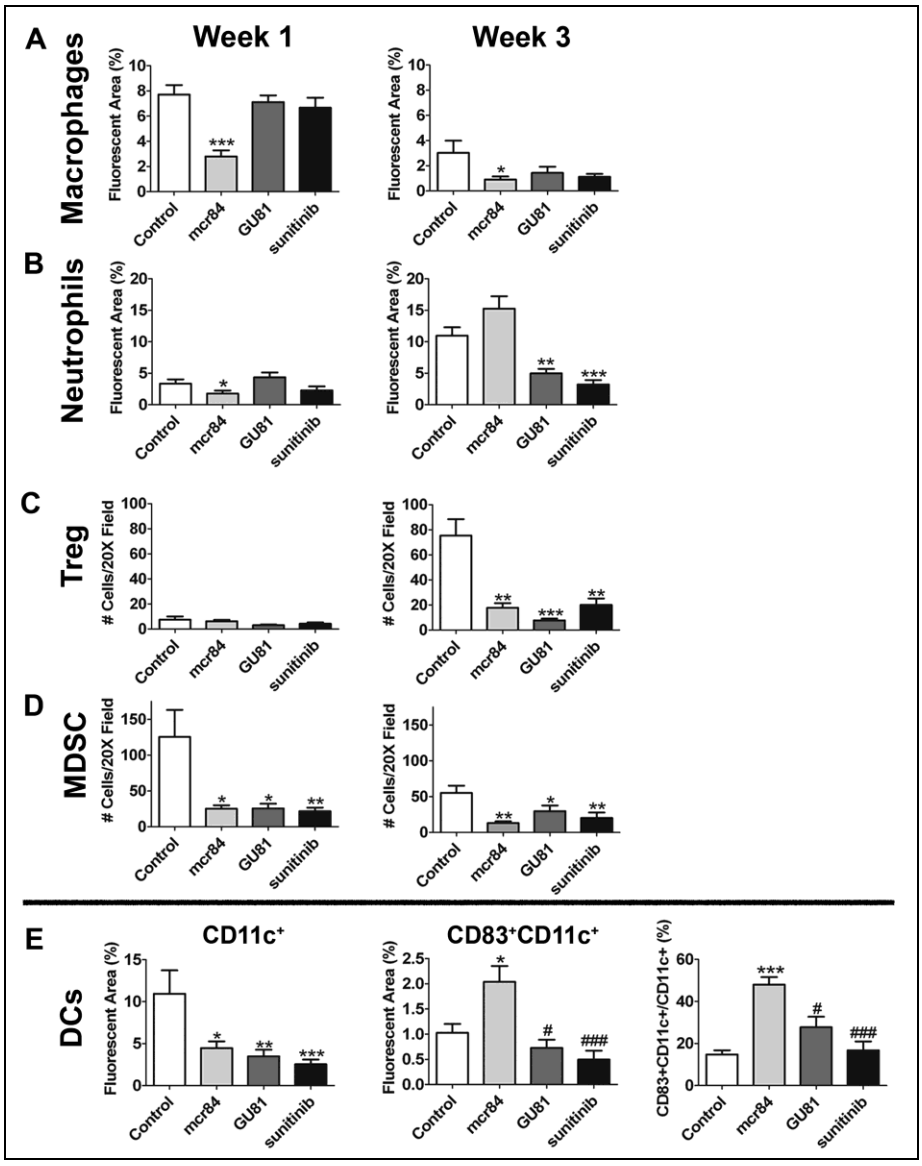

Figure 2.7. **mcr84 reduces immune suppressor cells and increases mature dendritic cell infiltration in the inflammatory 4T1 breast cancer model.** (A-B) Tumor sections were analyzed by immunofluorescence at the one and three week time points using CD68, a macrophage marker (A), and 7/4, a neutrophil marker (B). (C-E) Tumor sections were evaluated by immunofluorescence for (C) Tregs, colocalization of $CD25^+$ and $FoxP3^+$ (D) and MDSCs, colocalization of $CD11b^+$ and $Gr1^{+.}$ Dendritic cells were characterized using $CD11c^+$ (total DCs), mature dendritic cells, defined as colocalization of CD83 and CD11c and % of $CD11c^+$ cells that were $CD83^+$ (Week 1 only). Data are displayed as mean ± SEM and represents 5 images (Total magnification, 200X) per tumor and three tumors per group. Images were overlayed and analyzed using Elements software. *p=0.05, **p=0.01, ***p<0.001 vs control; #p=0.05, ###p<0.001 vs mcr84. **Adopted from (Roland et al. 2009)**.

2.2.4 Effect of anti-VEGF therapy on immune cell infiltration in the transgenic MMTV-PyMT breast tumor model.

The MMTV-PyMT transgenic mouse expresses the polyomavirus middle T antigen driven by the MMTV-LTR promoter (Guy et al. 1992). Polyomavirus middle T oncogene expression results in the generation of multifocal mammary carcinomas in 100% of female mice. We treated 52 day old transgenic MMTV-PyMT females with control IgG, mcr84, GU81 or sunitinib for four weeks (Table 2.1). Similar to the MDA-MB-231 model, we found that mcr84 controlled tumor growth after four weeks of therapy compared to control-treated tumors (Figure 2.8 (A)). Tumors from mcr84-treated animals had a decrease in vascular area and macrophage infiltration ($CD11b^{+}Gr1^{-}$ cells) compared to control-treated tumors (Figure 2.8 (B&C)) and an increase in neutrophils ($CD11b^{-}Gr1^{+}$ cells; Figure 2.8 (D)). Additionally, mcr84-treated tumors also had a significant reduction in MDSC and Treg infiltration compared to control, GU81, and sunitinib treated tumors (Figure 2.8 (E&F)).

With these studies, we have extended our previous observations (Roland et al. 2009) into an immunocompetent model system and have further validated that VEGF is an important cytokine that regulates immune cell trafficking into breast tumors.

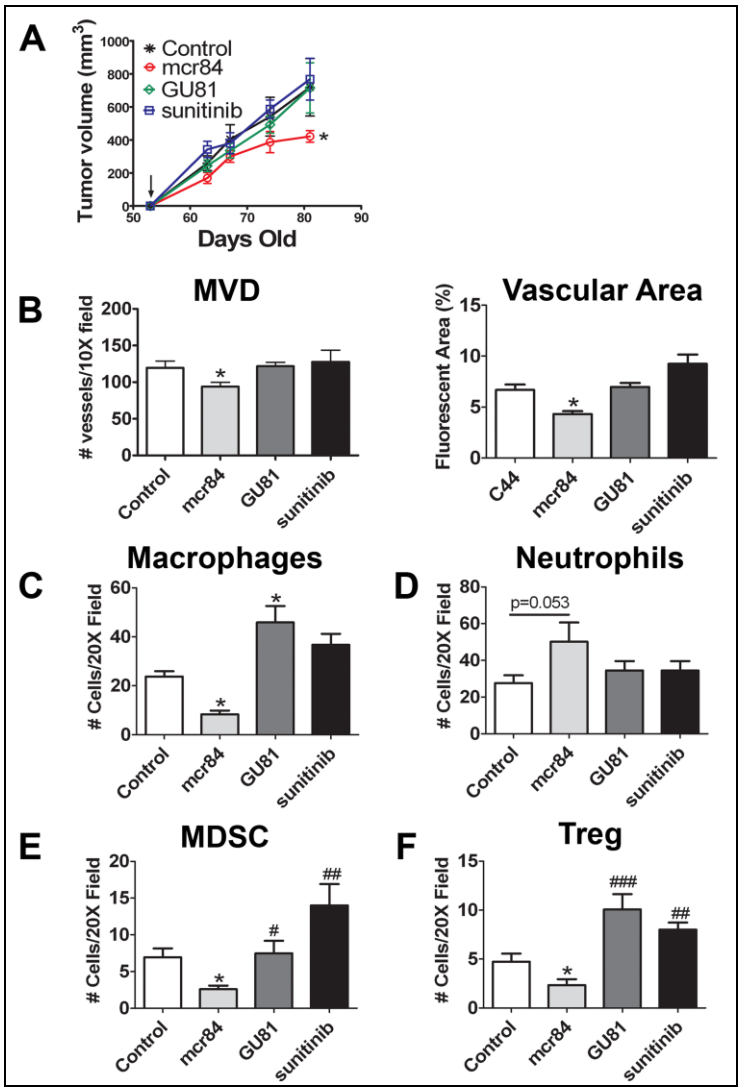

Figure 2.8. Effect of anti-VEGF therapy on immune cell infiltration in the transgenic MMTV-PyMT breast tumor model. (A) Treatment with 250 µg twice weekly of either control IgG or mcr84, 120 µg daily GU81 or 200 µg daily sunitinib was initiated when transgenic females were 52 days old (arrow) and continued for 4 weeks (n=5/group). Tumor volumes were measured twice weekly and mean tumor volume +/- SEM is displayed. (B-D) Tumor sections were analyzed by immunofluorescence using MECA-32, an endothelial cell marker (B), macrophages ($CD11b^{+}Gr1^{-}$ cells) (C) and neutrophils ($CD11b^{-}Gr1^{+}$) (D). (E-F) Tumor sections were evaluated by immunofluorescence for (E) MDSCs, co-localization of $CD11b^{+}$ and $Gr1^{+}$ (F) Tregs, co-localization of $CD25^{+}$and $FoxP3^{+}$. Data are displayed as mean ± SEM and represents 5 images per tumor and three tumors per group. Total magnification, 200X, except for Meca-32 staining (100X). Images were overlayed and using Elements software. *p=0.05, **p=0.01, ***p<0.001, ##p=0.01 vs mcr84. **Adopted from (Roland et al. 2009)**.

2.2.5 Immune cell infiltration and cytokine expression during the course of tumor progression in the MMTV-PyMT transgenic breast cancer model

The MMTV-PyMT breast cancer model features mammary specific expression of the polyoma middle-T antigen and 100% of transgenic female mice exhibit multifocal mammary adenocarcinoma. In addition, 90% of transgenic females will develop lung disease by 12 weeks of age (Guy et al. 1992). Disease progression has been extensively studied and closely mirrors human tumor progression. In this model, disease progresses from hyperplastic to advanced metastatic disease over the course of 16 weeks when mice are placed on an Fvb background (Figure 2.9) (Lin et al. 2003).When compared to the wild-type mammary fat pad, there is significant hyperproliferation of the mammary epithelium in transgenic mice at 6 weeks of age (Figure 2.9 (A)). This advances to an adenoma stage at 8 weeks, an early carcinoma at 10 weeks, and a late carcinoma by 12 weeks of age (Figure 2.9 (A)). By 16 weeks of age, all of the animals examined had macroscopic lung disease (Figure 2.9 (B&C)).

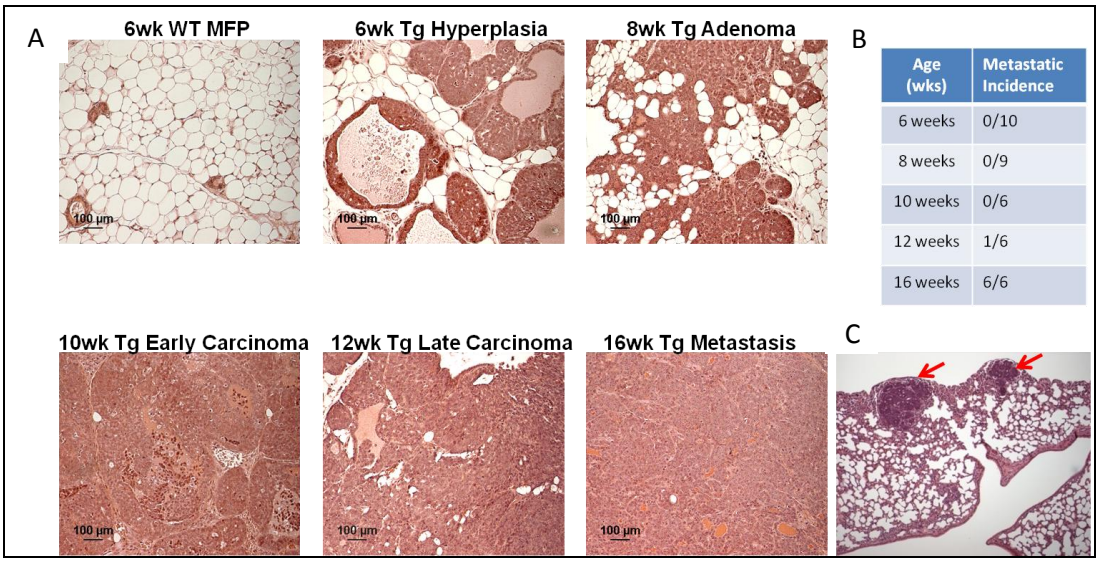

Figure 2.9 Disease progression in the MMTV-PyMT transgenic breast cancer model. Tumor (A) and lung (C) tissue was harvested from mice at 6, 8, 10, 12, and 16 weeks of age, formalin fixed, paraffin embedded, sectioned, and stained with hematoxylin and eosin. (B) Lungs from transgenic female mice were examined for macroscopic metastatic disease at the time of sacrifice and the number of mice with disease at each time point was noted. Pictures are representative of a minimum of 3 animals/group.

To further describe tumor progression in the MMTV-PyMT model of breast cancer, angiogenesis and immune cell infiltration was characterized throughout the course of tumor progression (Figure 2.10). Microvessel density (MVD) decreases during the course of tumor progression, where there are significantly fewer vessels in tumors from 12 and 16 week old transgenic mice compared to tumors from 6 week old transgenic mice (Figure 2.10(A)). Macrophage and neutrophil infiltration is constant throughout the course of tumor progression, except there are significantly fewer in tumors from 16 week old mice when compared to 6 week old mice (Figure 2.10 (B&C)). The number of MDSCs

and T-regs in the tumor peak when the mice reach 10 weeks of age, interestingly, this in the time when the tumors transition from hyperplastic to invasive lesions (Figure 2.10 (D&E)). In contrast to the tumor, the number of MDSCs sharply increases in the spleen when mice reach 12 weeks of age. This is the time when mice begin to exhibit macroscopic metastatic disease (Figure 2.10 (F)).

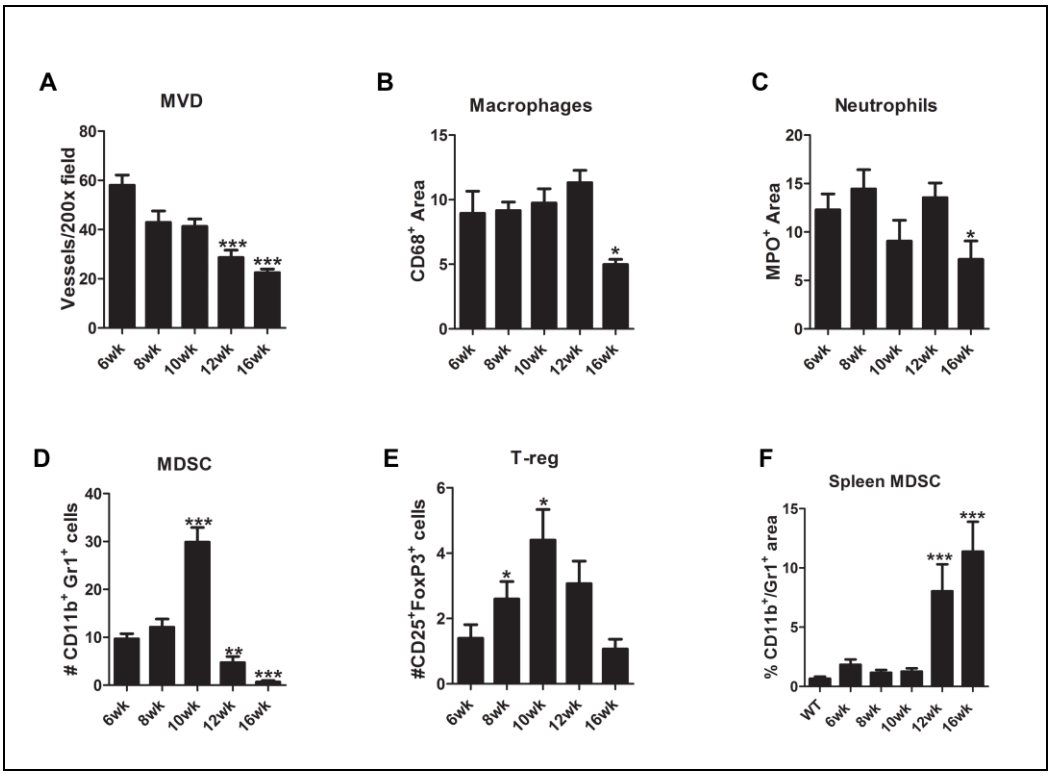

Figure 2.10. MVD and immune cell infiltration change as tumor progress in the MMTV-PyMT transgenic breast cancer model. Animals were sacrificed at 6, 8, 10, 12, and 16 weeks of age. Tumor (A-E) or spleen tissue (F) was snap frozen and sectioned for immunohistochemistry. The number of MECA-32$^+$ vessels/200X field was used as a measure of MVD (A). CD68$^+$ and MPO$^+$ area was used to assess macrophage and neutrophil infiltration, respectively (B&C). MDSCs are described as the number of CD11b$^+$ Gr1$^+$ cells (D&F). T-regs are described as the number of CD25$^+$ FoxP3$^+$ cells (E). Total magnification 200X. Images were overlayed and using Elements software. *p=0.05, **p=0.01, ***p<0.001 vs 6 week Tg, Mann-Whitney test. A minimum of 3 animals/group and 5 pictures/animal were used for analysis.

To further explore the changes in tumor MDSC levels during the course of tumor progression, we examined the levels of cytokines known to influence MDSC infiltration and differentiation. IL-1β and IL-10 levels significantly increase in tumors from 10 week old mice (Figure 2.11 (A&C)). These patterns of expression closely mirror the pattern of MDSC infiltration during the course of tumor progression. Linear regression analysis reveals a positive correlation between both IL-1β ($r^2 = 0.81$) (Figure 2.11(B)) and IL-10 and MDSC infiltration ($r^2 = 0.92$) (Figure 2.11 (D)).

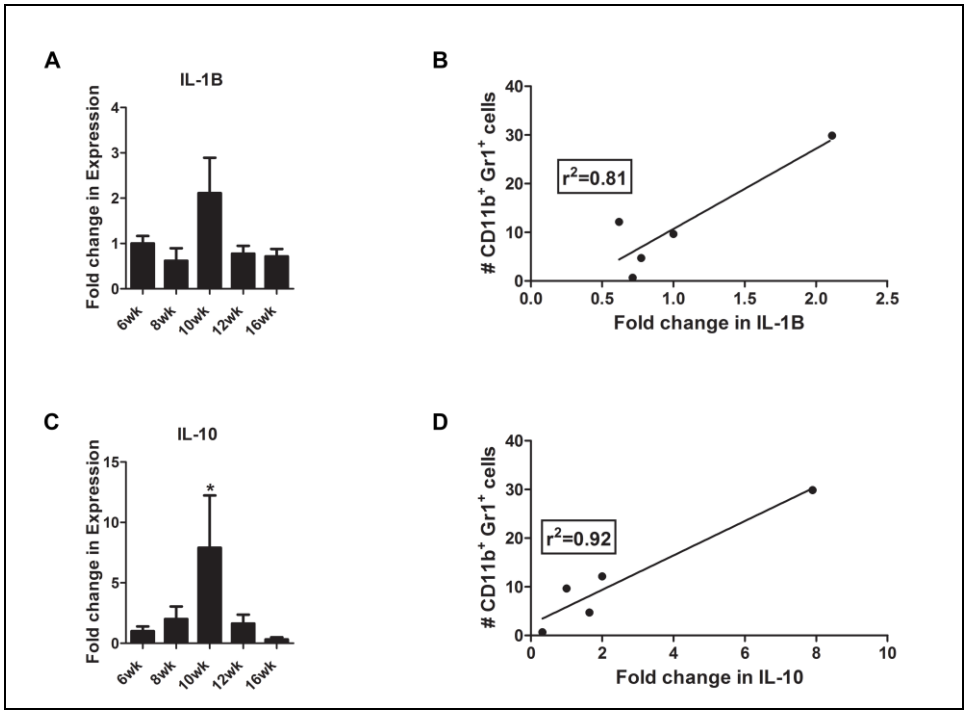

Figure 2.11. Cytokine levels correlate with MDSC infiltration during the course of tumor progression in the MMTV-PyMT model. Cytokine levels, IL-1β (A) and IL-10 (C), were analyzed by quantitative PCR from tumor samples at various time points. Linear regression analysis was used to determine the correlation between IL-1β (B) or IL-10 (D) and MDSC infiltration. A minimum of 3 tumors/group were used for analysis, which was performed in triplicate. *p=0.05, Mann-Whitney test.

*2.2.6 Tumor cytokine profile changes are induced by anti-VEGF therapy***.**

To address some of the differences we found in immune cell infiltration with anti-VEGF therapy, we analyzed intra-tumoral cytokine levels in tumor lysates from the various treatment groups in the MDA-MB-231 and 4T1 models (Tables 2.3 & 2.4).

Cytokine	Week	Control	r84	bev	MF1	RAFL-2	GU81	sunitinib
IL1β	1	1.877	1.887	**4.987**	0.898	3.417	2.46	1.577
IL1β	4	2.195	2.044	3.56	1.633	0.8987	**14.12**	1.876
IL10	1	0.213	0.282	0.888	0	**1.944**	1.672	1.422
IL10	4	3.124	**1.011**	3.967	2.099	1.415	1.438	**1.064**
IL12	1	167.8	153	220.2	95.49	**301.7**	219.1	145.4
IL12	4	277.6	233.3	245.1	139.1	88.2	270.2	189.9
IL2	1	n.d.	n.d.	n.d.	n.d.	n.d.	n.d.	n.d.
IL2	4	0.277	n.d.	0.329	n.d.	n.d.	n.d.	n.d.
IL4	1	n.d.	n.d.	n.d.	n.d.	n.d.	n.d.	n.d.
IL4	4	n.d.	n.d.	n.d.	n.d.	n.d.	n.d.	n.d.
IL5	1	n.d.	n.d.	0.125	n.d.	**0.379**	0.265	0.193
IL5	4	0.478	0.18	0.477	0.251	0.152	0.259	0.213
CXCL1	1	10.51	9.62	31.6	**6.865**	10.25	12.81	10.76
CXCL1	4	30.96	33.78	32.77	36.48	**12.69**	44.05	56.86
IFNγ	1	n.d.	n.d.	n.d.	n.d.	n.d.	n.d.	n.d.
IFNγ	4	0.435	0.181	0.291	0.111	**n.d.**	0.082	**0.055**
TNFα	1	n.d.	n.d.	n.d.	n.d.	n.d.	n.d.	n.d.
TNFα	4	n.d.	n.d.	n.d.	n.d.	n.d.	n.d.	n.d.
Total MMP-9		142.6	175.5	204.2	115	**90.9**	162.5	99.02
active MMP-9		89.15	109.4	111	66.95	**48.07**	85.61	63.79

Table 2.3. Anti-VEGF therapy modulates intra-tumoral cytokine levels in MDA-MB-231 human breast tumor xenografts. Mean pg/mg total protein is displayed. N=3 tumors/group assayed in duplicate at the one and four week time points. Values in red indicate cytokine levels that decreased significantly compared to control; values in blue indicate cytokine levels that increased significantly compared to control, all $p<0.01$ or $p<0.001$ by one-way ANOVA, Bonferroni Multiple Comparison Test. n.d., not detected. **Adopted from (Roland et al. 2009)**.

Cytokine	Week	Control	mcr84	GU81	sunitinib
IL1β	1	52.16	37.82	21.16	27.88
IL1β	3	41.69	**102.9**	64.31	79.41
IL10	1	11.67	8.544	**7.481**	7.096
IL10	3	6.268	7.547	3.961	8.011
IL12	1	422.4	527.1	198.8	286.6
IL12	3	191.8	545	**816.7**	172.4
IL2	1	2.209	1.77	1.473	1.572
IL2	3	1.581	1.555	1.771	1.748
IL4	1	1.696	1.38	**1.161**	1.085
IL4	3	1.147	1.159	0.8129	1.365
IL5	1	1.189	1.031	0.9213	0.8637
IL5	3	1.239	1.183	1.175	1.222
IL6	1	31.19	**12.74**	10.4	13.69
IL6	3	8.92	**20.69**	8.84	10.1
CXCL1	1	209.7	119	**78.14**	134.2
CXCL1	3	137.4	**395.5**	286.4	323.2
IFNγ	1	2.363	1.57	**1.02**	1.426
IFNγ	3	2.205	1.625	0.9552	1.24
TNFα	1	6.77	6.003	4.917	5.634
TNFα	3	5.519	4.54	5.376	5.486
Active TGFβ	1	250.6	268.8	312.6	233.6
Active TGFβ	3	252.5	312.3	175.9	133.4
serum IL6	3	8.844	**35.22**	32.04	52.60

Table 2.4. Anti-VEGF therapy modulates intra-tumoral and serum cytokine levels in 4T1 murine breast tumor xenografts. Mean pg/mg total protein if displayed. N=3 tumors/group assayed in duplicate at the one and three week time points. Values in red indicate cytokine levels that decreased significantly compared to control; values in blue indicate cytokine levels that increased significantly compared to control, all $p<0.01$ or $p<0.001$ by one-way ANOVA, Bonferroni Multiple Comparison Test. n.d., not detected. **Adopted from (Roland et al. 2009)**.

MDSC accumulation is driven by many factors, including VEGF and IL-1β (Bunt et al. 2006; Bunt et al. 2007; Huang et al. 2007). Given that there were differences in MDSC infiltration following different anti-VEGF therapies, we hypothesized that this may be due to aberrations in intra-tumoral IL-1β levels. In the MDA-MB-231 model, we found that inhibition of both VEGFR1 and VEGFR2 activation either via blocking ligand binding (bevacizumab) or receptor activation (GU81) resulted in significant increases in MDSC infiltration (Figure 2.4 (C)). In this model, intra-tumoral IL-1β levels were increased significantly following one week of bevacizumab therapy and four weeks of GU81 therapy (Table 2.3; Figure 2.12 (A)). By linear regression analysis, we found that changes in IL-1β levels as a result of anti-VEGF therapy were highly correlative with changes in MDSC infiltration at the one and four week time points (Figure 2.12 (B)).

In the 4T1 model tumors from mcr84-treated animals had increased levels of IL-1β after three weeks of therapy (Figure 2.12 (C)). Furthermore, following one week of therapy we found a trend in which increases in IL-1β correlated positively with MDSC infiltration (Table 2.4). However, after chronic anti-VEGF therapy (three week time point), increases in intra-tumoral IL-1β levels correlated negatively with changes in intra-tumoral MDSCs (Figure 2.12 (D); Table 2.4). These results suggest that IL-1β has a bi-modal effect on MDSC migration such that IL-1β concentrations $\leq$ 5 pg/mg or $\geq$ 50 pg/mg result in reduced recruitment

of MDSCs. We also evaluated intra-tumoral levels of IL-6, a downstream effector of IL-1β previously show to be important for MDSC infiltration (Bunt et al. 2006; Bunt et al. 2007), and found that levels of this cytokine did not correlate with MDSC number after 3 weeks of therapy (Table 2.4). This indicates that IL-6 is not the downstream mediator of IL-1β-mediated MDSC infiltration in the 4T1 breast cancer model, and suggests that another downstream target of IL-1β may modulate MDSC infiltration in this model.

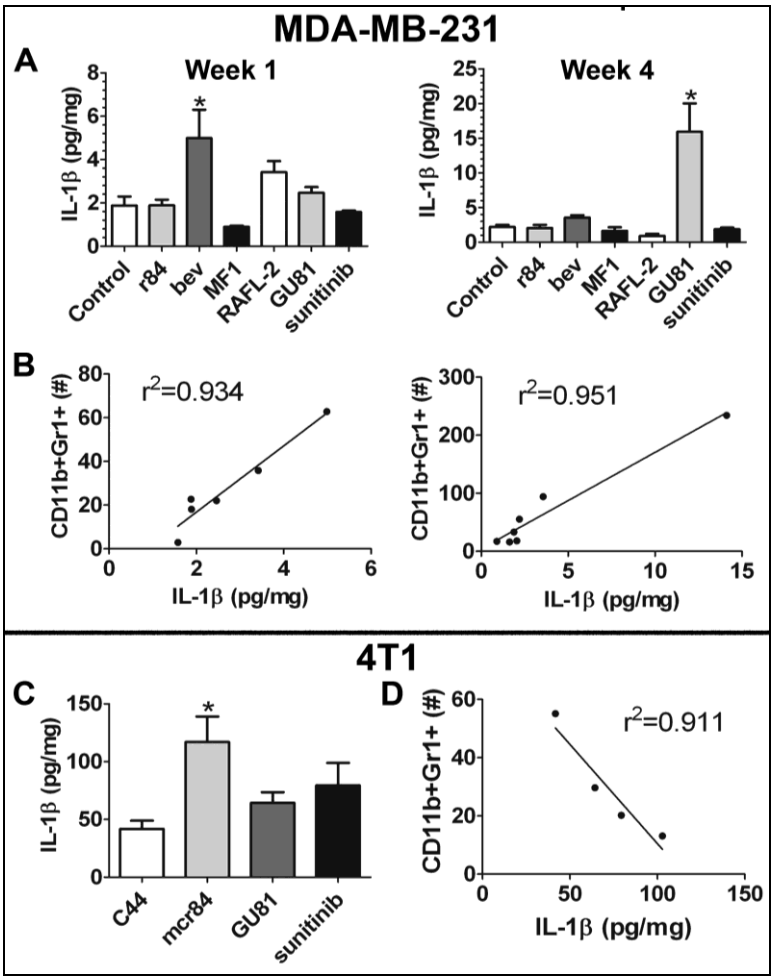

Figure 2.12. Changes in intra-tumoral IL-1β levels following anti-VEGF therapy correlate with intra-tumoral MDSCs. (A) MDA-MB-231 intra-tumoral IL-1β levels after one and four weeks of anti-VEGF therapy were determined by electrochemiluminescence. (B) By linear regression analysis, changes in MDA-MB-231 intra-tumoral IL-1β levels following anti-VEGF therapy positively correlate with intra-tumoral $CD11b^{+}Gr1^{+}$ (MDSCs) after one and four weeks of therapy. Each dot represents the mean IL-1β and MDSC for each treatment group. (C) 4T1 intra-tumoral IL-1β levels after three weeks of anti-VEGF therapy were determined by electrochemiluminescence. (D) By linear regression analysis, changes in 4T1 intra-tumoral IL-1β levels following anti-VEGF therapy negatively correlate with intra-tumoral $CD11b^{+}Gr1^{+}$ (MDSCs) after three weeks of therapy. Each dot represents the mean IL-1β and MDSC for each treatment group. *p=0.05

CXCL1 (KC, GRO) is expressed by macrophages, neutrophils, endothelial cells and has neutrophil chemoattractant activity (Armstrong et al. 2004). IL-1β can induce CXCL1 expression via a different mechanism than IL-6 (Tsakiri et al. 2008). In 4T1 tumors, we found that changes in CXCL1 levels were correlative with changes in IL-1β after one and three weeks of anti-VEGF therapy (Table 2.4, Table 2.5). Furthermore, changes in CXCL1 levels with anti-VEGF therapy negatively correlated with changes in MDSC infiltration at both time points (Figure 2.13 (A); Table 2.5), suggesting an alternative mechanism for MDSC recruitment in the presence of anti-VEGF therapy and increased levels of IL-1β.

Previously, we have shown that mice treated with r84 have no detectable level of free VEGF in serum (Roland et al. 2009). Therefore, we sought to investigate an alternative mechanism for the increased vascular area seen in 4T1 tumor-bearing animals treated chronically with mcr84 (Figure 2.5 (D)). Though VEGF is the primary stimulant for tumor angiogenesis, IL-1β can also stimulate *in vitro* endothelial cell migration and proliferation (Mantovani et al. 1992) and angiogenesis in mouse models of cancer via up regulation of VEGFR2 (Maruyama et al. 1999; Nakao et al. 2005). Tumors treated with mcr84 had a three-fold increase in VEGFR2 expression compared to control-treated tumors (data not shown). Furthermore, we found by linear regression analysis, that increases in vascular area seen with anti-VEGF therapy correlated with changes in

IL-1β and IL-6 (Figure 2.13 (B&C); Table 2.5), suggesting an alternative pathway for angiogenesis in the presence of anti-VEGF therapy.

	Week 1							**Week 3**					
r^2	IL-1β	IL-6	CXCL1	TNF-α	IFN-γ	IL-2	**r^2**	IL-1β	IL-6	CXCL1	TNF-α	IFN-γ	IL-2
IL-6	**0.825**						IL-6	**0.818**					
CXCL1	**0.834**	**0.952**					CXCL1	**0.945**					
TNF-α	**0.967**	**0.804**	**0.882**				TNF-α	**0.668**	**0.964**				
IFN-γ	**0.959**	**0.934**	**0.953**	**0.961**			IFN-γ						
IL-2	**0.978**	**0.899**	**0.858**	**0.916**	**0.966**		IL-2						
IL-4	**0.901**	0.75	0.647	0.767	**0.819**	**0.936**	IL-4						
IL-10	**0.884**	**0.865**	0.743	0.763	**0.866**	**0.955**	IL-10						
MDSC	0.741	**0.937**	**0.793**		**0.818**	**0.858**	MDSC	**0.911**	0.418	**0.986**			
Treg	**0.964**	0.671	0.725	**0.956**	**0.878**	**0.891**	Treg				0.138	**0.831**	0.305
Vascular area							**Vascular Area**	**0.845**	**0.894**	0.642			

Table 2.5. Changes in 4T1 intra-tumoral cytokine levels with anti-VEGF therapy correlate with changes in immune cell infiltration. Data are displayed as r^2 as determined by Pearson correlation test; $p<0.075$ for all bolded values. Values in red indicate significant negative correlation; values in blue indicate a significant positive correlation. For example, as graphically displayed in Figure 5D, as IL-1β levels increase following three weeks of anti-VEGF therapy (week 3, column1) MDSCs infiltration decreases (row 8; $r^2=0.911$). **Adopted from (Roland et al. 2009).**

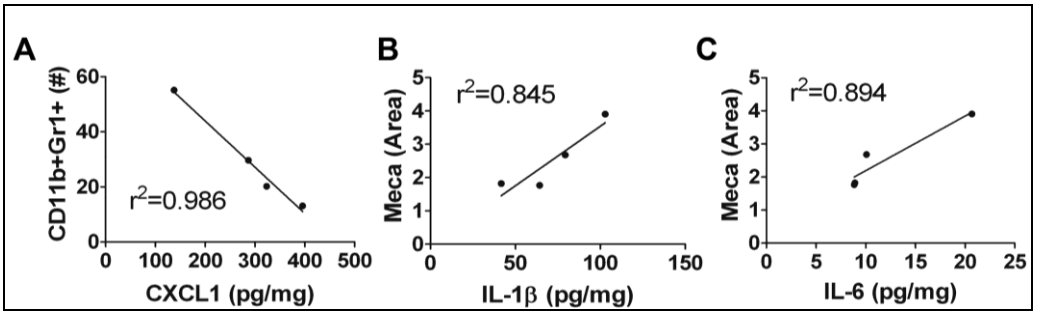

Figure 2.13. CXCL1, IL-1β, and IL-6 are differentially related to MDSC infiltration and vascular area in 4T1 tumors following anti-VEGF therapy. (A-C) Intra-tumoral IL-1β, CXCL1 and IL-6 were determined by electrochemiluminescence and ELISA. (A) Changes in intra-tumoral CXCL1 levels following anti-VEGF therapy negatively correlate with intra-tumoral $CD11b^{+}Gr1^{+}$ (MDSCs) after three weeks of therapy. (B-C) Changes in intra-tumoral IL-1β (B) and IL-6 (C) positively correlate with vascular area after chronic anti-VEGF therapy. Each dot represents the mean cytokine level for each treatment group. N=4/grp, assayed in duplicate. **Adopted from (Roland et al. 2009)**.

The development, recruitment, and activation of Tregs in the tumor microenvironment are not completely understood. Though TGF-β can induce peripheral Treg, it is not required for the generation of a thymic-derived subset of these cells. Recently, IL-2, IFN-γ and TNF-α have been implicated in Treg generation (Chen et al. 2007; Zheng et al. 2007; Feng et al. 2008). In this study we found that only IFN-γ levels correlated with Treg infiltration during both acute and chronic therapy, indicating IFN-γ may direct the development or migration of Treg in the face of anti-VEGF therapy (Table 2.5).

Recent evidence indicates that Treg infiltration may be mediated by myeloid cells in the tumor microenvironment, whereby myeloid cell depletion can reduce Treg homing to tumors (Qin 2009). Furthermore, macrophages are the key

cell type responsible for Treg expansion in certain immunosuppressive settings (Perruche et al. 2008). Re-examination and analysis of our previous data revealed that macrophage infiltration correlated with Treg accumulation in the PyMT-MMTV (r^2 = 0.99) and 4T1 (r^2 = 0.86) models following anti-VEGF therapy (Figure 2.14 (A&B)). Furthermore, MDSC number correlated with Treg accumulation in 4T1 (r^2 = 0.743) but not MMTV-PyMT tumors (r^2 = 0.43) (Figure 2.14 C&D)).

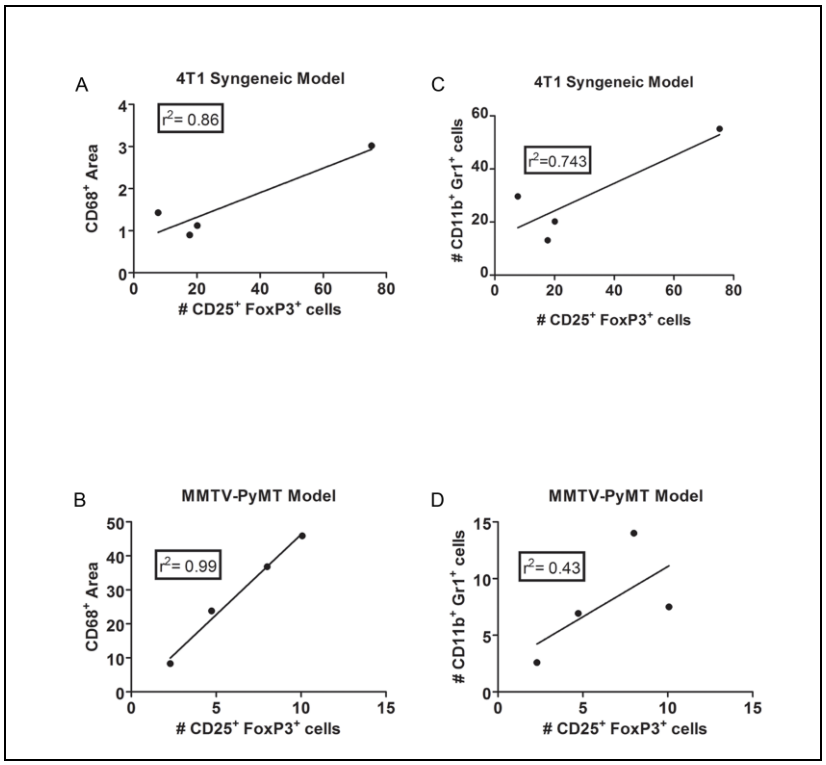

Figure 2.14. Macrophage infiltration correlates with the accumulation of CD25$^+$ FoxP3$^+$ regulatory T-cells in two pre-clinical models of breast cancer following anti-VEGF therapy. Mice in each experiment received therapy with either control antibody (C44), mouse-chimeric r84 (inhibits the VEGF: VEGFR2 interaction), sunitinib (inhibits VEGFR1, VEGFR2 PDGFRβ, c-kit), or GU81 (inhibits VEGFR1 and VEGFR2). (A, B) By linear regression analysis, changes intra-tumoral T_{reg} number following anti-VEGF therapy positively correlate with CD68$^+$ macrophage levels after four weeks of therapy in the 4T1 syngeneic (A) and MMTV-PyMT transgenic breast cancer models (B). Each dot represents the mean for CD68$^+$ area and the number of T_{regs} in each treatment group. (C, D) By linear regression analysis, changes in intra-tumor T_{reg} number positively correlate with the number of CD11b+ Gr1+ MDSCs following four weeks of therapy in the 4T1 syngenic (C) but not the MMTV-PyMT transgenic (D) breast cancer model. Each dot represents the mean for the number of MDSCs and T_{regs} in each treatment group. **Adopted from (Lynn 2010)**.

2.2.7 Identification of potential biomarkers of response to anti-VEGF therapy

Given the changes we observed in inflammatory cytokines in response to various anti-angiogenesis strategies, we sought to investigate whether changes in

serum levels of these cytokines would correlate with tumor progression. High levels of serum IL-1β and IL-6 levels correlated with delayed tumor progression in animals bearing 4T1 tumors treated with mcr84 and GU81, whereas low levels of these cytokines corresponded to tumor progression (Figure 2.15 (A-C)). However, low levels of IL-6 in the sera of sunitinib-treated animals correlated with tumor progression (Figure 2.15 (D)). These findings highlight the importance of the inflammatory cytokine profile in tumor progression and identify possible biomarkers of response to r84 or other anti-VEGF agents in breast cancer.

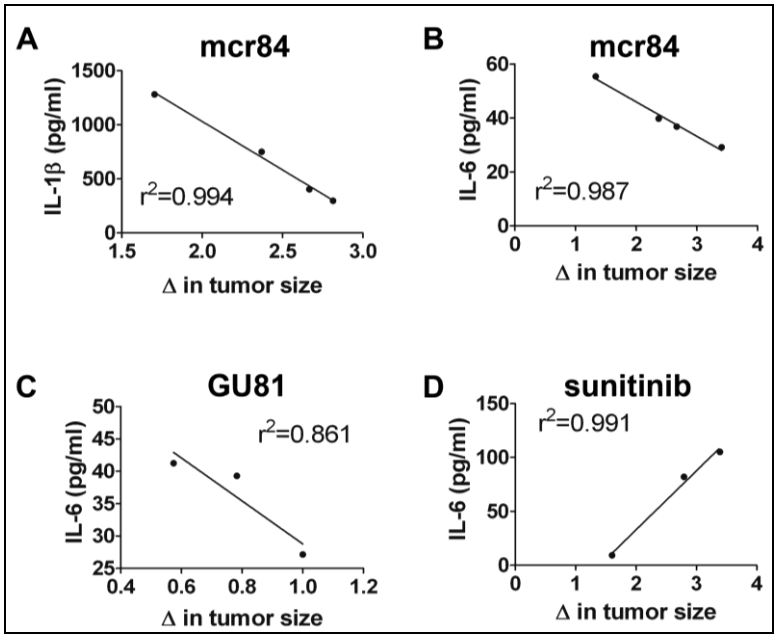

Figure 2.15. Identification of potential biomarkers of response. Serum levels of IL-1β and IL-6 were determined by electrochemiluminescence and ELISA, respectively from animals treated with anti-VEGF therapy bearing 4T1 tumors. Change (Δ) in tumor size was calculated as week three tumor weight/mean week one tumor weight for each individual therapy group. (A-C) By linear regression analysis, changes in serum levels of IL-1β (A) and IL-6 (B,C) negatively correlate with Δ in tumor size for animals treated with mcr84 and GU81. (D) Changes in IL-6 levels with sunitinib therapy positively correlate with Δ in tumor size. **Adopted from (Roland et al. 2009)**.

2.3 Discussion

In this report, we provide data that demonstrate the effectiveness of anti-VEGF therapy as a modulator of immune cell infiltration, and intra-tumoral and serum cytokine levels in multiple preclinical models of breast cancer. It is becoming increasingly clear that the effect of anti-VEGF agents extends beyond the inhibition of angiogenesis, as many immune cells express VEGFRs, including macrophages, neutrophils, MDSCs, DCs and T-cells (Dikov et al. 2005; Huang et al. 2007; Murdoch et al. 2008) (Folkman 1995; Folkman 2007). We and others have shown a reduction in macrophages in tumors from animals treated with anti-VEGF therapy (Salnikov et al. 2006; Dineen et al. 2008; Roland et al. 2009). In preclinical models of colon cancer, sunitinib treatment reduced the accumulation of MDSCs and plasmacytoid dendritic cells in tumors compared to control treatment (Ozao-Choy et al. 2009). In metastatic renal cell carcinoma patients, sunitinib therapy reduced the level of circulating MDSCs and reduction in MDSCs in response to sunitinib therapy correlated with an increase in T-cell IFN-γ production (Ko et al. 2009). These studies suggest that sunitinib or other anti-VEGF therapies function as modulators of antitumor immunity. Here, we demonstrate that inhibition of VEGF binding to VEGFR2 with r84 is more effective than other anti-VEGF strategies in controlling breast tumor growth and the infiltration of immune suppressor cells.

Using the MDA-MB-231 human breast cancer model, we demonstrate that inhibition of VEGF binding to VEGFRs with bevacizumab or r84 effectively controls tumor growth (Figure 2.1 (A)). Furthermore, only selective inhibition of VEGF binding to VEGFR2 with r84 is able to prevent an increase in MVD from week 1 to week 4 of therapy (Figure 2.1 (B)). Therapy with r84 and bevacizumab is able to control tumor burden in this model by modulating the cells of the tumor microenvironment, as neither VEGF nor any of the anti-VEGF agents tested were able to modulate tumor cell proliferation *in vitro* (data not shown). In contrast anti-VEGF therapy may regulate tumor cell migration in this model (Figure 2.2 (A)). Similar to the MDA-MB-231 model, we found that mcr84 controlled tumor growth in the MMTV-PyMT model after four weeks of therapy (Figure 2.8 (A)). Tumors from mcr84-treated animals also had a decreased vascular area (Figure 2.8 (B)). Interestingly, when these experiments were repeated using the immunocompetent 4T1 inflammatory breast cancer model, mcr84 and the VEGFR1 & VEGFR2 binding peptoid, GU81, were able to control tumor growth (Figure 2.5 (A&B). Though mcr84 was able to reduce MVD as seen in the MDA-MB-231 model, 4T1 tumors from animals treated with chronic mcr84 had an increased vascular area compared to controls (Figure 2.5 C&D). In an effort to explain this increase in vascular area, we evaluated intra-tumoral cytokine levels in animals from all treatment groups at the one and three week time points (Table 2.4). Though hypoxia and VEGF are the main angiogenic stimuli, other cytokines,

including IL-1β, IL-6 and TNF-α can induce angiogenesis (Aoki et al. 1999; Maruyama et al. 1999; Amano et al. 2004; Nakao et al. 2005). For example, in cardiac myocytes IL-1β increases VEGFR2 expression (Maruyama et al. 1999). In mcr84-treated tumors, we found increased levels of IL-1β and VEGFR2 compared to control-treated tumors (Figure 2.12 (C),data not shown). By linear regression analysis, increases in intra-tumoral IL-1β following anti-VEGF therapy correlated with increased vascular area (Figure 2.13 (B)). VEGFR2 is the main receptor responsible for VEGF-induced angiogenesis and is activated by VEGF-A, C, or D (Achen et al. 1998; Cao et al. 1998). It is plausible that VEGF-C/D may bind to increased levels of VEGFR2, resulting in increased VEGFR2 signaling. Increased VEGFR2 signaling can then promote the increased vascular area observed in mcr84- treated tumors.

The effects of anti-VEGF therapy extend beyond its effects on tumor blood vessels. In both the MDA-MB-231 and 4T1 models, chronic anti-VEGF therapy reduced macrophage infiltration in all treatment groups. In contrast, only mcr84 was able to reduce macrophage infiltration in the MMTV-PyMT model, where both GU81 and sunitinib increased macrophage infiltration (Figure 2.8 (C)). In non-tumor bearing animals, monocyte and macrophage migration is driven in part by placental growth factor (PlGF), VEGF and VEGFR1 (Clauss et al. 1996). However, we have previously shown that VEGFR2 is expressed on macrophages from tumor-bearing animals, and is the dominant receptor driving

VEGF-induced macrophage chemotaxis in those animals (Figure 2.3) (Dineen et al. 2008; Roland et al. 2009). Therefore, the reduction in macrophage migration seen following anti-VEGF therapy is likely due to the inhibition of VEGFR2 signaling (Figure 2.4 (A); Figure 2.7 (A); Figure 2.8 (C)). However, as MF1 is the only agent used that does not inhibit VEGFR2 activation, the reduction in macrophage infiltration seen in these tumors is likely due to decreased PlGF signaling through VEGFR1, as this is known to be important to monocyte migration (Clauss et al. 1996). Interestingly, the inhibition of both VEGFR1 and VEGFR2 activation with bevacizumab, GU81, or sunitinib did not reduce macrophage infiltration better than agents that inhibited the activation of a single VEGFR alone (r84, MF1, or RAFL-2). Macrophage infiltration (as measured by CD68 expression) does not seem to be regulated during the course of tumor progression (Figure 2.10 (B)), however, macrophage phenotype is regulated as tumors progress (discussed extensively in Chapter Three).

Neutrophils are often described as 'first responders' and are capable of mediating the angiogenic switch in engineered animal models of cancer (Salnikov et al. 2006; Pahler et al. 2008). In contrast to these data, neutrophil infiltration is not regulated during the course of tumor progression in the MMTV-PyMT transgenic breast cancer model (Figure 2.10 (C)). The mechanism underlying the increase in neutrophils after anti-VEGF therapy is unclear. VEGF can stimulate neutrophil migration *in vitro* via VEGFR1 activation (Ancelin et al. 2004).

Furthermore, these cells were shown to express VEGFR1 and VEGFR2 by RT-PCR, suggesting that even though VEGFR2 is present, VEGFR1 is the primary receptor mediating VEGF-induced migration of these cells. In support of this, we have previously shown an increase in neutrophil infiltration in r84-treated tumors (Roland et al. 2009). In this study, we have further characterized the effect of anti-VEGF therapy on neutrophil infiltration utilizing an immunocompetent model of breast cancer. In the 4T1 model, tumors from animals treated with agents that block VEGFR1 activation (GU81 and sunitinib) had reduced neutrophil infiltration compared to control-treated tumors. In contrast, tumors from animals treated with mcr84, where VEGFR1 signaling was intact, had an increase in neutrophil infiltration (Figure 2.7 (B)), suggesting that VEGFR1 is the dominant receptor involved in VEGF-mediated neutrophil migration in tumor-bearing animals. Neutrophil infiltration was also increased following treatment with mcr84 but not GU81 or sunitinib in the MMTV-PyMT breast cancer model (Figure 2.8(D)). It is important to note, that the differentiation of MDSCs into neutrophils following VEGFR2-specific therapy may also contribute to neutrophil accumulation in this model. Alternatively, recent evidence indicates that macrophages can reduce neutrophil infiltration by inhibiting CXCL8-dependent chemotaxis (Pahler et al. 2008). Therefore, macrophage numbers often correlate inversely with neutrophil levels. We have found that in general anti-VEGF strategies reduce macrophage infiltration; however only selective inhibition of

VEGF-activation of VEGFR2 by receptor specific agents resulted in marked accumulation of neutrophils (Pahler et al. 2008; Roland et al. 2009). Interestingly, neutrophil numbers in the blood are an independent prognostic indicator of response to anti-VEGF therapy in patients with renal cell carcinoma, whereby increased neutrophil number correlates with a decreased overall survival following anti-VEGF therapy (Heng et al. 2009).

VEGF is a key mediator in the development and maturation of dendritic cells (Huang et al. 2007). Activation of VEGFR1 on dendritic cells inhibits hematopoetic stem cell differentiation along the dendritic cell lineage, whereas VEGFR2 is important for dendritic cell maturation (Huang et al. 2007). Previously, using the MDA-MB-231 model, we found an increase in mature dendritic cells in animals treated with r84, but not bevacizumab (Roland et al. 2009). In this study, we demonstrate that this effect is seen after only one week of therapy, as inhibition of VEGF binding to VEGFR2 with mcr84 reduced the number of total dendritic cells, while increasing the mature fraction of these cells (Figure 2.7 (E)). Though the antigen presenting ability of these cells is not known, in human breast cancer specimens, increased CD83+ dendritic cells is associated with an improved prognosis (Iwamoto et al. 2003).

The role of VEGF MSDC differentiation and migration has been characterized in recent years (Gabrilovich et al. 2001; Gabrilovich and Nagaraj

2009). In mouse models and patients with cancer, these immunosuppressive cells are increased in the blood, spleen and tumors (Gabrilovich and Nagaraj 2009; Ko et al. 2009; Ozao-Choy et al. 2009). Many factors induce MDSC expansion and activation, including VEGF, IL-1β, and IL-6, making these attractive targets for MDSC inhibition. In this study, we reveal an interesting connection between these cytokines in mediating MDSC infiltration into tumors. MDSC infiltration is highly correlative with IL-1β and IL-10 levels in the MMTV-PyMT model during the course of tumor progression (Figure 2.11). In MDA-MB-231 tumors, treatment with anti-VEGF agents that block both VEGFR1 and VEGFR2 (bevacizumab and GU81), but not other receptor tyrosine kinases resulted in increased intra-tumoral IL-1β levels and MDSC accumulation (Figure 2.4 (C), Figure 2.12 (A)). It is interesting to note that sunitinib, which also blocks both VEGFR1 and VEGFR2 signaling, does not result in increased IL-1β and MDSC accumulation. This is likely due to the fact that sunitinib also blocks PDGFRβ, GSF-1R, Flt-3, and cKit, any of which may be important for increased expression of IL-1β. Furthermore, changes in IL-1β levels in response to anti-VEGF therapy were highly correlative with changes in MDSC infiltration at the one and four week time-points (Figure 2.12 (B)), indicating that IL-1β is a key cytokine mediating the infiltration of MDSCs following anti-VEGF therapy. Interestingly, in the 4T1 immunocompetent model of breast cancer, changes in intra-tumoral IL-1β levels correlate negatively with changes in MDSC infiltration after three weeks

of therapy (Figure 2.12 (D), Table 2.5), where increases in IL-1β following treatment with mcr84 were associated with reduced MDSC infiltration. These findings indicate a possible bimodal role of IL-1β in MDSC infiltration, where a low level of IL-1β induces MDSC infiltration and increased levels following anti-VEGF therapy inhibit MDSC infiltration. Interestingly, mcr84 was also able to reduce MDSC infiltration in the MMTV-PyMT model but in contrast to other models, sunitinib increased MDSCs. Unfortunately IL-1β levels were not examined in this model, making the interpretation of these results difficult.

MDSCs do not express receptors for IL-1β; however, they do express receptors for IL-6, which is capable of inducing MDSC infiltration in the absence of IL-1β signaling (Bunt et al. 2007). Therefore, we investigated other cytokines that may be involved in regulating immune cell recruitment. Similar to IL-1β, tumors from animals treated chronically with mcr84 had increased IL-6 and CXCL1 levels. However, only changes in CXCL1, not IL-6, correlated negatively with changes in MDSC infiltration, as seen with IL-1β (Figure 2.13 (A), Table 2.5). Therefore, we propose that CXCL1 is an inhibitor of MDSC infiltration subsequent to markedly increased IL-1β levels following anti-VEGF therapy.

Treg are immune suppressor cells that maintain peripheral tolerance (Linehan and Goedegebuure 2005). Like MDSCs, these cells are increased in the blood and tumors of cancer patients and mouse models of cancer (Linehan and

Goedegebuure 2005). The generation of Tregs is a complicated process that involves many cytokines, such as IL-2, TGF-β, IFN-γ and TNF-α (Chen et al. 2007; Zheng et al. 2007; Feng et al. 2008). Tregs accumulate during the early carcinoma stage of tumor progression in the MMTV-PyMT transgenic breast cancer model (Figure 2.10 (E)). Though acute anti-VEGF therapy did not affect Treg infiltration, we found reduced levels of Treg after chronic anti-VEGF therapy in all treatment groups in the 4T1 model (Figure 2.7 (C)). In contrast, Tregs were reduced following treatment with mcr84 but increased following chronic GU81 or sunitinib therapy in the MMTV-PyMT model (Figure 2.8 (F)). Furthermore, only changes in intra-tumoral IFN-γ levels correlated with changes in Treg infiltration, further confirming its importance in Treg infiltration/generation (Table 2.5). Recent evidence indicates that Treg infiltration may be mediated by myeloid cells in the tumor microenvironment, whereby myeloid cell depletion can reduce Treg homing to tumors (Qin 2009). Furthermore, macrophages are the key cell type responsible for Treg expansion in certain immunosuppressive settings (Perruche et al. 2008). In this study, we found that macrophage infiltration does correlate with Treg accumulation in the PyMT-MMTV and 4T1 models following anti-VEGF therapy (Figure 2.14 (A&B)). Furthermore, MDSC number correlates with Treg accumulation in 4T1 but not MMTV-PyMT tumors (Figure 2.14 C&D)), leading us to hypothesize that

macrophages may be the primary mediators of Treg infiltration in immunocompetent mouse models of breast cancer.

Finally, having demonstrated changes in intra-tumoral cytokine levels and immune cell infiltration with anti-VEGF therapy, we looked at serum levels of IL-β and IL-6, as potential biomarkers of response to anti-VEGF therapy. For animals treated with mcr84 or GU81, we found that decreases in serum levels of IL-1β and IL-6 were highly correlative with changes in tumor size in the presence of anti-VEGF therapy (Figure 2.15 (A-C)). Interestingly, increases in serum IL-6 levels in sunitinib-treated animals correlated with increases in tumor size, suggesting different mechanisms for the cytokine aberrations seen between selective versus broad spectrum anti-VEGF strategies (Figure 2.15 (D)).

In conclusion, we have demonstrated differences in the ability of anti-VEGF therapy to affect tumor vasculature and modulate immune cell infiltration, intra-tumoral and serum cytokine levels depending on the mechanism of VEGF inhibition. We have demonstrated that selective inhibition of VEGF binding to VEGFR2 with r84 is effective at controlling tumor growth, inhibiting the infiltration of suppressive immune cells (MDSC, Treg, macrophages) while increasing the mature fraction of dendritic cell infiltrates. Furthermore, we have identified two possible biomarkers (IL-1β and IL-6) for assessing the efficacy of anti-VEGF therapy in breast cancer patients.

CHAPTER THREE

THE PLEIOTROPHIN-ALK SIGNALING AXIS PROMOTES AN ANTI-INFLAMMATORY MACROPHAGE PHENOTYPE IN MOUSE MODELS OF BREAST CANCER

3.1 Introduction

The concept surrounding the development of anti-VEGF of therapy was based upon the fact that VEGF functions as an endothelial cell proliferation, migration, and survival factor (Ferrara and Henzel 1989; Alon et al. 1995; Gerber et al. 1998). It was thought that by blocking VEGF activation of endothelial cells in the tumor microenvironment, which are genetically stable and accessible, the vascular network supplying the tumor would be damaged severely resulting in dramatically reduced delivery of oxygen and nutrients to tumor cells. However, the modest clinically efficacy of anti-VEGF strategies has revealed that there is much left to understand. At best we are able to improve overall survival but patients are not cured using anti-VEGF therapy either alone or in combination

with chemotherapy (Hurwitz et al. 2004; Sandler et al. 2006; Norden et al. 2008; Rini et al. 2008; Friedman et al. 2009; Miles et al. 2010; Robert et al. 2011).

The majority of human mammary tumors are innately resistant or will acquire resistance to anti-VEGF therapy (Ellis and Hicklin 2008), suggesting that these tumors may activate alternate angiogenesis pathways. The alternate angiogenic growth factors fibroblast growth factor (FGF 1 and 2), ephrin A1 and 2, angiopoietin (Ang-1 and 2), placental growth factor (PlGF), and stromal cell-derived factor 1 alpha (SDF-1α) have been implicated in resistance to anti-VEGF therapy (reviewed in (Grepin and Pages 2010)). Furthermore, many of these growth factors affect immune cell infiltration and function in the tumor microenvironment (Kitayama et al. 1994; Berardi et al. 1995; Zhao et al. 1995; Byrd et al. 1999; Ribatti et al. 1999; Takagi et al. 2000; Selvaraj et al. 2003; Burger and Kipps 2006; Lewis et al. 2007; Lewis and Hughes 2007; Lin et al. 2007; Nakayama et al. 2007; Schulz et al. 2009). It is important to note that the VEGFRs are expressed on endothelial cells, tumor cells, and many host immune cells. Therefore, to better understand the effects of anti-VEGF therapy it is important to consider the effects of VEGF on all cells in the tumor microenvironment.

Inflammatory cells comprise a major portion of the overall tumor mass and of these, macrophages represent an abundant and important cell type (Pollard

2004). In fact, macrophages regulate the angiogenic switch in MMTV-PyMT tumors (Lin et al. 2006). VEGF stimulates macrophage chemotaxis (Sawano et al. 2001) into the tumor microenvironment, and we and others have shown that anti-VEGF therapy can reduce macrophage infiltration in pre-clinical tumor models (Salnikov et al. 2006; Whitehurst et al. 2007; Dineen et al. 2008; Roland et al. 2009; Roland et al. 2009). We found that macrophages harvested from tumor-bearing animals express VEGFR1 and VEGFR2, whereas those harvested from non-tumor bearing mice are $VEGFR1^{+}$ but deficient in VEGFR2. Furthermore, when VEGFR2 is expressed, it becomes the dominant receptor driving VEGF-induced chemotaxis. Additionally, we found that specific blockade of VEGF:VEGFR2 interaction is sufficient to inhibit macrophage chemotaxis (Dineen et al. 2008; Roland et al. 2009). Interestingly, analysis of human peripheral blood from cancer patients and healthy volunteers revealed a population of $VEGFR2^{+}/CD45^{bright}/CD14^{+}$ monocytes; this population was significantly more prominent in blood from cancer patients compared to that of healthy volunteers, confirming our pre-clinical findings (Vroling et al. 2007).

There are two general classes or phenotypes of macrophages in the tumor microenvironment: pro-inflammatory and anti-inflammatory, both which can be grouped into numerous subclasses. Pro-inflammatory macrophages are stimulated by interferon γ (IFN γ) and microbial products (LPS) and have an increased ability to endocytose and destroy pathogens (Ezekowitz and Gordon 1984; Adams 1989;

Mosser and Handman 1992). Recent publications also suggest the Notch pathway as a critical mediator in the pro-inflammatory activation of macrophages (Outtz et al. 2010; Wang et al. 2010). In fact, macrophages deficient for the Notch pathway regulated transcription factor RBP-J display an anti-inflammatory cytokine profile despite stimulation with pro-inflammatory activators (IFNγ and LPS) (Wang et al. 2010). Pro-inflammatory macrophages are potent effector cells that produce inflammatory cytokines (IL-6, IL-12, TNFα) and are capable of destroying tumor cells.

Anti-inflammatory macrophages can be stimulated by a diverse array of molecules including IL-4, IL-13, IL-10, TGF-β, and glucocortocoids (Mantovani et al. 2002; Gordon 2003). The physiological functions of anti-inflammatory macrophages are to promote collagen deposition, angiogenesis, and tissue repair (Hesse et al. 2001; Szekanecz and Koch 2001; Rosenkilde and Schwartz 2004; Strieter et al. 2005; Strieter et al. 2005). In the context of tumor biology, anti-inflammatory macrophages secrete angiogenic and anti-inflammatory cytokines (IL-10, TGF-β, and VEGF), which suppress the immune system and promote tumor progression (reviewed in (Allavena et al. 2008)). Macrophage depletion inhibits tumor growth and metastasis in pre-clinical models of breast cancer, suggesting the majority of macrophages in the tumor microenvironment display an anti-inflammatory phenotype (Lin et al. 2006; Zeisberger et al. 2006).

A growing body of clinical evidence also suggests that macrophage infiltration promotes tumor progression. One meta-analysis confirms that in clinical studies that examine macrophage infiltration, 80% found that macrophage infiltration conferred a worse prognosis (Bingle et al. 2002). In breast cancer specifically, an increase in macrophage hotspots correlates with decreased relapse-free and overall survival (Leek et al. 1996; Leek and Harris 2002). Experimental evidence for the tumor promoting capabilities of macrophages in pre-clinical models of breast cancer is equally compelling. Genetic ablation of colony stimulating factor-1 (CSF-1) in the MMTV-PyMT transgenic breast cancer model results in delayed tumor progression and potent metastasis inhibition (Lin et al. 2001). Anti-sense nucleotides and antibodies targeting CSF-1 or its receptor (CSF-1R) have also been used in transgenic and xenograft breast cancer models to inhibit macrophage infiltration, resulting in delayed tumor progression and reduced metastasis (Aharinejad et al. 2009; Abraham et al. 2010).

Macrophages assist tumor cells in every step of the metastatic cascade. Multiphoton microscopy has allowed for the direct visualization of tumor cell intravasation in the MMTV-PyMT transgenic breast cancer model; interestingly tumor cell intravasation occurs in direct association with perivascular macrophages (Wyckoff et al. 2007). Furthermore, genetic depletion of macrophages significantly reduces tumor cell ability to invade into the vasculature (Wyckoff et al. 2007). Macrophages are also mediators of tumor cell

extravasation, seeding, and growth at the metastatic site in animal models of breast cancer metastasis (Qian et al. 2009). More specifically, intravital imaging confirms that tumor cell extravasation into the lung occurs in direct cell-cell contact with macrophages following i.v. injection of tumor cells (Qian et al. 2009). Perivascular macrophages at the metastatic site recognize extravasating tumor cells, physically interact with them, and assist their invasion into the lung (Qian et al. 2009). This distinct macrophage population can be described as $F480^{+}CD11b^{+}Gr1^{-}CCR2^{hi}CX3CR1^{hi}$ and $VEGFR1^{hi}$. Macrophage depletion using genetic or chemical means significantly reduces tumor cell seeding of the metastatic site, suggesting that macrophage involvement in this process is critical (Qian et al. 2009). Most compelling and interesting is the evidence that genetic or chemical depletion of macrophages even after initial seeding has occurred is still able to reduce total metastatic burden (Qian et al. 2009). Following extravasation, tumor cells may continue to influence macrophage differentiation into an anti-inflammatory subpopulation that can increase tumor cell survival and growth at the metastatic site (Qian et al. 2009). The abundance of clinical and pre-clinical data linking macrophages to disease progression and metastasis in breast cancer makes these cells an attractive therapeutic target. Even more exciting is the pre-clinical data suggesting that inhibition of macrophage function has the potential to prevent metastasis and significantly reduce metastatic burden even when disseminated disease is already present.

Pleiotrophin (PTN), an 18 kDa heparin-binding cytokine, is expressed extensively during development, but expression in adult tissues is restricted except during times of inflammation and remodeling (Rauvala 1989; Vanderwinden et al. 1992; Silos-Santiago et al. 1996; Yeh et al. 1998). The primary receptor for PTN is receptor protein tyrosine phosphatase (RPTP)β/ζ. RPTPβ/ζ maintains steady-state phosphorylation levels of a number of substrates including anaplastic lymphoma kinase (ALK), β-catenin, β-adducin and others under normal cellular conditions. PTN binding inactivates RPTPβ/ζ, allowing phosphorylation of ALK and other targets to persist. The result is a net increase in substrate phosphorylation following PTN stimulation, which can promote cell proliferation, migration, differentiation, and transformation (Milner et al. 1989; Courty et al. 1991; Fang et al. 1992; Laaroubi et al. 1994; Perez-Pinera et al. 2006). PTN is an important angiogenic cytokine in many models of breast cancer (Perez-Pinera et al. 2007) and is expressed highly by approximately 60% of primary breast tumors (Fang et al. 1992; Riegel and Wellstein 1994). In this study, I illustrate that anti-VEGF therapy can modulate PTN expression in multiple pre-clinical mouse models of breast cancer. Once expressed, PTN induces the expression of VEGFR2 on macrophages and promotes an anti-inflammatory, metastatic macrophage phenotype. Our data further demonstrates that this phenomena is dependent on ALK signaling in these cells, as inhibition with either the small molecule receptor tyrosine kinase inhibitor crizotinib, which targets ALK, or ALK siRNA is

sufficient to abrogate VEGFR2 and anti-inflammatory macrophage marker expression following PTN stimulation *in vitro*. As seen in our previous studies, treatment with the anti-VEGF agent mcr84 reduces macrophage infiltration *in vivo* (Roland et al. 2009; Roland et al. 2009). However, the macrophages that remain following anti-VEGF therapy exhibit an increase in VEGFR2 and anti-inflammatory marker expression. This suggests that while anti-VEGF therapy reduces macrophage infiltration into the tumor, compensatory expression of PTN can promote an anti-inflammatory phenotype in those macrophages that are either (1) in the tumor prior to therapy or (2) migrate into the tumor in response post anti-VEGF therapy. I found that blockade of ALK in combination with anti-VEGF therapy prevents macrophage VEGFR2 and anti-inflammatory marker expression and significantly decreases metastatic burden in the MMTV-PyMT transgenic breast cancer model.

3.2 Results

3.2.1 Pleiotrophin levels correlate with ALK phosphorylation and anti-inflammatory macrophage marker expression during the course of tumor progression in the MMTV-PyMT breast cancer model

The MMTV-PyMT transgenic mouse expresses the polyomavirus middle T antigen driven by the MMTV-LTR promoter (Guy et al. 1992). Polyomavirus middle T oncogene expression results in the generation of multifocal mammary

carcinomas in 100% of female mice. Tumor progression in this model closely mimics the progression seen in human mammary carcinoma (Lin et al. 2003) and advances from hyperplastic to advanced metastatic disease over the course of 16 weeks (Figure 2.9).

I examined PTN expression during the course of tumor progression in this model and found that PTN expression peaks when mice reach 8 weeks of age (Figure 3.1 (A-C)). Interestingly, this is also the time period when lesions are transitioning from hyperplasia to invasive carcinoma. Furthermore, macrophage phenotype is regulated during this transition period. While total macrophage number is constant throughout the course of tumor progression (Figure 2.10 (B)), I discovered that ALK phosphorylation (P-ALK) is increased in tumor-associated macrophages when mice reach 8-10 weeks of age, coinciding with increased PTN expression (Figure 3.1 (D)). Furthermore, our analysis reveals that approximately 90% of P-ALK$^+$ cells are also positive for the macrophage markers CD68 and F4/80, indicating that macrophages are the primary cell type regulated through the PTN-ALK signaling axis in the tumor microenvironment (data not shown). In fact, linear regression analysis demonstrates a positive correlation between PTN expression and ALK phosphorylation (r^2=0.67) (data not shown). Next, I examined the number of mouse mannose receptor (MMR$^+$) macrophages during the course of tumor progression. MMR serves as a carbohydrate recognition receptor on macrophages; its expression is decreased upon activation by

pathogens (Shepherd et al. 1997) and IFNα and IFNγ (Ezekowitz 1985; Mokoena and Gordon 1985; Schreiber et al. 1993) and increased upon stimulation with IL-4 and IL-10 (Stein et al. 1992; Dewals et al. 2010), indicating that MMR is a marker of alternatively activated macrophages [reviewed in (Mantovani et al. 2002). I found that MMR^+ cells also increase in the tumor when mice reach 8 weeks of age (Figure 3.1 (E)). Linear regression analysis further suggests that PTN may be promoting MMR expression on tumor associated macrophages (r^2=0.80) (data not shown). Another marker of anti-inflammatory macrophages (YM-1) is also increased when mice reach 8 weeks of age and correlates with PTN expression (Figure 3.1 (F)). YM-1 is a heparan binding protein synthesized and secreted by alternatively activated macrophages (Chang et al. 2001; Raes et al. 2002). YM-1 expression is increased through stimulation with IL-4 (Raes et al. 2002) and IL-13 (Nair et al. 2003) and decreased through stimulation with IFNγ (Welch et al. 2002). Both MMR and YM-1 are involved in decreasing inflammation (O'Brien et al. 2010). Finally, I examined the number of $VEGFR2^+$ macrophages present in the tumor during progression to malignancy and discovered that these are most abundant when mice reach 8 weeks of age (Figure 3.1 (G&H)) and these numbers positively correlate with PTN expression (r^2=0.74).

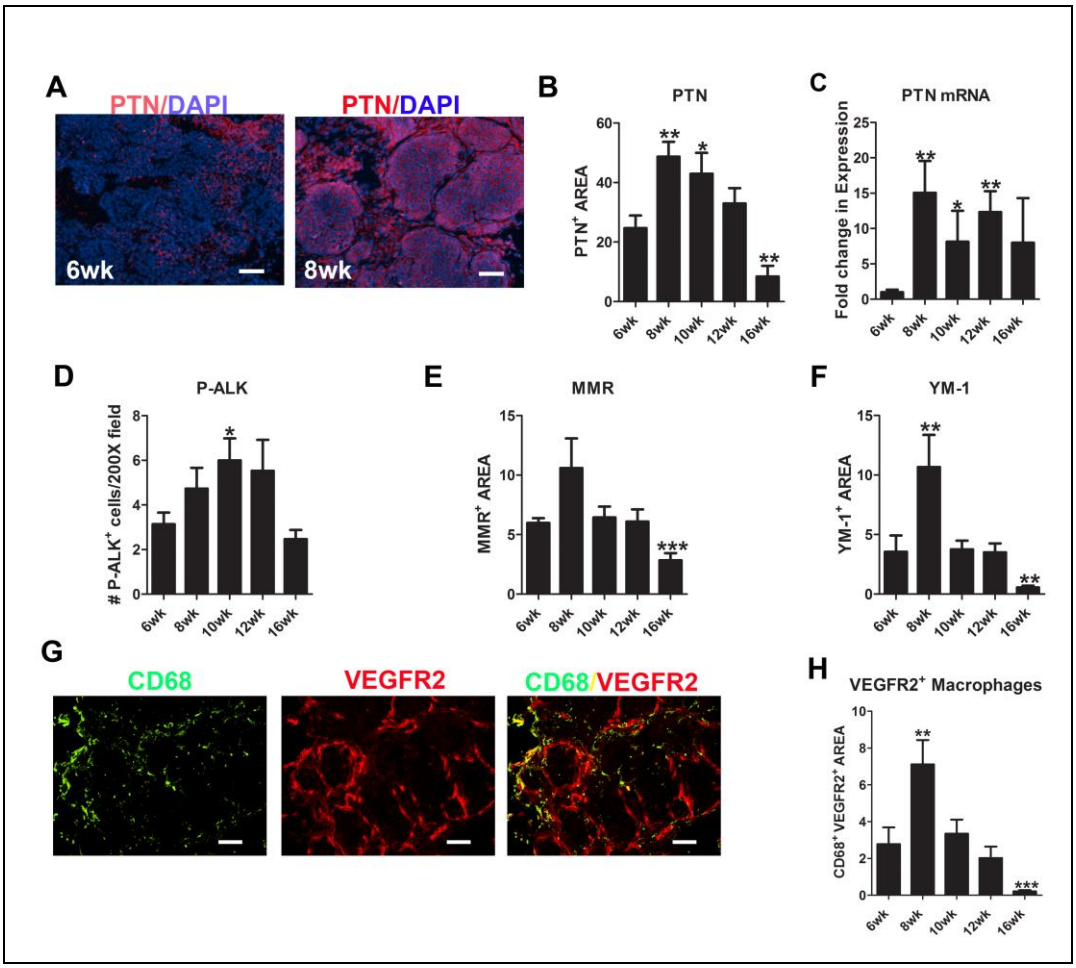

Figure 3.1. PTN expression correlates with ALK phosporylation, VEGFR2 expression, and anti-inflammatory macrophage marker expression during the course of tumor progression in the MMTV-PyMT transgenic breast cancer model. Transgenic female mice were sacrificed at various time points. Tumor tissue was snap frozen in liquid nitrogen, sectioned and stained for PTN (A&B), P-ALK (D), MMR (E), YM-1 (F), CD68, and VEGFR2 (G&H). Tumor RNA was harvested at various time points and RT-qPCR was performed to analyze PTN mRNA expression (C). Data are displayed as mean ± SEM and represents 5 images (Total magnification, 200X) per tumor and four tumors per group. Images were analyzed using Elements software. qPCR analysis represents 4 tumors per group, performed in triplicate. *p=0.05, **p=0.01, ***p<0.001 vs. 6 wk, Mann-Whitney test. Scale bar = 50 µm.

3.2.2 VEGFR2$^+$ macrophages represent an alternatively activated, anti-inflammatory subpopulation

We have previously reported VEGFR2 expression on tumor-associated and systemic macrophages harvested from animals bearing pancreatic (Dineen et al. 2008) and breast (Roland et al. 2009) orthotopic xenografts. In this study, I characterize the VEGFR2$^+$ macrophage population in a spontaneous, immunocompetent breast cancer model. Flow cytometry analysis confirms the presence of a VEGFR2$^+$ tumor-associated macrophage (CD11b$^+$) population in 12 week old MMTV-PyMT female mice (Figure 3.2 (A)). When these cells were separated into F4/80$^+$ and F4/80$^+$ VEGFR2$^+$ subpopulations for qPCR analysis, I found that VEGFR2$^+$ macrophages have decreased expression of the Notch pathway mediators Dll4 and Hes1 (Figure 3.2 (B)), which are critical for pro-inflammatory macrophage differentiation (Wang et al. 2010). Furthermore, the anti-inflammatory markers MMR and YM-1, as well as the protease MMP-9, were significantly increased in the VEGFR2$^+$ macrophage population, further implicating VEGFR2 as a marker of anti-inflammatory macrophages (Figure 3.2 (B)). Interestingly, ALK expression is relatively constant in both macrophage subpopulations, suggesting that either population has the potential to respond to PTN stimulation (Figure 3.2 (B)). Finally, peritoneal macrophages were harvested from MMTV-PyMT and wild-type littermates and examined for pro- and anti-inflammatory marker expression using immunocytochemistry (ICC). I found that systemic macrophages harvested from tumor bearing animals have decreased

expression of the pro-inflammatory markers iNOS and MCP-1, whereas expression of the anti-inflammatory markers MMR and VEGFR2 were increased in systemic macrophages from tumor-bearing animals (Figure 3.2 (C& D)).

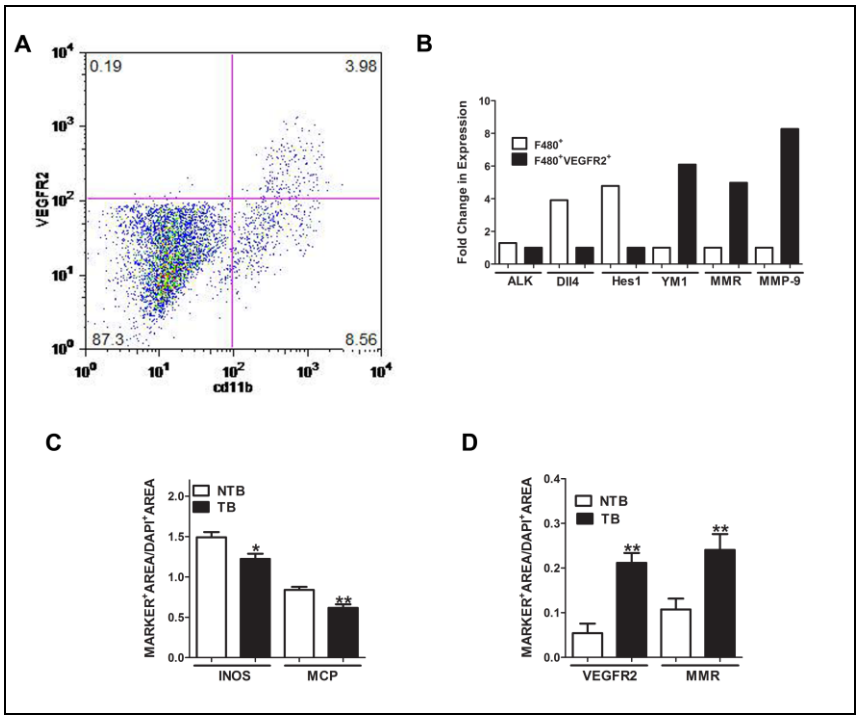

Figure 3.2. VEGFR2$^+$ macrophages are found in the tumor and peritoneal cavity of MMTV-PyMT transgenic mice and display an anti-inflammatory phenotype. (A) Fresh tumor tissue was harvested from 12 week old MMTV-PyMT female mice and subjected to flow cytometry, which confirms the presence of a VEGFR2$^+$ cd11b$^+$ tumor-associated macrophage population (top, right quandrant). Scatter-plot is representative of two independent experiments. (B) Fresh tumor tissue was harvested from 8 week old transgenic female mice and subjected to FACs to separate F4/80$^+$ and F4/80$^+$ VEGFR2$^+$ macrophage populations. The 8 week time point was chosen to maximize the number of VEGFR2$^+$ macrophages harvested. RNA was collected from the two subpopulations and subjected to RT-qPCR to characterize ALK, Dll4, Hes1, YM-1, MMR, and MMP-9 mRNA expression. Graph is representative of 3 independent experiments. (C&D) Peritoneal macrophages were harvested from 12 week old MMTV-PyMT or wild-type littermates, plated on chamber slides, and analyzed for pro (C), and anti-inflammatory (D) marker expression using ICC. Data are displayed as mean ± SEM and represents 5 images (Total magnification, 200X) per animal and three animals per group. Images were analyzed using Elements software. *p=0.05, **p=0.01 vs. NTB, Mann-Whitney test.

3.2.3 PTN promotes an anti-inflammatory macrophage phenotype through an ALK-dependent signaling mechanism.

We and others have shown that PTN induces the expression of VEGFR2 on macrophages *in vitro* (Sharifi et al. 2006; Dineen et al. 2008; Chen et al. 2009). In this study, I further characterize macrophage phenotypic changes following PTN stimulation. Mouse macrophages, RAW 264.7 cells, were stimulated with serum free media (SFM) or PTN prior to the analysis of pro- and anti-inflammatory macrophage marker expression using ICC. The pro-inflammatory markers iNOS and MCP-1 were decreased following PTN stimulation (Figure 3.3 (A)), whereas the anti-inflammatory markers YM-1, MMR, arginase (ARG), and VEGFR2 increased significantly in response to PTN stimulation (Figure 3.3 (B)). This data indicates that PTN promotes an anti-inflammatory macrophage phenotype.

To further investigate the mechanism by which PTN promotes an anti-inflammatory macrophage phenotype and to examine the function of ALK signaling in this process, RAW 264.7 cells were stimulated with PTN in the presence or absence of the ALK inhibitor crizotinib or siRNA targeting ALK. ALK phosphorylation is significantly increased following stimulation with PTN and importantly this phosphorylation is completely abrogated in the presence of crizotinib (Figure 3.4 (B&C)). Furthermore, targeting ALK expression with siRNA constructs decreased significantly the expression of ALK (Figure 3.4 (A))

and PTN fails to promote ALK phosphorylation in the presence of ALK siRNA (Figure 3.4 (D)), demonstrating the specificity of the P-ALK antibody. As shown previously, PTN stimulates the expression of VEGFR2 on macrophages *in vitro;* however, PTN fails to promote VEGFR2 expression in the presence of either crizotinib or ALK siRNA (Figure 3.3 (C, D, F)). Furthermore, PTN does not stimulate MMR expression in the presence of crizotinib or ALK siRNA (Figure 3.3 (C, E, G)). These data provide significant evidence that PTN signals through ALK to promote an anti-inflammatory macrophage phenotype.

Furthermore, I performed cytokine analysis (Millipore MPXMCYTO-70K) of conditioned media from RAW 264.7 cells stimulated with SFM, PTN, crizotinib, or PTN + crizotinib and found that there are very few cytokine changes induced by any of the treatment conditions. Only 7 of the 32 cytokines analyzed had more than a 2-fold change in cytokine expression following any of the treatment conditions (Table 3.1). Furthermore, none of these changes were correlative with the changes in VEGFR2 or MMR expression observed following treatment with PTN in the presence or absence of crizotinib. Interestingly, IL-4, IL-10, and IL-13, which are known to stimulate anti- inflammatory marker expression on macrophages, were not detected (IL-4) (data not shown) or were not regulated following treatment with PTN in the presence or absence of crizotinib (Table 3.1). This suggests that PTN may directly regulate the

expression of these anti-inflammatory molecules rather than acting through a secondary cytokine mediator.

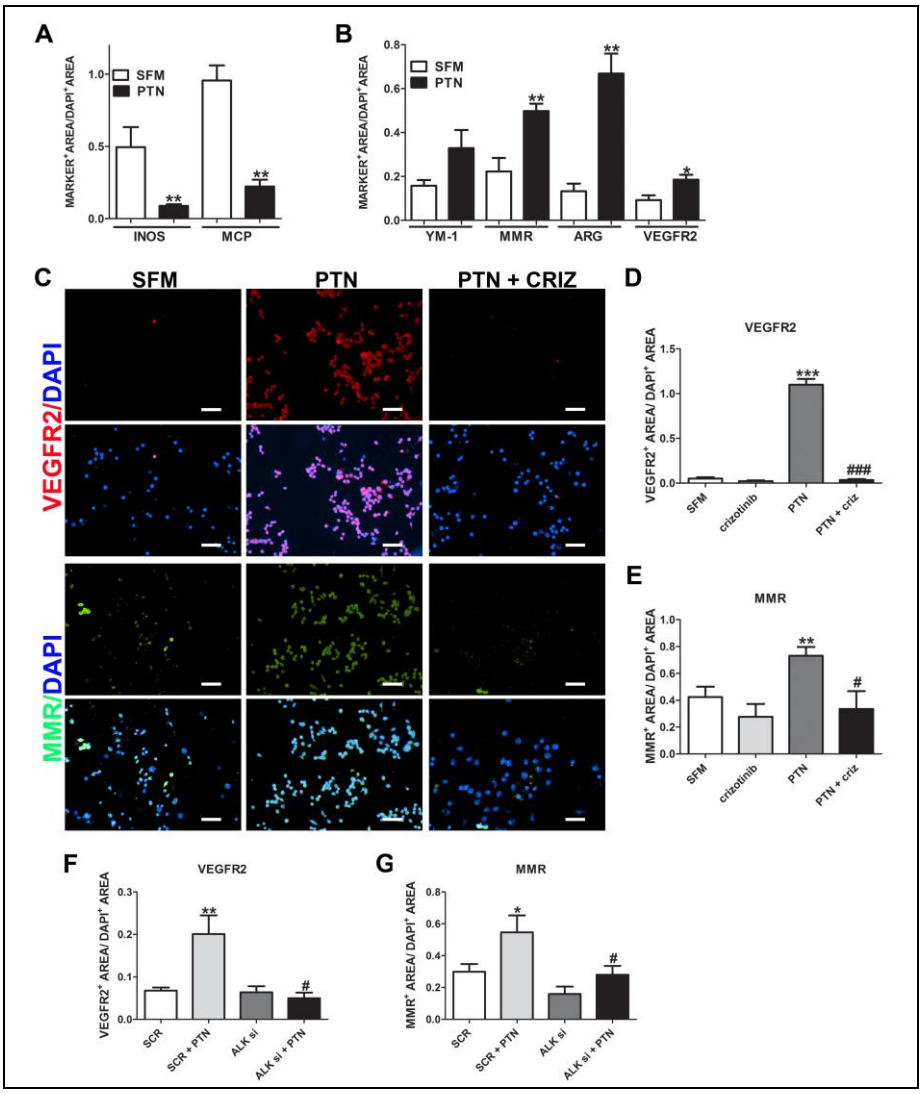

Figure 3.3. PTN promotes an anti-inflammatory macrophage phenotype through an ALK-dependent signaling mechanism. (A&B) RAW 264.7 cells were stimulated overnight with either SFM or PTN (10 ng/ml). Cells were fixed and the expression of Inos, MCP, YM-1, MMR, ARG, and VEGFR2 was analyzed by ICC. (C-E) RAW 264.7 cells were stimulated overnight with PTN (100 ng/ml) in the presence or absence of crizotinib (2 µM). Cells were fixed and the expression of VEGFR2 and MMR was analyzed by ICC. (F-G) RAW 264.7 cells were transfected with either scrambled (SCR) or ALK siRNA (20 µM) 48 hours prior to stimulation with PTN (100 ng/ml) overnight. Cells were fixed and the expression of VEGFR2 and MMR was analyzed by ICC. Data are displayed as mean ± SEM and represents 10 images (Total magnification, 200X) per group, performed in triplicate. Images were analyzed using Elements software. *p=0.05, **p=0.01, ***p<0.001 vs. SFM; $^{\#}$p=0.05, $^{\#\#\#}$p<0.001 vs. PTN; Mann-Whitney test. Scale bar = 50 µm.

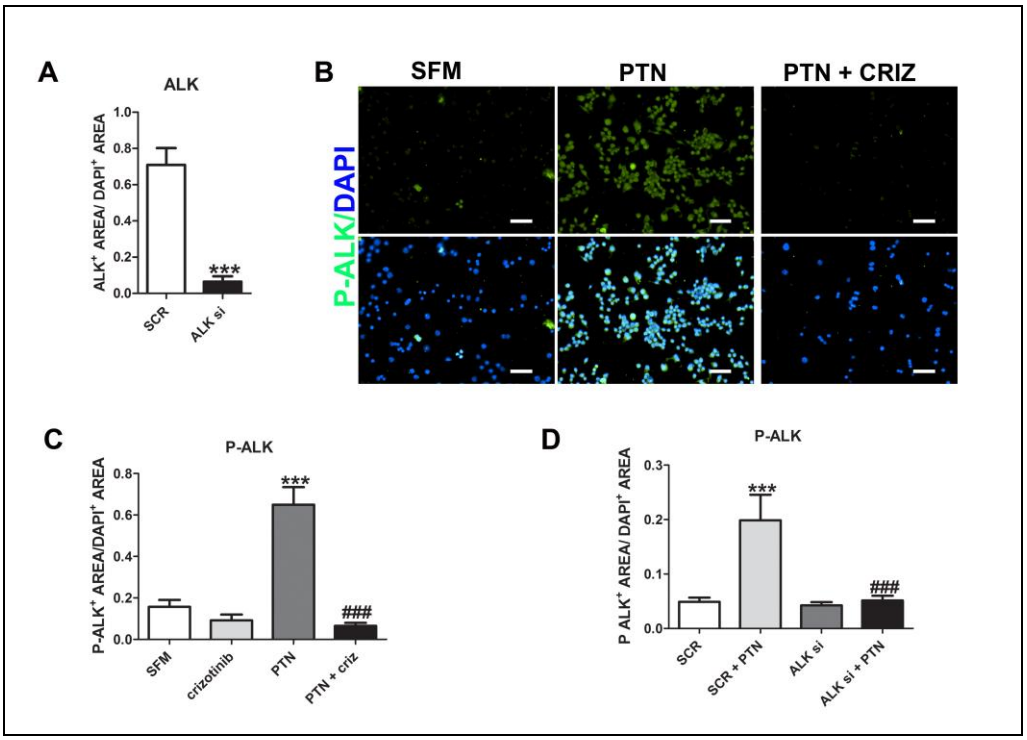

Figure 3.4. PTN promotes ALK phoshorylation, which is abrogated in the presence of crizotinib or ALK siRNA *in vitro*. (A) RAW 264.7 cell were transfected with either SCR or ALK siRNA (20 µM) 48 hours prior to analysis of ALK expression using ICC. (B&D) RAW cells were stimulated overnight with PTN (100 ng/ml) in the presence or absence of crizotinib (2 µM). Cells were analyzed for ALK phosphorylation using ICC. (D) RAW 264.7 cells were transfected with either scrambled (SCR) or ALK siRNA (20 µM) 48 hours prior to stimulation with PTN (100 ng/ml) overnight. Cells were fixed and analyzed for ALK phosphorylation using ICC. Data are displayed as mean ± SEM and represents 10 images (Total magnification, 200X) per group, performed in triplicate. Images were analyzed using Elements software. ***$p<0.001$ vs. SFM; ###$p<0.001$ vs. PTN; Mann-Whitney test. Scale bar = 50 µm.

	IL-6	IL-17	MIG	MIG	IL-1b	TNFa	IL-15	IL-10	IL-13	MMR	VEGFR2
SFM CM	1.00	1.00	1.00	1.00	1.00	1.00	1.00	1.00	1.00	1.00	1.00
PTN CM	0.57	0.97	0.27	0.27	0.25	0.93	1.06	0.77	0.92	1.74	22.00
CRIZ CM	0.48	0.33	0.67	0.67	0.98	0.49	0.99	0.73	0.62	0.65	0.42
PTN+CRIZ CM	0.41	0.42	1.03	1.03	0.40	0.65	0.02	0.88	0.69	0.79	0.68

Table 3.1. Changes in cytokine expression *in vitro* following treatment with PTN in the presence or absence of crizotinib. RAW 264.7 cells were stimulated overnight with SFM, PTN (100 ng/ml), crizotinib (2 μM), or the combination of PTN and crizotinib. Conditioned media was collected and analysis was performed using the Millipore Milliplex mouse cytokine array (MPXMCYTO-70K). Numbers displayed represent the average of two independent experiment performed in duplicate. All values were normalized to expression levels in SFM conditions. MMR and VEGFR2 expression levels were taken from the Figure 3.3 and normalized to SFM conditions. Expression levels greater than 1.5 are green and those less than 0.5 are red.

3.2.4 mcr84 increases PTN expression and anti-inflammatory macrophage numbers in two immunocompetent breast cancer models.

mcr84 is a mouse IgG2a,k chimeric form of r84, a monoclonal antibody that binds VEGF and specifically inhibits VEGF from binding to and signaling through VEGFR2 (Sullivan et al. 2010). We have reported previously the use of mcr84 in the MMTV-PyMT model of breast cancer, where it controls tumor growth and angiogenesis. mcr84 also inhibits the infiltration of MDSCs, Tregs, and macrophages in this model (Roland et al. 2009). In this study, I define PTN expression and macrophage phenotype following treatment with mcr84 in the MMTV-PyMT and 4T1 breast cancer models. Growth of 4T1 tumors cells in the mammary fat pad of BALB/c mice is an inflammatory model of breast cancer in which immune cells comprise 40-50% of the overall tumor mass (DuPre and Hunter 2007; DuPre et al. 2007). Surprisingly, I found that PTN expression is increased in the tumor following treatment with mcr84 in the MMTV-PyMT (Figure 3.5 (A&B)) and 4T1 (Figure 3.5 (F)) breast cancer models. Furthermore, the number of tumor-associated $VEGFR2^{+}$ macrophages is also increased following treatment with mcr84 in both models (Figure 3.5 (E& I)), despite an overall reduction in total macrophage number (Figure 3.8 (A&B)) (Roland et al. 2009). Further characterization of macrophage phenotype reveals an increase in anti-inflammatory macrophages following treatment with mcr84 as ARG (Figure 3.5 (D)), YM-1 (Figure 3.5 (C)) and MMR (Figure 3.8 (C&E) expression all

increase in tumors from mcr84 treated animals compared to control animals in the MMTV-PyMT model. Furthermore, there is an increase in MMR expression in tumors from mcr84 treated animals bearing 4T1 tumors (Figure 3.5 (H)). Finally, P-ALK^{+} macrophage numbers increase following treatment with mcr84 in both models (Figure 3.5 (G); Figure 3.8 (C& D)), suggesting that PTN signaling through ALK may be an important regulator of macrophage phenotype in the tumor microenvironment.

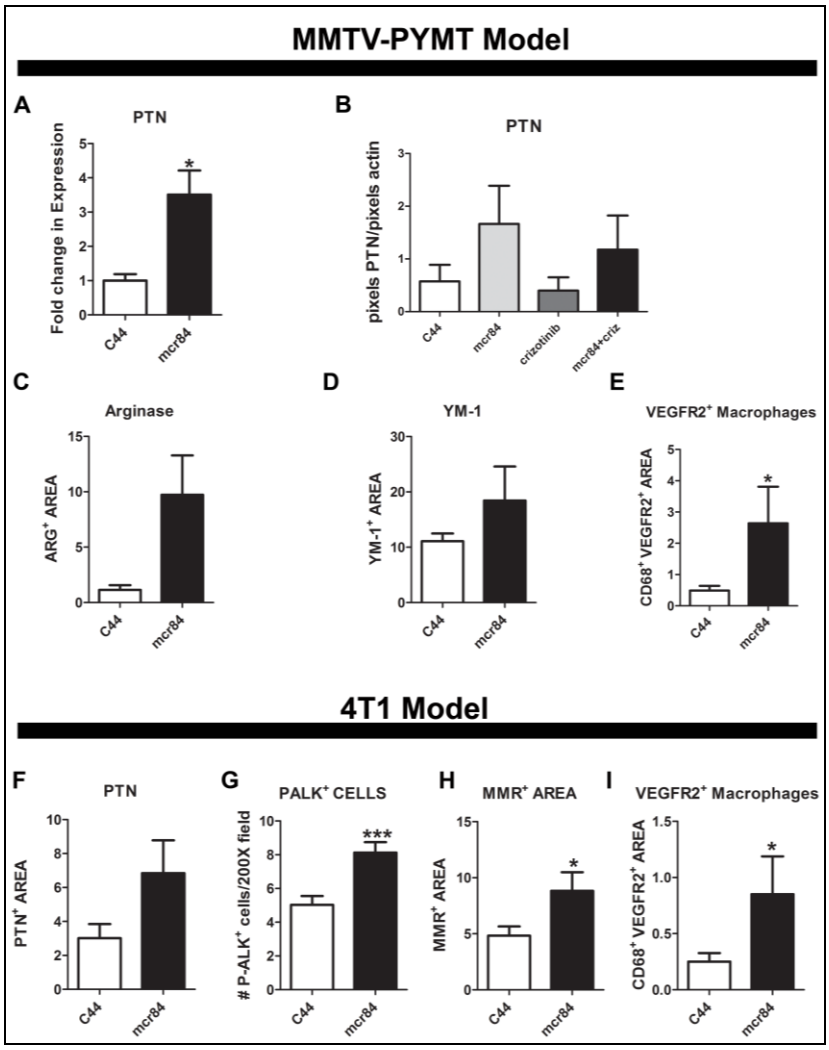

Figure 3.5. Treatment with mcr84 increases PTN expression and anti-inflammatory macrophage numbers in two immunocompetent breast cancer models. (A-E) MMTV-PyMT transgenic female mice were treated with either control antibody (C44) or mcr84 (250 µg/twice weekly) for 4 weeks beginning when mice reached 8 weeks of age. Tissue was snap frozen in liquid nitrogen, sectioned, and stained for PTN (A), ARG (C), YM-1 (D), CD68, and VEGFR2 (E). In (B) crizotinib treatment was also added (50 mg/kg/day). Tumor lysates were made and analyzed by western blot. Image J software was used to analyze the relative PTN expression (PTN pixels/actin pixels) for each sample. (F-I) 10,000 4T1 cells were injected into the mammary fat pad of Balb/C mice. Treatment with C44 or mcr84 began 14 days post tumor cell injection and continued for 3 weeks. Tissue was snap frozen in liquid nitrogen, sectioned, and stained for PTN (F), P-ALK (G), MMR (H), CD68, and VEGFR2 (I). Data are displayed as mean ± SEM and represents 5 images (Total magnification, 200X) per tumor and four tumors per group. Images were analyzed using Elements software. *p=0.05, **p=0.01, ***p<0.001 vs. C44, Mann-Whitney test.

3.2.5 Crizotinib controls tumor growth and alters tumor histology in combination with mcr84 in the MMTV-PyMT model

I have discovered that treatment with mcr84 increases PTN expression and macrophage ALK phosphorylation in two independent breast cancer models. Furthermore, PTN promotes an anti-inflammatory macrophage phenotype through an ALK-dependent mechanism *in vitro* and correlates with anti-inflammatory macrophage levels *in vivo*. This data led us to combine the use of mcr84 and the ALK inhibitor crizotinib in the MMTV-PyMT model. mcr84 significantly reduces primary tumor burden alone and in combination with crizotinib. Crizotinib alone, however, has no effect on primary tumor burden (Figure 3.6 (A)). *In vitro* analysis confirms that the IC_{50} for crizotinib is relatively high for both Met-1 cells, which are derived from a MMTV-PyMT tumor (Borowsky et al. 2005), and macrophages (Figure 3.6 (B)). These values are well above the maximum achievable *in vivo* concentration of 0.5 μM (data not shown). ALK phosphorylation is inhibited potently at *in vivo* concentrations of 0.1 μM, which I am able to sustain at the 50 mg/kg/day dose (data not shown), suggesting that any anti-tumor effects seen are a result of effects beyond direct tumor cell toxicity. Hematoxylin and eosin staining reveals no striking differences in tumor histology between the control IgG (C44), mcr84, and crizotinib treated animals, however, tumors from animals treated with the combination of mcr84 and crizotinib (combo) appeared to be less invasive and showed preservation of the ductal

structure and surrounding basement membrane (Figure 3.6 (C), bottom right panel). To further characterize tumor phenotype, trichrome staining was performed. Trichrome stains collagen fibers, allows the visualization of intact basement membrane, and assists in the assessment of tumor invasiveness. There is an increase in intact basement membrane surrounding the hyperproliferating mammary epithelium in tumors from combo treated animals, further suggesting that tumors from these animals are less invasive than those from the other treatment groups (Figure 3.6 (D), bottom right panel).

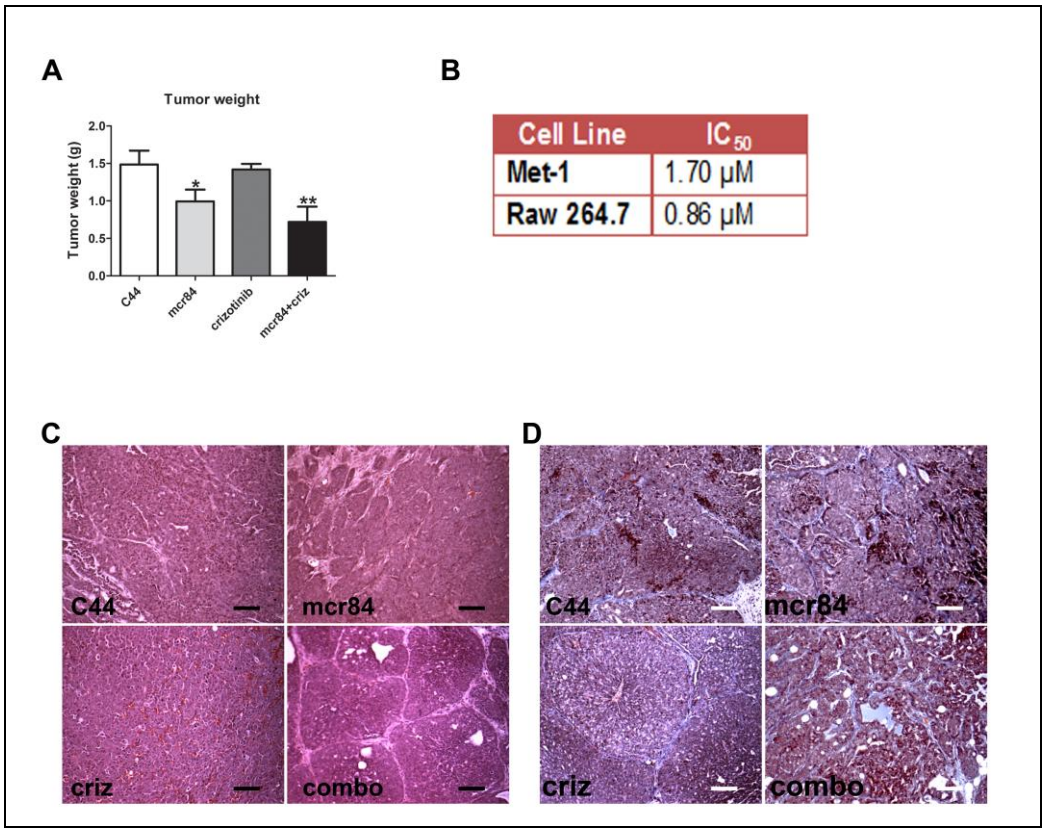

Figure 3.6 Crizotinib controls tumor growth and alters tumor histology in combination with mcr84 in the MMTV-PyMT breast cancer model. (A) MMTV-PyMT female mice began therapy at 8 weeks of age; therapy was continued for 4 weeks. C44 and mcr84 was given at 250 µg/twice weekly, i.p. Crizotinib was given at 50/mg/kg/day by oral gavage. Animals were sacrificed at the end of therapy and total tumor burden was excised and weighed. Data are displayed as mean ± SEM and represents 8 animals/group and 2 independent experiments. (B) MTS assays were performed to determine the *in vitro* sensitivity of Met-1 and RAW 264.7 cells to crizotinib. Numbers represent the average of 3 independent experiments performed in duplicate. (C-D) Tumor tissue was harvested, fixed in formalin, sectioned, and stained with hematoxylin and eosin (C) or Trichrome (D). Images representative of at least 4 tumors from each group are shown. Note the dramatic reduction in the number of invasive cells induced by combination therapy. *p=0.05, **p=0.01, vs. C44, Mann-Whitney test. Total magnification 200X. Scale bar = 50 µm.

3.2.6 Crizotinib and mcr84 control tumor angiogenesis both alone and in combination in the MMTV-PyMT model.

We have previously shown that mcr84 inhibits angiogenesis in the MMTV-PyMT model (Roland et al. 2009) and confirm these findings here using two independent endothelial cell markers: Meca-32 (Figure 3.7 A&B) and endomucin (Figure 3.7 (C)). Furthermore, crizotinib alone significantly reduced MVD (Figure 3.7 (A-C)), despite having no effect on primary tumor growth (Figure 3.6 (A)). The combination of mcr84 and crizotinib also significantly decreased MVD, however, this decrease is not more than the reduction seen with either agent alone (Figure 3.7 A-C). These findings suggest that inhibition of MVD alone is not sufficient to decrease primary tumor growth in the MMTV-PyMT model.

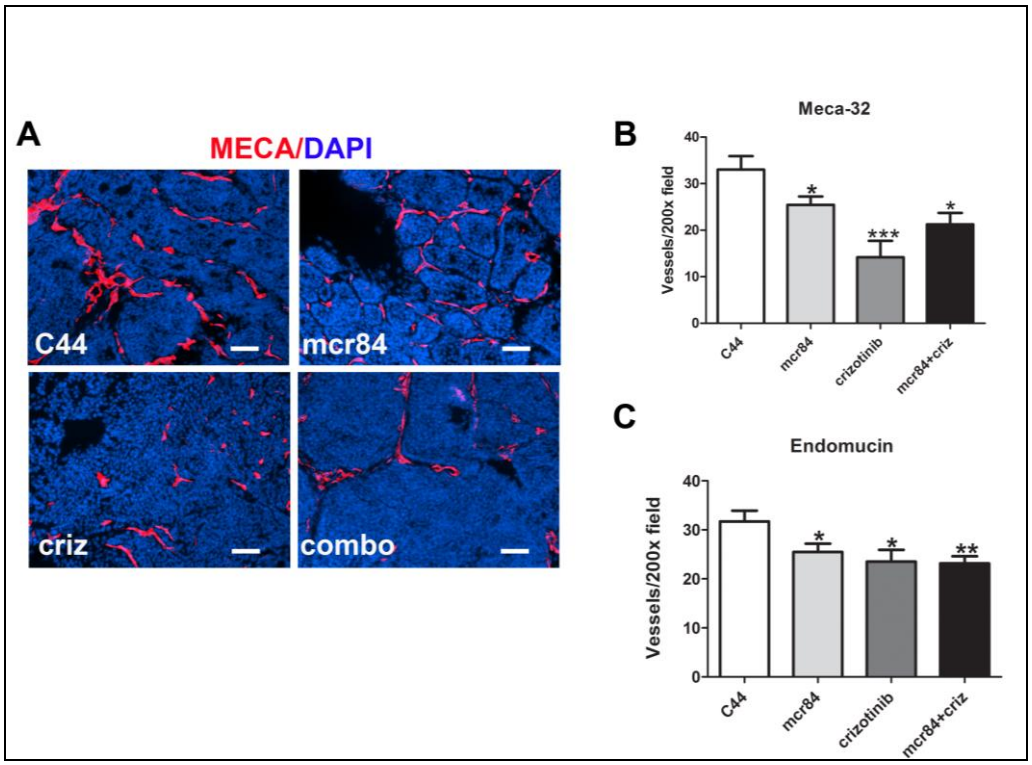

Figure 3.7. mcr84 and crizotinib inhibit angiogenesis alone and in combination in the MMTV-PyMT model. Mice were sacrificed at 12 weeks of age, following 4 weeks of therapy. Tissue was snap frozen in liquid nitrogen and stained for the endothelial cell markers Meca-32 (A&B) and endomucin ©. Data are displayed as mean ± SEM and represents 5 images (Total magnification, 200X) per tumor and four tumors per group. Images were analyzed using Elements software. *p=0.05, **p=0.01, ***p<0.001 vs. C44, Mann-Whitney test. Scale bar = 50 µm.

3.2.7 mcr84 increases PTN expression and anti-inflammatory VEGFR2$^+$ macrophage levels in vivo through an ALK dependent signaling mechanism

We have described previously a decrease in macrophage infiltration following treatment with mcr84 and r84 in multiple mouse models of breast cancer, including the MMTV-PyMT model (Roland et al. 2009; Roland et al. 2009). In this study, I demonstrate a significant decrease in F4/80$^+$ macrophages

following treatment with mcr84 either alone or in combination with crizotinib (Figure 3.8 (A&B)), confirming our previous results. When I further characterized the macrophage population following treatment with mcr84, I found that the number of P-ALK$^+$ macrophages increased in tumors from mcr84 treated animals. This increase is completely abrogated when mcr84 is combined with the ALK inhibitor crizotinib (Figure 3.8 (C&D)). As previously discussed, the number of MMR$^+$ macrophages is also increased following treatment with mcr84, however, this increase is again reduced when mcr84 is combined with crizotinib (Figure 3.5 (H); Figure 3.8 (C&E)). Furthermore, co-localization studies suggest that virtually all P-ALK$^+$ macrophages are also MMR$^+$, however, the reverse does not seem to be true, as only a subpopulation of MMR$^+$ macrophage are also P-ALK$^+$ (Figure 3.8 (C)). An increase in YM-1 expression in tumors from mcr84 treated animals was observed in this study and again this increase was reduced significantly in tumors from mice treated with a combination of mcr84 and crizotinib (Figure 3.5 (D); Figure 3.8 (F&G)). Finally, I looked at the number of VEGFR2$^+$ tumor-associated macrophages in animals treated with mcr84 and found that this number was increased significantly compared to animals treated with C44, confirming our previous results (Figure 3.5 (E&I); Figure 3.8 (H&I). Furthermore, this increase was inhibited when animals were treated with the combination of mcr84 and crizotinib (Figure 3.8 (H&I)). I also analyzed the percentage of tumor-associated macrophages that are VEGFR2$^+$ following therapy. I found that following

treatment with C44 approximately 4% of macrophages are VEGFR2^{+}, whereas 17% of macrophages are VEGFR2^{+} following treatment with mcr84 (Figure 3.8 (J)). Treatment with crizotinib alone or in combination with mcr84 significantly reduced the percentage of VEGFR2^{+} macrophages compared to both C44 and mcr84 treatment (0.07% and 0.78%, respectively) (Figure 3.8 (J)). These data provides significant evidence that the mcr84 dependent upregulation of PTN in the tumor results in an increase of anti-inflammatory VEGFR2^{+} macrophages, despite decreasing total macrophage infiltration. Furthermore, this increase in anti-inflammatory macrophages is dependent on ALK signaling, as treatment with crizotinib inhibits the switch from pro- to anti-inflammatory macrophages.

I performed cytokine analysis on tumors from MMTV-PyMT mice treated with C44, mcr84, crizotinib, and mcr84 + crizotinib (Millipore, MPXMCYTO-70K) and found that while the expression of several cytokines changed following therapy with the various treatment regimens, none of these changes were correlative with the changes in PTN or MMR^{+}, YM-1^{+},VEGFR2^{+} macrophage levels (Table 3.2). 14 of the 32 cytokines analyzed had more than a 2-fold change in cytokine expression following any of the treatment conditions (Table 3.2). I found that most of the changes in cytokine expression followed one of two distinctive patterns. Cytokine levels were either reduced in all treatment groups (GM-CSF, IL-13, and IL-15) or in treatment groups receiving crizotinib alone or in combination with mcr84 (IL-17, IL-1β, IL-12 (p70), Mip1b, Mip2, TNFα,

MCP-1, G-CSF). Interestingly, cytokines known to stimulate an anti-inflammatory macrophage phenotype were not detected in any of the samples tested (IL-4) (data not shown) or were unchanged following any of the treatment regimens (IL-10) (Table 3.2). IL-13, which can promote an anti-inflammatory macrophage phenotype, was decreased in all treatments groups (Table 3.2). This *in vivo* data along with the *in vitro* cytokine analysis (Table 3.2) strongly suggests that PTN directly modulates macrophage phenotype, rather than acting through a secondary cytokine mediator.

Analysis of MMTV-PyMT tumors treated with other anti-VEGF strategies including GU81 and sunitinib, which inhibit signaling through both VEGFR1 and VEGFR2, (Roland et al. 2009; Lynn et al. 2010), demonstrates that neither PTN nor anti-inflammatory macrophage levels are increased (data not shown). To determine whether VEGFR1 signaling may promote PTN expression by tumor cells, I moved into an *in vitro* system. Met-1 cells, which are derived from a MMTV-PyMT tumor (Borowsky et al. 2005), express both VEGFR1 and VEGFR2 (data not shown). When these cells are stimulated with the VEGFR1 specific ligand (VEGF-B), there is a 5-fold increase in PTN expression; this phenomena is not seen when VEGF-A (VEGF), a ligand for both VEGFR1 and VEGFR2, is added (Figure 3.8 (K)). Met-1 cells produce a significant amount of endogenous VEGF (Lynn et al. 2010). When r84 is added to Met-1 culture media, shuttling the available VEGF to bind and signal exclusively through VEGFR1,

PTN expression is increased 2-fold (Figure 3.8 (L)). Furthermore, addition of a VEGFR1 blocking antibody either alone or in combination with r84, potently inhibits PTN expression, further implicating VEGFR1 signaling as an upstream mediator of PTN expression in Met-1 cells (Figure 3.8 (L)).

.

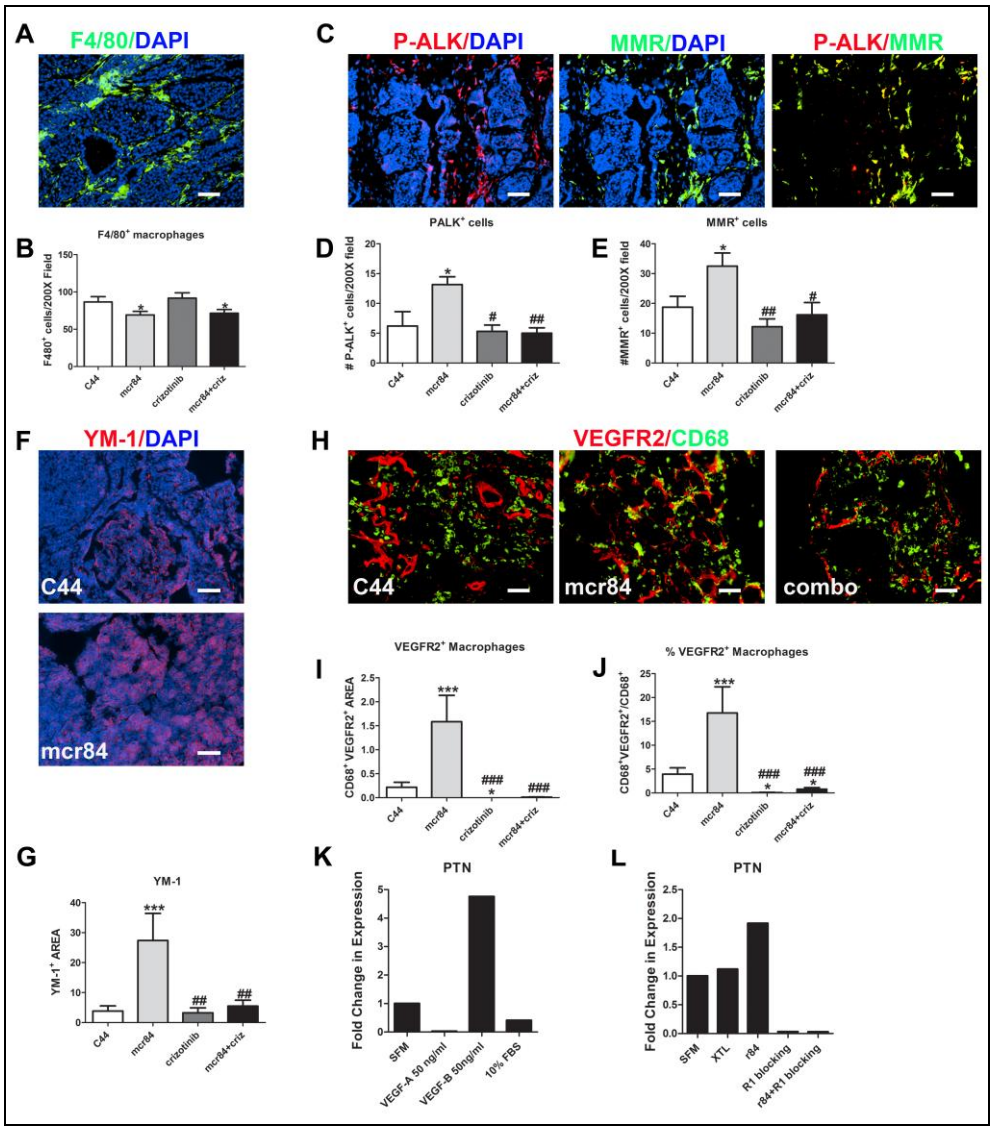

Figure 3.8 mcr84 increases PTN expression and anti-inflammatory VEGFR2^{+} macrophage levels *in vivo* through an ALK dependent signaling mechanism. Mice were sacrificed at 12 weeks of age, following 4 weeks of therapy. Tissue was snap frozen in liquid nitrogen and stained for F4/80 (A&B), P-ALK (C&D), MMR (C&E), YM-1 (F&G), and CD68 and VEGFR2 (H-J). Data are displayed as mean ± SEM and represents a minimum of 5 images (Total magnification, 200X) per tumor and four tumors per group. Images were analyzed using Elements software. *p=0.05, **p=0.01, ***p<0.001 vs. C44; $^{\#}$p=0.05, $^{\#\#}$p=0.01, $^{\#\#\#}$p<0.001 vs. mcr84, Mann-Whitney test. Scale bar = 50 µm. Met-1 cells were allowed to reach 70% confluence prior placement in SFM. Exogenious VEGF-A and VEGF-B was added in (K). Control antibody (XTL), r84, or a VEGFR1 (R1) blocking antibody was added in (L). RNA was isolated following 48 hours treatment. PTN levels were assessed using RT-Qpcr. Graphs are representative of 2 independent experiments.

	GM-CSF	IL-13	IL-15	IL-12 (p70)	MIP-1b	MIP-2	TNFa	LIF	IL-1a	IL-17
C44	1.00	1.00	1.00	1.00	1.00	1.00	1.00	1.00	1.00	1.00
mcr84	0.26	0.12	0.38	0.64	0.78	0.57	0.58	0.42	0.34	1.15
crizotinib	0.00	0.00	0.00	0.34	0.08	0.11	0.13	0.19	0.00	0.41
mcr84+crizotinib	0.26	0.33	0.25	0.34	0.39	0.14	0.33	1.11	1.15	1.35

	IL-1b	MCP-1	G-CSF	KC	IL-10	IL-6	MMR+	YM-1+	P-ALK+	VEGFR2+	PTN
C44	1.00	1.00	1.00	1.00	1.00	1.00	1.00	1.00	1.00	1.00	1.00
mcr84	0.60	0.61	1.34	0.43	0.64	0.79	1.74	7.14	2.13	4.27	2.91
crizotinib	0.49	0.84	1.01	0.71	0.63	0.79	0.65	0.84	0.85	0.02	0.70
mcr84+crizotinib	0.59	0.42	0.44	0.36	0.54	1.39	0.86	1.42	0.81	0.20	2.06

Table 3.2. Changes in tumor cytokine expression *in vivo* following treatment with mcr84, crizotinib, and the combination of mcr84 and crizotinib. MMTV-PyMT transgenic female mice received therapy as described in the Materials and Methods. Tumor lysates were collected and analysis was performed using the Millipore Milliplex mouse cytokine array (MPXMCYTO-70K). Values represent averages of 4 tumors/group, performed in duplicate. All values were normalized to expression levels in C44 treated tumors. MMR, YM-1, P-ALK, and VEGFR2+ levels were takes from Figure 3.8 and normalized to levels found in C44 treated tumors. PTN levels were taken from Figure 3.5 (I) and normalized to levels found in C44 treated tumors. Expression levels greater than 1.5 are green and those less than 0.5 are red.

3.2.8 Crizotinib decreases metastatic burden both alone and in combination with mcr84 in the MMTV-PyMT breast cancer model.

Clinical data confirms that macrophage infiltration confers a worse prognosis for many cancer types, including breast cancer (Leek et al. 1996; Bingle et al. 2002; Leek and Harris 2002). Furthermore, a wealth of pre-clinical data demonstrates that macrophages are intimately involved in disease progression and metastasis in multiple pre-clinical breast cancer models (Lin et al. 2001; Wyckoff et al. 2007; Aharinejad et al. 2009; Qian et al. 2009; Abraham et al. 2010). These observations led us to investigate what role, if any, the P-ALK$^+$ macrophage population may have in regulating metastasis in the MMTV-PyMT model. When I examined the P-ALK$^+$ macrophages in the lung, I found that this macrophage population is completely absent from the lungs of wild-type mice (Figure 3.9 (B)). Furthermore, there is a significant population of P-ALK$^+$ macrophages in the lungs of MMTV-PyMT mice treated with C44, however, this population is decreased in mice treated with crizotinib alone or in combination with mcr84 (Figure 3.9 (A&B)). Interestingly, when I combined the use of CD31, P-ALK, and DAPI staining to visualize metastatic lesions in the lung, I found that P-ALK$^+$ macrophages cluster around micrometastatic lesions (Figure 3.9 (C)). Using PyMT mRNA as a measure of tumor burden, I found that metastatic burden is reduced significantly in animals treated with crizotinib (Figure 3.9 (D)). This was unexpected, as crizotinib had no effect or primary tumor burden (Figure 3.6 (A)). Furthermore, mcr84, which does reduce primary tumor burden (Figure 3.6 (A)),

does not reduce metastatic burden (Figure 3.9 (D)). Importantly the combination of mcr84 and crizotinib reduces primary tumor burden (Figure 3.6 (A)) and significantly reduces metastatic tumor burden in the MMTV-PyMT model (Figure 3.9 (D)). In fact, metastatic tumor burden is reduced 5-fold when compared to metastatic burden at the start of therapy (fold change of 1.0 vs. 0.22) (Figure 3.9 (D)), suggesting that combination therapy not only prevents further metastatic growth but also reduces the burden of already disseminated disease.

To further analyze the function of P-ALK$^+$ macrophages in metastasis, I moved to an *in vitro* invasion assay. In this assay, the ability macrophages to promote Met-1 tumor cell invasion was examined. Neither PTN nor crizotinib promote Met-1 cell invasion (Figure 3.9 (E)). However, PTN- stimulated RAW 264.7 cells significantly increase Met-1 cell invasion compared to RAW 264.7 cells stimulated with serum-free media. Furthermore, this increase in tumor cell invasion is inhibited when cells are treated with the combination of PTN and crizotinib (Figure 3.9 (F)). Crizotinib treatment has no effect on the ability of RAW 264.7 cells to stimulate Met-1 cell invasion in the absence of PTN (Figure 3.9 (F)). This data suggests that P-ALK$^+$ macrophages may promote tumor cell invasion *in vivo* during the metastatic processes of intravasation, extravasation, or both.

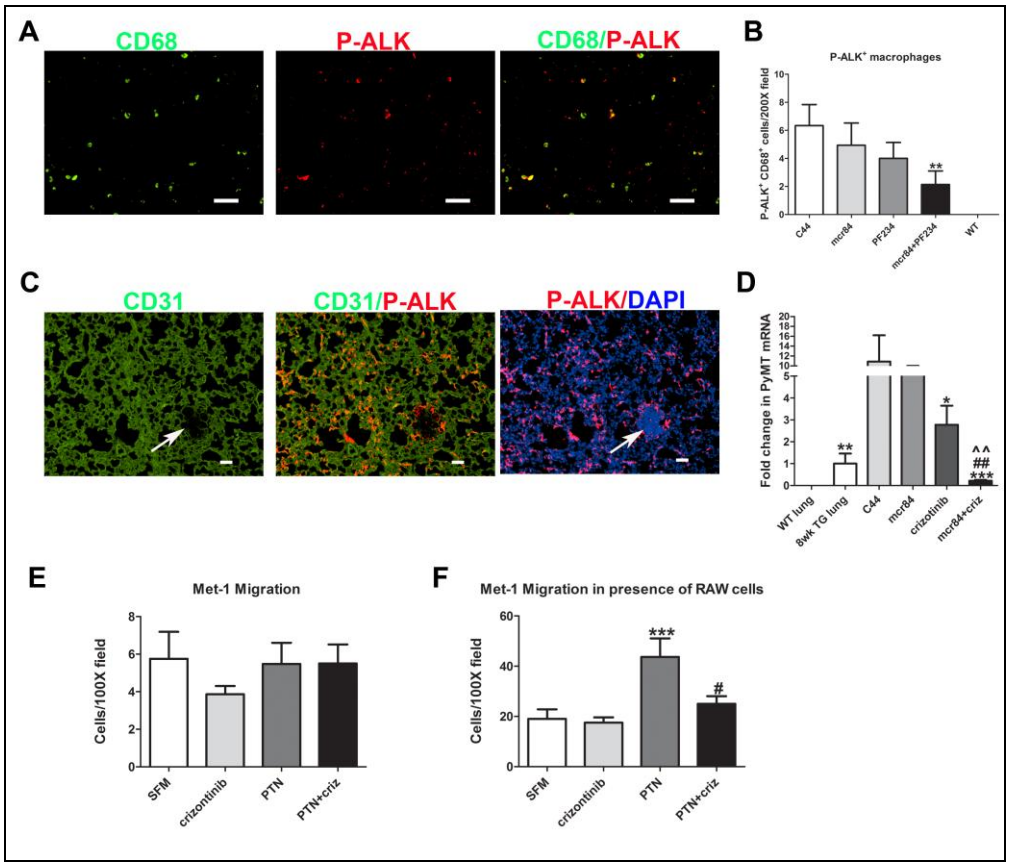

Figure 3.9 Crizotinib reduces PTN-induced ALK phosphorylation and metastatic tumor burden alone and in combination with mcr84 in the MMTV-PyMT breast cancer model. Mice were sacrificed at 12 weeks of age, following 4 weeks of therapy. Lung tissue was snap frozen in liquid nitrogen and stained for CD68, P-ALK (A&B), and CD31, P-ALK, ©. Data are displayed as mean ± SEM and represents a minimum of 5 images (Total magnification, 200X (A); 100X (C)) per tumor and four tumors per group. Images were analyzed using Elements software. *p=0.05, **p=0.01, ***p<0.001 vs. C44, Mann-Whitney test. Scale bar = 50 µm. (D) RNA was harvested from the entire left lobe of the lung, DNAse treated, and subjected to RT-Qpcr using primers specific for PyMT Mrna. Data are displayed as mean ± SEM and represents a minimum of 4-6 animals/per group *p=0.05, **p=0.01, vs. control; $^{\#\#}$p=0.01, vs. mcr84; ^^p=0.01 vs. crizotinib, Mann-Whitney test. (D) 20, 000 Met-1 cell were added to the top of a gelatin-coated transwell insert and allowed to invade overnight towards PTN (250 ng/ml), crizotinib (2 µM) or the combination of PTN and crizotinib. (E) 50,000 RAW 264.7 cells were plated and allowed to adhere 18 hours in the presence of DMEM+5% FBS. Serum-containing media was removed and cells were placed in SFM containing PTN (250 ng/ml), crizotinib (2 µM) or the combination of PTN and crizotinib overnight. The stimulatory media was removed and replaced with SFM 6 hours prior to the addition of gelatin-coated inserts. 20, 000 Met-1 cells were added to the top of the inserts and allowed to invade overnight. Inserts were fixed in methanol and mounted bottom-up using Prolong Gold plus DAPI. Data are displayed as mean ± SEM and represents a minimum of 20 images (Total magnification, 100X) per group, performed in triplicate. Images were analyzed using Elements software. ***p<0.001 vs. SFM; $^{\#}$p=0.05 vs. PTN, Mann-Whitney test.

3.3 Discussion

Our analysis of PTN and anti-inflammatory macrophage levels during the course of tumor progression reveals a sharp increase in both entities at the 8-10 week time point (Figure 3.1). Previous studies (Lin et al. 2003) as well as our own histological analysis (Figure 2.9) demonstrate that this is the time period when lesions are progressing from hyperplastic or adenoma/MIN lesions to invasive carcinoma. Total macrophage depletion using the CSF-$1^{op/op}$ model delays progression to malignancy, indicating that macrophages are involved in disease progression in the MMTV-PyMT model (Lin et al. 2006). My data indicates that not only macrophage number but also macrophage phenotype is regulated during the course of tumor progression (Figure 3.1). Furthermore, the positive correlations between PTN expression and anti-inflammatory macrophage levels during the course of tumor progression along with previous publications citing PTN's ability to promote the expression of VEGFR2 on macrophages (Sharifi et al. 2006; Dineen et al. 2008; Chen et al. 2009), strongly suggest that PTN is regulator of macrophage phenotype in the tumor microenvironment.

We have reported previously VEGFR2 expression on tumor-associated and systemic macrophages harvested from animals bearing pancreatic (Dineen et al. 2008) and breast (Roland et al. 2009) orthotopic xenografts. In this study, I identified the $VEGFR2^{+}$ macrophage population in a spontaneous,

immunocompetent breast cancer model (Figure 3.2). For the first time, I also further characterized the tumor-associated VEGFR2^{+} macrophage population and found that they exhibit an anti-inflammatory expression profile (Figure 3.2 (B)). Furthermore, peritoneal macrophages harvested from MMTV-PyMT mice exhibit increased expression of VEGFR2 and the anti-inflammatory marker MMR (Figure 3.2 (D)), providing evidence that VEGFR2 expression coincides with anti-inflammatory marker expression not only in the tumor but also in systemic macrophages from tumor-bearing animals.

We and others have shown that PTN induces the expression of VEGFR2 on macrophages *in vitro* (Sharifi et al. 2006; Dineen et al. 2008; Chen et al. 2009). While others have reported this phenomenon as the transdifferentiation of macrophages into endothelial cells, I have found that these cells continue to express F4/80 (Figure 3.2 (B)) and represent a subpopulation of macrophages rather than endothelial cells. In this study, I demonstrate that PTN has a significant impact on macrophage phenotype *in vitro*. PTN increases VEGFR2 expression and anti-inflammatory macrophage marker expression (Figure 3.3). Furthermore, I provide novel evidence that PTN modulates macrophage phenotype in an ALK-dependent manner (Figure 3.3). In addition, extensive cytokine anaylsis suggests that PTN directly regulates macrophage phenotype rather than acting through a secondary cytokine mediator, as cytokines known to induce an anti-inflammatory phenotype (IL-4, IL-10, IL-13) are not regulated

following PTN-stimulation (Table 3.1). Furthermore, none of the 32 cytokines analyzed changed in a manner that was correlative with the changes in VEGFR2 or MMR expression observed following treatment with PTN (Table 3.1). However, it is possible that PTN regulates the expression of a cytokine not examined in this study and it is this unidentified cytokine that potentiates an anti-inflammatory macrophage phenotype following PTN stimulation.

In this study, I provide evidence that blockade of VEGF-A induced activation of VEGFR2 decreases macrophage infiltration but increases PTN expression and $VEGFR2^{+}$ anti-inflammatory macrophage levels in two immunocompetent breast cancer models (Figure 3.4, Figure 3.9) (Roland et al. 2009). Furthermore, treatment with the combination of mcr84 and crizotinib abrogates these anti-inflammatory macrophage increases in the MMTV-PyMT model (Figure 3.9). Other studies have demonstrated reduced disease progression and angiogenesis following macrophage depletion in pre-clinical breast cancer models (Lin et al. 2001; Lin et al. 2006; Wyckoff et al. 2007; Aharinejad et al. 2009; Abraham et al. 2010), however, no studies have measured the therapeutic efficacy of preventing the pro-inflammatory to anti-inflammatory macrophage switch. In this study, I report that primary tumor burden is reduced in animals treated with mcr84 alone and in combination with crizotinib (Figure 3.6 (A)). *In vitro* analysis confirms that the IC_{50} for crizotinib is relatively high for both Met-1 cells and macrophages (1.7 and 0.86 μM, respectively) (Figure 3.6 (B)). These

values are well above the maximum achievable *in vivo* concentration of 0.500 µM (data not shown). ALK phosphorylation is inhibited at *in vivo* concentrations of 0.100 µM, which I am able to sustain at the 50/mg/kg/day dose (data not shown), suggesting that any anti-tumor effects seen are due to regulation of macrophage phenotype rather than direct effects on tumor cell or macrophage survival.

Tumors from animals treated with the combination of mcr84 and crizotinib appear to be less invasive when compared to tumors from other treatment groups, and much of the ductal structure and surrounding basement membrane is intact (Figure 3.5 C&D)). Interestingly, crizotinib does not significantly alter tumor histology when used as a single agent, despite reducing angiogenesis (Figure 3.5 (C&D); Figure 3.6). In the MMTV-PyMT model approximately 90% of P-ALK^{+} cells are macrophages (data not shown). Furthermore, macrophages regulate the angiogenic switch in this model (Lin et al. 2006), suggesting that crizotinib indirectly affects angiogenesis by modulating macrophage phenotype. In contrast, total macrophage depletion slows disease progression and angiogenesis (Lin et al. 2001; Lin et al. 2006; Wyckoff et al. 2007; Aharinejad et al. 2009; Abraham et al. 2010). Close examination of anti-inflammatory macrophage levels following treatment with control IgG and crizotinib reveals that ALK phosphorylation, MMR expression, and YM-1 expression are not significantly inhibited in tumors from crizotinib treated mice (Figure 3.9). However, crizotinib potently inhibits the increase in anti-

inflammatory marker expression induced by mcr84 treatment (Figure 3.9). This phenomenon is puzzling and may suggest that a higher dose of crizotinib is needed to decrease ALK phosphorylation in a subpopulation of macrophages of the tumor microenvironment. In contrast to other anti-inflammatory macrophage markers, crizotinib significantly reduces VEGFR2 expression on tumor associated macrophages as a single agent, indicating that VEGFR2 expression may be more sensitive to ALK inhibition compared to other anti-inflammatory macrophage markers (Figure 3.9). The failure of crizotinib to significantly modulate anti-inflammatory marker expression *in vivo* may explain the lack of change in tumor histology following treatment with this agent. In this experiment, the dose of crizotinib used was 50 mg/kg/day, however, I have found that mice can tolerate doses up to 150 mg/kg/day and expect that I could see a significant decrease in P-ALK^{+}, MMR^{+}, YM-1^{+} macrophages and delayed tumor progression with single agent crizotinib at this dose.

Clinical data confirm that macrophage infiltration confers a worse prognosis for many cancer types, including breast cancer (Leek et al. 1996; Bingle et al. 2002; Leek and Harris 2002). Furthermore, a wealth of pre-clinical data demonstrates that macrophages are intimately involved in metastasis in multiple pre-clinical breast cancer models (Lin et al. 2001; Wyckoff et al. 2007; Aharinejad et al. 2009; Qian et al. 2009; Abraham et al. 2010). Macrophages assist tumor cells in every step of the metastatic cascade. Multiphoton microscopy

has allowed for the direct visualization of tumor cell intravasation in the MMTV-PyMT transgenic breast cancer model; interestingly tumor cell intravasation occurs in direct association with perivascular macrophages (Wyckoff et al. 2007). Furthermore, genetic depletion of macrophages significantly reduces tumor cell invasion into the vasculature (Wyckoff et al. 2007). Macrophages are also mediators of tumor cell extravasation, seeding, and growth at the metastatic site in animal models of breast cancer metastatsis (Qian et al. 2009). Perivascular macrophages at the metastatic site recognize extravasating tumor cells, physically interact with them, and assist their invasion into the lung (Qian et al. 2009). Macrophage depletion using genetic or chemical means significantly reduces tumor cell seeding of the metastatic site, suggesting macrophage involvement in this process is critical.

When I examined the P-ALK^{+} macrophages in the lung, I found that this macrophage population is completely absent from the lungs of wild-type mice (Figure 3.9 (B)). Furthermore, there is a significant population of P-ALK^{+} macrophages in the lungs of MMTV-PyMT mice treated with control IgG, however, this population is decreased in mice treated with crizotinib alone or in combination with mcr84 (Figure 3.9 (A&B)).

Metastatic burden is reduced significantly in animals treated with crizotinib (Figure 3.9 (D)). This was unexpected, as crizotinib has no effect or

primary tumor burden or histology (Figure 3.6). These data suggest that even partial inhibition of P-ALK^{+} macrophage infiltration into the lung (Figure 3.9 (D)) is sufficient to decrease metastatic spread in the MMTV-PyMT model. Furthermore, mcr84 does not significantly reduce metastatic burden (Figure 3.9 (D)). Recent studies have demonstrated an increase in tumor cell invasion and metastasis following anti-VEGF therapy in both clinical and pre-clinical models, however, I did not see this phenomenon following treatment with mcr84 (Figure 3.9 (D)) (Ebos et al. 2009; Paez-Ribes et al. 2009; de Groot et al. 2010; Keunen et al. 2011). While mcr84 does not significantly alter tumor histology or decrease metastatic burden as a single agent, it also does not increase metastatic burden, despite increasing the number of anti-inflammatory macrophages. It is important to note that the effects of anti-VEGF therapy extend far beyond its effects on endothelial cells and even macrophages. We have previously reported a reduction in MDSCs and Tregs following therapy with mcr84 in the MMTV-PyMT model, which may impact the metastatic potential of tumor cells (Roland et al. 2009). Furthermore, We have shown previously that when VEGFR2 is expressed, it becomes the primary receptor driving VEGF induced macrophage chemotaxis. Specific inhibition of the VEGF:VEGFR2 signaling axis is sufficient to inhibit macrophage migration *in vitro* and *ex vivo* and macrophage infiltration *in vivo* (Figure 3.9 (A)) (Dineen et al. 2008; Roland et al. 2009; Roland et al. 2009). Together this data suggests that anti-VEGF therapy reduces macrophage

infiltration into the tumor, however, compensating expression of PTN can promote VEGFR2 expression and an anti-inflammatory phenotype in those macrophages that are either (1) in the tumor prior to therapy or (2) migrate into the tumor in response to a non-VEGF cytokine. Furthermore, I do not see an increase in the number of P-ALK$^+$ macrophages in the lungs of mice treated with mcr84 (Figure 3.9 (B)), which may explain why there is no increase in metastatic burden in these animals. While P-ALK$^+$ cells are 2-fold more abundant in the primary tumors of mcr84 treated vs. control IgG treated animals (6.2 vs. 13.1 cells/200X field, respectively) (Figure 3.8 (D)), there are slightly fewer P-ALK$^+$ cells in the lungs of mcr84 treated animals (Figure 3.9 (B)). It is possible that mcr84 inhibits the homing of VEGFR2$^+$ macrophage to the lung through inhibition of the VEGF:VEGFR2 signaling axis.

The combination of mcr84 and crizotinib reduces primary tumor burden (Figure 3.6 (A)) and significantly reduces metastatic tumor burden in the MMTV-PyMT model (Figure 3.9 (D)). In fact, metastatic tumor burden is reduced 5-fold when compared to metastatic burden at the beginning of therapy (fold change of 1.0 vs. 0.22) (Figure 3.9 (D)), suggesting that combination therapy prevents further metastatic growth and reduces the burden of already disseminated disease. This data indicates that metastatic burden can be decreased by targeting the VEGF and ALK signaling pathways.

To further analyze the function of P-ALK$^+$ macrophages in metastasis, I moved to an *in vitro* invasion assay. PTN- stimulated macrophages significantly increase Met-1 cell invasion and this invasion is inhibited when cells are treated with the combination of PTN and crizotinib (Figure 3.9 (F)). Furthermore, crizotinib treatment has no effect on the ability of macrophages to stimulate Met-1 cell invasion in the absence of PTN (Figure 3.9 (F)). It is important to note that while PTN-stimulated macrophages increase tumor cell invasion to a greater degree than unstimulated cells, even unstimulated macrophages promote tumor cell invasion compared to SFM alone (Figure 3.9 (E&F)). This data suggests that P-ALK$^+$ macrophages may promote tumor cell invasion during the metastatic processes of intravasation or extravasation or both.

In conclusion, our data suggest a working model whereby VEGF binding to VEGFR1 on the surface of tumor cells promotes the expression of PTN. Once expressed, PTN stimulates ALK phosphorylation on tumor associated macrophages. These macrophages express YM-1, ARG, MMR, and VEGFR2 and promote anti-inflammation, angiogenesis, immune tolerance, and metastatsis. Importantly, these phenomena can be inhibited using either ALK siRNA or the RTKi crizotinib, which is currently in Phase III clinical trials for the treatment of lung cancer (Figure 3.10).

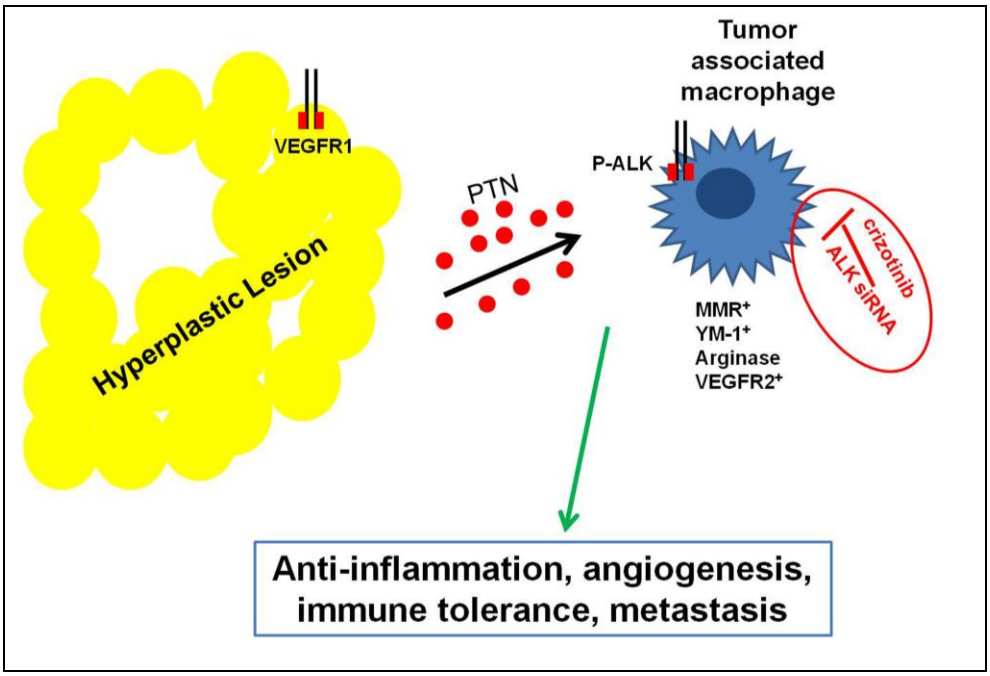

Figure 3.10. The pleiotrophin – ALK signaling axis promotes an anti-inflammatory and pro-metastatic macrophage phenotype in murine models of breast cancer. VEGF activates VEGFR1 on tumor cells, inducing PTN expression. PTN leads to ALK phosphorylation and the expression of MMR, YM-1, ARG, and VEGFR2 on tumor associated macrophages. These macrophages are anti-inflammatory and promote angiogenesis, immune tolerance and metastasis. Importantly, the PTN-induced changes in macrophage characteristics can be inhibited by either ALK siRNA or crizotinib.

CHAPTER FOUR

CONCLUSIONS AND FUTURE DIRECTIONS

4.1 Conclusions

The evidence for immune cell involvement in tumor progression and metastasis is compelling in human breast cancer and mouse pre-clinical breast cancer models. Macrophages are one of the most studied immune cell types in the context of breast cancer and a wealth of data indicates that these cells promote tumor progression and metastasis. However, macrophages are a diverse population of cells and classifying these into anti-tumor *versus* pro-tumor subpopulations is difficult. This has become increasing clear as even blockade of the pro-inflammatory macrophage cytokine CCL2 (MCP-1) is able to inhibit metastasis in mouse models of breast cancer (Qian et al. 2011). My data indicate that PTN signals through ALK to promote an anti-inflammatory macrophage phenotype and blockade of this pathway reduced metastasis in the MMTV-PyMT

model of breast cancer. This is exciting as the ALK inhibitor used in my studies, crizotinib, is expected to receive FDA approval within the year for the treatment of lung cancer patients harboring the ELM4-ALK fusion protein. My data suggests that crizotinib may be used in combination with anti-VEGF and/or chemotherapy to reduce metastatic disease in breast cancer patients.

4.2 Future Directions

Crizotinib inhibits not only ALK but also c-Met, a receptor tyrosine kinase involved in epithelial to mesenchymal transition (EMT) and tumor cell invasion [reviewed in (Elliott et al. 2002)]. The c-Met ligand, hepatocyte growth factor (HGF), and c-Met are overexpressed in a number of invasive cancer types, including breast cancer [reviewed in (Tuck et al. 1996)]. HGF and c-Met are expressed in the MMTV-PyMT transgenic breast cancer model and by Met-1 cells at the mRNA level, however, these levels do not change following treatment with mcr84, crizotinib, or the combination of mcr84 and crizotinib (data not shown). Studies are currently underway to evaluate the levels of c-Met and phosphorylated c-Met in MMTV-PyMT tumors from each treatment group. I cannot rule out that c-Met inhibition by crizotinib may contribute to the anti-metastatic effects observed in this study until the evaluation of c-Met phosphorylation is complete. However, evaluation of the epithelial marker E-cadherin and the mesenchymal marker vimentin in tumors from mice in each

treatment group reveal that the levels of these proteins do not change. Therefore, crizotinib does not inhibit EMT in this model. Furthemore, histological examination of tumors from crizotinib treated animals indicate that these tumors are as invasive as tumors from control treated mice, providing further evidence that crizotinib has no significant effect on primary tumor progression in the MMTV-PyMT model. In addition, I am currently using an *in vitro* invasion assay to determine whether HGF promotes Met-1 cell invasion and if this invasion can be inhibited with crizotinib at physiologically relevant concentrations.

I have described a novel $VEGFR2^{+}$ $P\text{-}ALK^{+}$ subpopulation of macrophages in multiple mouse models of breast cancer, however, this population of macrophages has not been described in human breast cancer. To determine if the observations made in pre-clinical breast cancer models could be translated to breast cancer patients, I have performed a human breast cancer tissue microarray. PTN expression and $VEGFR2^{+}$ and $P\text{-}ALK^{+}$ macrophages levels were examined in 10 human breast cancer samples of various histology. Preliminary results from this array reveal a significant population of $VEGFR2^{+}$ $P\text{-}ALK^{+}$ tumor-associated macrophages in patients with breast carcinoma, however, this population of macrophages is was not found in the 2 samples of normal human breast tissue examined. Our pre-clinical data suggest that $P\text{-}ALK^{+}$ and $VEGFR2^{+}$ macrophages may be indicators of disease progression and therefore, could be used as prognostic indicators. To demonstrate this, we would require hundreds of tumor

samples from breast cancer patients and a collaborative effort to obtain the treatment status and survival time of these patients.

Recent studies have demonstrated an increase in tumor cell invasion and metastasis following anti-VEGF therapy in both clinical and pre-clinical models, however, I did not see this phenomena following treatment with mcr84 (Ebos et al. 2009; Paez-Ribes et al. 2009; de Groot et al. 2010; Keunen et al. 2011). This is quite perplexing, as the number of anti-inflammatory macrophages is increased significantly in the primary tumor following mcr84 therapy. I do not see an increase in the number of anti-inflammatory macrophages in the lungs of mice treated with mcr84, which may explain why there is no increase in metastatic burden in these animals. It is possible that mcr84 inhibits the homing of $VEGFR2^{+}$ macrophage to the lung through inhibition of the VEGF:VEGFR2 signaling axis.

To determine if VEGFR2 expression is critical for TAM homing to the lung, I have developed at breeding strategy to genetically delete VEGFR2 in macrophages. The lab has obtained $VEGFR2^{lox/lox}$ and LysM Cre mice. These were bred to produce mice with myeloid specific deletion of VEGFR2. and then These mice have now been crossed with $VEGFR2^{lox/lox}$ MMTV-PyMT transgenic mice and the first offspring were born on July 20, 2011. Progeny will include MMTV-PyMT female mice with myeloid specific deletion of VEGFR2 and

littermate control mice, which will carry the MMTV-PyMT transgene and the VEGFR2$^{lox/lox}$ allele but will lack Cre expression. These progeny will be sacrificed at 12 weeks of age and metastatic burden will be assessed using H&E staining and the qPCR metastasis assay. Dr. Michael Dellinger will be overseeing the completion of this project following my departure from the Brekken lab.

I have repeated these studies using the 4T1 inflammatory breast cancer model, however, there were some significant complications. In this study, 10,000 4T1 cells were implanted into the MFP of Balb/C mice. Tumors were allowed to establish for 14 days and then a tumor resection was performed in half of the animals by Dr. Christina Roland. I initiated therapy in all animals on day 15 post tumor cell injection. Animals received either control IgG (C44), mcr84 (i.p. 250 µg/twice weekly), or crizotinib (50/mg/kg/day, 1 mg/day, oral gavage). While I did see a modest decrease in metastatic burden in mice receiving the combination of mcr84 and crizotinib, this decrease did not reach statistical significance (data not shown). When I examined the primary tumor for the expression of the P-ALK^{+} anti-inflammatory macrophages, I found that crizotinib did not decrease ALK phosporylation in this model (Figure 4.1). Dr. Brekken and I consulted Pfizer on this matter and they suggested that in some models it is necessary to use crizotinib at 100 mg/kg/day or 150 mg/kg/day to achieve maximum inhibition of ALK phoshorylation. Therefore, a crizotinib dose escalation study must be performed in the 4T1 model to determine the concentration of crizotinib

necessary to inhibit ALK phosphorylation in this model. Once the optimal dose has been established, the 4T1 resection study described above can be repeated.

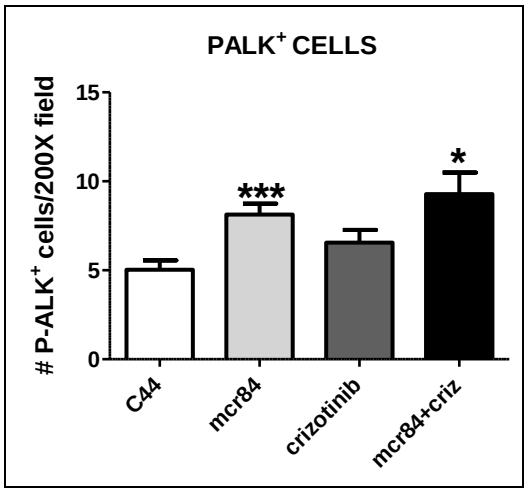

Figure 4.1. Crizotinib (50 mg/kg/day) did not reduce ALK phosphorylation in the 4T1 breast cancer model. Tumor tissue was snap frozen in liquid nitrogen and stained for P-ALK.. Data are displayed as mean ± SEM and represents a minimum of 5 images (Total magnification, 200X) per tumor and four tumors per group. Images were analyzed using Elements software. *p=0.05, **p=0.01, ***p<0.001 vs. C44, Mann-Whitney test.

As mentioned above, recent studies report an increase in tumor cell invasion and metastasis following anti-VEGF therapy. In many of these studies, invasion and metastasis parameters were assayed some time after therapy withdrawal. It may be interesting to repeat the mcr84/crizotinib study in the context of mcr84 withdrawal. More specifically, MMTV-PyMT mice would be given control IgG (C44) or mcr84 for a specific period of time, then therapy

would be withdrawn. At the time of withdrawal, mice in each treatment arm would be randomized to receive either vehicle or crizotinib until the time of sacrifice. I would hypothesize that in this experiment metastatic burden would be increased following withdrawal of mcr84 due to the increased number of anti-inflammatory macrophages that may now home to the lung. Furthermore, crizotinib may be able to prevent this mcr84 induced increase in metastasis by reversing the pro-inflammatory to anti-inflammatory macrophage switch, as we have preliminary data indicating that crizotinib can reduce anti-inflammatory marker expression ex vivo in peritoneal macrophages harvested from animals bearing MMTV-PyMT tumors. This experiment is relevant to the clinical setting where patients generally receive anti-VEGF therapy every 21 days until therapy is withdrawn due to toxicity or tumor progression.

CHAPTER FIVE

MATERIALS AND METHODS

5.1 Chapter One: Materials and Methods

Cell Culture

MDA-MB-231 and MCF-7, and RAW 264.7 cells were obtained from ATCC (Manassas, VA) and maintained accordingly. Tumor conditioned media was obtained by culturing MDA-MD-231 or MCF-7 cells in serum-free Dulbecco's Minimal Essential Media (DMEM) for 48 hours at 80% confluence.

Isolation of peritoneal macrophages

Peritoneal macrophages were collected by washing the peritoneal cavity with ice-cold RPMI medium with pen/strep (10 mL x 2 washes) and collecting the lavage fluid. The lavage fluid from TB (n=3) and NTB (n=3) was pooled and centrifuged at 1000 rpm for 5 min. The cells were plated overnight and washed with PBS the following morning. This procedure yielded cells that were > 95% positive for F4/80. These cells were used for ICC and transwell assays.

Macrophage stimulation

RAW 264.7 (RAW) cells were incubated for 12 hours in chamber slides in the presence or absence of PTN or tumor-conditioned media from MDA-MB-231 or MCF-7 cells. Cells were fixed in fresh acetone and stained using T014 (an anti-VEGFR2 antibody purified in our laboratory, (Feng et al. 2000)).

Histology and immunohistochemical studies

Formalin-fixed, paraffin-embedded tissues were sectioned by molecular pathology core laboratory at the University of Texas Southwestern Medical Center (Dallas, TX). Paraffin-embedded sections were deparaffinized by immersion in xylenes and rehydrated in sequential ethanol. Sections were blocked with 20% Aquablock (East Coast Biologics, North Berwick, ME). Primary antibodies used include: F4/80 (Serotec, Raleigh, NC), T014 (rabbit anti-VEGFR2 purified in our laboratory) (Feng et al. 2000), anti-Mac-3 (Pharmingen, Franklin Lakes, NJ), and anti-PTN (Abcam, Cambridge, MA). The appropriate HRP- or fluorophore conjugated secondary antibody was used (Jackson Immunoresearch, West Grove, PA). Negative controls were performed by omitting the primary antibody. Fluorescent slides were cover-slipped using Prolong with DAPI (Invitrogen, Carlsbad, CA). Sections were examined on a Nikon E600 microscope and images captured with Photometrics coolsnap HQ camera using Metamorph Software.

Migration Assays

Migration assays were done using 24-well plates with 8 μm transwell inserts (Beckton Dickinson Labware, Franklin Lakes, NJ). RAW 264.7 cells were incubated in serum free media ± 100 ng / mL PTN (Sigma) for 6 hours prior to use in the assay 40,000 cells were loaded onto the top of a gelatin coated filter. The cells were allowed to migrate overnight. 40 ng of human VEGF (R&D, Minneapolis, MN) added to the lower chamber was used to stimulate chemotaxis. 2C3 or an isotype matched control antibody (C44) was used at 40 μg/mL. The inserts were fixed and stained using Diff-Quick method (Dade Behring, Newark, DE). Cells were counted in 5-10 high power fields per insert.

Statistics

Data were analyzed using GraphPad software (GraphPad Prism version 4.00 for Windows; GraphPad Software, San Diego C, www.graphpad.com). Results are expressed as mean ± SEM. Differences are analyzed by t-test or ANOVA and results are considered significant at $p < 0.05$.

5.2 Chapter Two: Materials and Methods

Cell Lines, Culture Conditions

The human breast carcinoma cell line MDA-MB-231 and murine breast carcinoma cell line 4T1 were obtained from ATCC (Manassas, VA). Cells were

maintained at 37^{o}C in a mixture of 5% CO_2 and 95% air in DMEM (Invitrogen; Carlsbad, CA; MDA-MB-231 cells) or RPMI 1640 (Invitrogen, Carlsbad, CA; 4T1 cells) supplemented with 10% fetal calf serum (Gemini Bio-Products, Woodland, CA). Cell lines were confirmed to be pathogen free and human cell lines were genotyped to confirm origin prior to implantation into animals.

Animal Tumor Models

6-8 week old female NOD/SCID mice or BALB/c were purchased from an on-campus supplier. The MMTV-PyMT transgenic mice in the FVB background (The Jackson Laboratory, Bar Harbor, ME) express the polyomavirus middle T antigen driven by the MMTV-LTR promoter (Guy et al. 1992). Polyomavirus middle T oncogene expression results in the generation of multifocal mammary carcinomas in 100% of female mice, followed by progression to pulmonary metastases in the vast majority of animals. Only female transgenic mice were used in these experiments and were obtained by breeding transgenic male mice with *wild-type* FVB female mice. Progeny were monitored for transgene expression by PCR analysis. Animals were housed in a pathogen free facility and all animal studies were performed on a protocol approved by the IACUC at the University of Texas Southwestern Medical Center.

5 x 10^6 MDA-MB-231 or 1 x 10^5 4T1 cells were injected into the mammary fat pad (MFP) of SCID or BALB/c mice, respectively using previously described

techniques (Zhang et al. 2002; Whitehurst et al. 2007). Caliper measurements were performed twice weekly and tumor volume was calculated as D x d^2 x 0.52, where D is the long diameter and d is the perpendicular short diameter.

Anti-VEGF therapy (Table 2.1)

Bevacizumab (Avastin®, Genentech, South San Francisco, CA) was purchased from the clinical pharmacy at UT-Southwestern. r84 and mouse chimeric r84 (mcr84) were provided by Peregrine Pharmaceuticals, Inc (Tustin, CA). The production and full characterization of r84, a human IgG1 specific for VEGF-A will be described in detail in a forth-coming manuscript (Sullivan et al). MF-1, a rat IgG specific for VEGFR1 was provided by ImClone Systems (New York, NY). The hybridoma producing RAFL-2, a rat IgG specific for VEGFR2 was obtained from Dr. Philip Thorpe and was produced and purified in our laboratory as described (Ran et al. 2003). GU81, a peptoid that binds and specifically inhibits VEGFR1 and VEGFR2 was produced as described previously (Astle et al. 2008; Udugamasooriya et al. 2008; Udugamasooriya et al. 2008; Udugamasooriya et al. 2008). Sunitinib, a receptor tyrosine kinase inhibitor which inhibits VEGFR1, VEGFR2, PDGFRβ, c-kit, Flt-3, and c-Ret was purchased from LC laboratories (Woburn, MA).

Therapy was initiated on day 26 post tumor cell injection for MDA-MB-231 experiments or day 12 for 4T1 experiments, when tumor volume reached

approximately 150 mm^3 or 15 mm^3, respectively. Therapy in the MMTV-PyMT model was initiated when the mice reached 8 weeks of age. Animals were randomized to receive intraperitoneal injection of IgG control, r84, bevacizumab, MF-1 or RAFL-2 (250 µg of the designated IgG) twice weekly (Tuesday & Friday), GU81 (120 µg daily by intraperitoneal osmotic pump; Alzet, Cupertino, CA), or sunitinib (200 µg/day by oral gavage). Animals were sacrificed at various time points post initiation of therapy: 1 week (MDA-MB-231 (n=4/group) and 4T1 models (n=6/group)), 3 weeks (4T1 model, n=4/group) or 4 weeks (MDA-MB-231 and MMTV-PyMT models; n=4/group). Tumor weights were determined at the time of sacrifice and necropsy.

PCR

RNA was prepared using TRIzol (Invitrogen) according to the manufacturer's instructions. The quality of RNA was evaluated using spectrophotometry. The cDNA used for subsequent for PCR was made using iScript (Bio-Rad Laboratories, Hercules, CA) and Choice DNA Taq polymerase (Denville Scientific, Metuchen, NJ) was used for subsequent PCR reactions. The expression of human *VEGFR1* (Hs00176573_m1), human *VEGFR2* (Hs00176676_m1), human *Nrp-1* (Hs1546494_m1), human *Nrp-2* (Hs00187290_m1), mouse *VEGFR1* (Mm00438980_m1), mouse *VEGFR2* (Mm00440099_m1), mouse *IL-10* (Mm01288386_m1), and mouse *IL-1β* (Mm99999061_m1) was analyzed by

quantitative real-time RT-PCR using an assay on demand (Mm00440111_m1) from Applied Biosystems. *GAPDH* (Applied Biosystems assay-on-demand) was used as an internal reference gene to normalize input cDNA. Quantitative real-time RT-PCR was performed in a reaction volume of 20 µl including 1 µl of cDNA, and each reaction was performed in triplicate. I used the comparative Ct method to compute relative expression values (Karlen et al. 2007). RNA isolated from human dermal microvascular endothelial cells (HDMECs) and murine brain endothelial cell line (bEnd.3) was used a positive control.

Isolation of Peritoneal Macrophages

Peritoneal macrophages were collected 6 weeks after tumor cell injection, by washing the peritoneal cavity with ice-cold RPMI medium with pen/strep (10 ml x 2 washes) and collecting the lavage fluid. The lavage fluid from tumor bearing (TB) (n=3) and non-tumor bearing (NTB) (n=3) was pooled and centrifuged at 1000 rpm for 5 minutes. The cells were plated overnight and washed with PBS the following morning. This procedure yielded cells that were > 95% positive for the macrophage marker F4/80. These cells were used for immunocytochemistry and transwell migration assays.

Migration Assays

Migration assays were done using 24-well plates with either 3 μm (peritoneal macrophages) or 8 μm (MDA-MB-231) transwell inserts (Beckton Dickinson Labware, Franklin Lakes, NJ). 40,000 peritoneal macrophages or 20,000 MDA-MB-231 cells in serum-free media were loaded onto the top of a gelatin coated or Matrigel coated (BD Biosciences, Bedford, MA) filters. Forty ng of VEGF (R&D, Minneapolis, MN) in the presence or absence of the indicated IgG at 40 μg/ml was added to the lower chamber and the cells were allowed to migrate overnight. The inserts were fixed and stained using Diff-Quick (VWR International, West Chester, PA). The number of cells per field (total magnification, 400x macrophages or 100x MDA-MB-231 cells) was counted manually. Each experiment was done in triplicate and 4-5 fields per insert were counted.

Immunohistochemistry

Tissue was snap frozen in liquid nitrogen, embedded in OCT media, and sectioned. Sections were fixed in acetone, briefly air-dried and blocked with 20% Aquablock (East Coast Biologics, North Berwick, ME) for 30-60 minutes. Primary antibodies were used at a final concentration of 5-10 μg/ml and include: rat anti-mouse endothelial cell (MECA-32, Developmental Studies Hybridoma Bank, University of Iowa), rabbit anti-mouse CD31 (abcam, Cambridge, MA), rat anti-endomucin (sc-69495, Santa Cruz Biotechnology, Santa Cruz, CA), goat

anti-F4/80 (sc-26642, Santa Cruz Biotechnology, Santa Cruz, CA), rabbit anti-MPO (HP9048, Cell Sciences, Canton, MA), rat anti-CD68 (AbD Serotec, Raleigh, NC), rat anti-neutrophil, 7/4 (MCA 7716, AbD Serotec, Raleigh, NC), and rat anti-CD83 (Michel-19, BioLegend, San Diego, CA). Primarily conjugated antibodies include PE-labeled Gr1 (RB6-8C5), FITC-labeled CD11b (M1/70), Alexa Fluor® 488-labeled CD11c (N418) from Biolegend (San Diego, CA), Alexa Fluor® 488-labeled CD25 and Phycoerythrin-labeled FoxP3 from eBioscience (San Diego, CA). Primary antibody was incubated on sections for one hour at room temperature or overnight at 4°C. Negative controls were performed by omitting the primary antibody. Following washes, the appropriate fluorophore conjugated secondary antibody was added (Jackson Immunoresearch, West Grove, PA). Fluorescent slides were cover-slipped using Prolong with DAPI (Invitrogen, Carlsbad, CA). Sections were examined on a Nikon E600 microscope and images captured with Photometrics Coolsnap HQ camera using Elements Software. Fluorescent images were captured under identical conditions (exposure time, high and low limits, and scaling). Images were thresholded to exclude background signal from secondary antibody alone.

Histology

Tumor and lung tissue was collected from MMTV-PyMT transgenic female mice at various ages, formalin fixed, paraffin embedded, sectioned, and stained with hematoxylin and eosin (H & E) by the Molecular Pathology Core Laboratory

ELISA/ Electrochemiluminescence

Tumor lysates were made from orthotopic tumors by mincing the tumor in lysis buffer. Protein content was assayed using BCA assay (Pierce, Rockford, IL). Mouse total and active MMP-9, serum IL-1β and IL-6 Quantikine Immunoassays were performed according to manufacturer's instructions (R&D Systems, Minneapolis, MN). Active TGFβ levels were assessed using Promega TGFβ ELISA kit according to the manufacturer's instructions (Promega, Madison, WI). Electrochemiluminescence assays were performed on biological triplicate samples using capture antibody precoated 96-well multispot plates from Meso Scale Discovery (MSD; Gaithersburg, MD). 75 µg-100 µg of total protein was added to each well and incubated with shaking for 4 h at room temperature. Specific protein levels were quantitated by adding 25 µl of 1 µg/ml specific detection antibody labeled with MSD SULFO-TAG reagent to each well and incubated with shaking for 1 h at room temperature. The plate was then washed three times with PBS/0.05% Tween 20 and 150 µl of 2x read buffer was added to each well. Plates were immediately read using the SECTOR Imager 6000, and

data were quantitated using Discovery Workbench and SOFTmax PRO 4.0 software.

Statistics

Data were analyzed using GraphPad software (GraphPad Prism version 4.00 for Windows; GraphPad Software, San Diego, CA, www.graphpad.com). Results are expressed as mean ± SEM. Spearman rank correlations were used to assess associations between immune parameters and cytokine levels. Data was analyzed by t-test or ANOVA and results are considered significant at $p < 0.05$.

5.3 Chapter Three: Materials and Methods

Cell Lines, Culture Conditions

The murine breast carcinoma cell line Met-1 was a kind gift of Dr. Philipp Scherer. Raw 264.7 cells were obtained from ATCC (Manassas, VA). Cells were maintained at 37^{o}C in a mixture of 5% CO_2 and 95% air in DMEM (Invitrogen; Carlsbad, CA) supplemented with 5% fetal calf serum (Gemini Bio-Products, Woodland, CA).

Animal Tumor Models and Treatment

The MMTV-PyMT transgenic mice in the FVB background (The Jackson Laboratory, Bar Harbor, ME) express the polyomavirus middle T antigen driven

by the MMTV-LTR promoter (Guy et al. 1992). Polyomavirus middle T oncogene expression results in the generation of multifocal mammary carcinomas in 100% of female mice, followed by progression to pulmonary metastases in the vast majority of animals. Only female transgenic mice were used in these experiments and were obtained by breeding transgenic male mice with *wild-type* FVB female mice. Progeny were monitored for transgene expression by PCR analysis. Animals were housed in a pathogen free facility and all animal studies were performed on a protocol approved by the IACUC at the University of Texas Southwestern Medical Center.

4-6 week old female BALB/c were purchased from an on-campus supplier. 1 x 10^4 4T1 cells were injected into the mammary fat pad (MFP) of SCID or BALB/c mice, respectively using previously described techniques (Zhang et al. 2002; Whitehurst et al. 2007).

Mouse chimeric r84 (mcr84) were provided by Peregrine Pharmaceuticals, Inc (Tustin, CA). Crizotinib was provided Pfizer (New York, NY). Therapy in the MMTV-PyMT model was initiated when the mice reached 8 weeks of age and continued for 4 weeks. Therapy was initiated on day 15 for 4T1 experiments and continued for 3 weeks. Animals were randomized to receive intraperitoneal injection of IgG control (C44) or mcr84 (250 μg of the designated IgG) twice weekly or crizotinib (50 mg/kg/day by oral gavage (1 mg/day).

Immunohistochemistry

Tissue was snap frozen in liquid nitrogen, embedded in OCT media, and sectioned. Sections were fixed in acetone, briefly air-dried and blocked with 20% Aquablock (East Coast Biologics, North Berwick, ME) for 30-60 minutes. Primary antibodies were used 1:50 to 1:200 and include: goat anti-PTN (ab10849, abcam, Cambridge, MA), rabbit anti-phospho ALK (ab73996, abcam, Cambridge, MA), FITC rat anti-MMR (123006, Biolegend, San Diego, CA), rabbit anti-YM-1(01404, Stem Cell Tech, Vancouver, BC, Canada), rat anti-CD68 (AbD Serotec, Raleigh, NC), rabbit anti-VEGFR2 (2479, Cell Signaling Technology, Danvers, MA), rat anti-mouse endothelial cell (MECA-32, Developmental Studies Hybridoma Bank, University of Iowa), rat anti-endomucin (sc-69495, Santa Cruz Biotechnology, Santa Cruz, CA), rat anti-F4/80 (MCA497, AbD Sertotec, Raleigh, NC), T014 (rabbit anti-VEGFR2 purified in our laboratory) (Feng et al. 2000), rat anti-CD31 (553370, BD Pharminogen, San Diego, CA), and goat anti-Arginase (sc-18351, Santa Cruz Biotechnology). Primary antibody was incubated on sections for one hour at room temperature or overnight at 4°C. Negative controls were performed by omitting the primary antibody. Following washes, the appropriate fluorophore conjugated secondary antibody was added (Jackson Immunoresearch, West Grove, PA). Fluorescent slides were cover-slipped using Prolong with DAPI (Invitrogen, Carlsbad, CA). Sections were examined on a Nikon E600 microscope and images captured with Photometrics Coolsnap HQ

camera using Elements Software. Fluorescent images were captured under identical conditions (exposure time, high and low limits, and scaling). Images were thresholded to exclude background signal from secondary antibody alone.

Flow Cytometry anb Fluorescent Activated Cell Sorting

Tumor lysates were prepared by mincing the tumor in digestion buffer consisting of 1 mg/ml collagenase (Sigma, St. Louis, MO) in DMEM supplemented with 5% FBS and 1X antibiotic/antimycotic (15240-062, Invitrogen). Tumors were incubated for 1 hour at 37° filtered through sequentially smaller filters (BD Biosciences, Franklin Lakes NJ). The single cell suspension was labeled with primary antibody for 30 minutes at 4°C. Antibodies specific for CD11b (FITC, 101206, Biolegend), VEGFR2 (PE, 121906, Biolegend), and F4/80 (APC, MCA497APC, AbD Serotec) were used. Flow cytometry was done on FACSCaliber (BD Biosciences). Cell sorting experiments were performed using a MoFlo Cell Sorter (Beckman Coulter). Propidium iodide (Sigma) positive cells were excluded and gates were adjusted on the negative control. These gates were then applied to tumor lysates. Data analysis was performed using FloJo software (Tree Star Inc, Ashland OR).

PCR

RNA was prepared using TRIzol (Invitrogen) according to the manufacturer's instructions. The quality of RNA was evaluated using spectrophotometry. The cDNA used for subsequent for PCR was made using iScript (Bio-Rad Laboratories, Hercules, CA). The expression of ALK, Dll4, Hes1, MMR, and YM-1 was examined using iQ SYBR Green Supermix (Bio-Rad Laboratories) and the following primer sequences: *ALK*: (5'-AGG TGT ATG AAG GCC AGG TG-3', 5'AGT TCC AGC AGG ATG AAG C-3'); *Dll4*: (5'-CTG TGA GCT GGG ACT CAG CAA G-3', 5'-ATG CTC ACA GTG CTG GCC ATA G-3'); *Hes1*: (5'-GCA GAC ATT CTG GAA ATG ACT GTG A-3', 5'-GAG TGC GCA CCT CGG TGT TA-3'); *YM-1*: (5'-TGA GAT CAC TTA CAC ACA TGA GCA AGA CT-3', 5'-TGT CTT TCT CCA CAG ATT CTT CCT CAA-3';) *MMR*: (5'-AGT TGG GTT CTC CTG TAG CCC AA-3', 5'-ACT ACT ACC TGA GCC CAC ACC TGC T-3'). *B-actin*: (5'-GAC GAG GCC CAG AGC AAG AGA-3', 5'- ACG TAC ATG GCT GGG GTG TTG-3') was used as an internal reference gene to normalize input cDNA. The expression of *PTN* (Mm00436062_m1) and *MMP-9* (Mm00442991_m1) was analyzed by quantitative real-time RT-PCR using an assay on demand (Mm00440111_m1) from Applied Biosystems. *GAPDH* (Applied Biosystems assay-on-demand) was used as an internal reference gene to normalize input cDNA. Quantitative real-time RT-PCR was performed in a reaction volume of 25 µl including 5 µl of

cDNA, and each reaction was performed in triplicate. I used the comparative Ct method to compute relative expression values (Karlen et al. 2007).

Isolation of Peritoneal Macrophages

Peritoneal macrophages were collected from MMTV-PyMT transgenic mice at 12 weeks of age by washing the peritoneal cavity with ice-cold RPMI medium with pen/strep (10 ml x 2 washes) and collecting the lavage fluid. The lavage fluid from tumor bearing (TB) (n=3) and non-tumor bearing (NTB) (n=3) mice was centrifuged at 1000 rpm for 5 minutes. The cells were plated overnight and washed with PBS the following morning. This procedure yielded cells that were > 95% positive for the macrophage marker F4/80. These cells were used for immunocytochemistry.

In vitro Macrophage Assays

RAW 264.7 cells were plated on chamber slides (BD Biosciences) and stimulated overnight with either SFM or PTN (10 ng/ml or 100 ng/ml) in the presence or absence of crizotinib (2 μM) or transfected with either scrambled (SCR) (Qiagen) or ALK siRNA (Integrated DNA Technologies, Coralville, IA) (20 μM) using the N-TER Nanoparticle siRNA transfection system (N2913, Sigma-Aldrich, St. Louis, MO) according to the manufacturer's directions for 48 hours prior to stimulation with SFM or PTN (100 ng/ml) overnight.

Immunocytochemistry

Peritoneal macrophages were plated on chamber slides and maintained overnight at 37^{o}C in a mixture of 5% CO_2 and 95% air in DMEM supplemented with 10% fetal calf serum. RAW 264.7 cells were plated on chamber slides and stimulated as described. Cells were fixed in acetone and blocked with 20% Aquablock for 30-60 minutes. Primary antibodies were used at 1:50-1:100 and included: rabbit anti-INOS (NB120-15323, Novus Biologicals, Littleton, CO), goat anti-CCL2 (MCP-1) (sc-1304, Santa Cruz Biotechnology), FITC rat anti-MMR (123006, Biolegend), rabbit anti-phospho ALK (ab73996, abcam), goat anti-ALK (sc-6346, Santa Cruz Biotechnology), T014, and rabbit anti-VEGFR2 (2479, Cell Signaling Technology) The slides were developed with fluorophore conjugated secondary antibody as described above.

Western Blot Analysis

Tumor lysates were made from MMTV-PyMT tumors by homogenizing the tumor in M-PER Mammalian Protein Extraction Reagent (78501, Thermo Scientific, Rockford, IL). Protein content was assayed using BCA assay (Pierce, Rockford, IL). 30 µg of protein was loaded onto a 10% SDS PAGE gel and transferred to a PVDF membrane. The membrane was blocked using 4% BSA prior to the addition of goat anti-PTN (ab10849, abcam) at 0.2 µg/mL in 4% BSA. HRP-labeled secondary antibody was used at 1:10,000. SuperSignal West Dura

Chemiluminescent Substrate was used for development (34076, Thermo Scientific). Image J software was used to analyze the relative PTN expression (PTN pixels/actin pixels) for each sample.

Histology

Tumor and lung tissue was collected from MMTV-PyMT transgenic female mice, formalin fixed, paraffin embedded, sectioned, and stained with hematoxylin and eosin (H & E) or Trichrome by the Molecular Pathology Core Laboratory.

Assay of PTN expression in Met-1 cells

Met-1 cells were allowed to reach 70% confluence prior placement in SFM in the presence or absence of VEGF-A (50 ng/ml) (293-VE-050, R&D Systems, Minneapolis, MN), VEGF-B (50 ng/ml) (751-VE-025, R&D Systems), Control antibody (XTL) (Peregrine Pharmaceuticals, Inc), r84, or a VEGFR1 neutralizing antibody (AF471, R&D Systems). RNA was isolated following 48 hours treatment. PTN levels were assessed using RT-qPCR as described above.

Milliplex Cytokine Array

Tumor lysates were made from MMTV-PyMT tumors by homogenizing the tumor in M-PER Mammalian Protein Extraction Reagent and protein content was assayed using BCA assay. Analysis of 32 mouse cytokines was performed on biological quadruplicate samples using the Milliplex Cytokine Array

(MPXMCYTO-70K, Millipore, Billerica, MA) according to the manufacturer's directions. 10 µg of total protein was added to each well. The assay was read using a Luminex 200 and 3.1 xPONENT software. Analysis was performed using Milliplex Analyst software.

Metastasis Assay

RNA was isolated from the left lobe of the lung using TRIzol (Invitrogen) according to the manufacturer's instructions. Any contaminating DNA was removed using DNA free (AM1906, Ambion,). The quality of RNA was evaluated using spectrophotometry. The cDNA used for subsequent for PCR was made using iScript (Bio-Rad Laboratories, Hercules, CA). The expression of PyMT mRNA in the lung was examined using iQ SYBR Green Supermix (Bio-Rad Laboratories) and the following primer sequences: 5'- CTC CAA CAG ATA CAC CCG CAC ATA CT-3', 5'-GCT GGT CTT GGTT CGC TTT CTG GAT AC-3'. Lung tissue from WT mice was used as a negative control.

Migration Assay

50,000 RAW 264.7 cells were plated and allowed to adhere 18 hours in the presence of DMEM + 5% FBS. Serum-containing media was removed and cells were placed in SFM containing PTN (250 ng/ml), crizotinib (2 µM) or the combination of PTN and crizotinib overnight. The stimulatory media was

removed and replaced with SFM 6 hours prior to the addition of gelatin-coated inserts. 20, 000 Met-1 cells were added to the top of the inserts and allowed to migrate overnight. Inserts were fixed in methanol, removed from the transwells and mounted bottom-up using Prolong Gold plus DAPI.

REFERENCES

(2009). "American Cancer Society: Cancer Facts and Figures 2009." Atlanta, GA: American Cancer Society.

(2009). Nexavar (sorafenib) package insert, 17.5 FDA-approved patient labeling; Bayer Healthcare Pharmaceuticals Inc. West Haven, CT, USA.

Abraham, D., et al. (2010). "Stromal cell-derived CSF-1 blockade prolongs xenograft survival of CSF-1-negative neuroblastoma." Int J Cancer 126(6): 1339-1352.

Achen, M. G., et al. (1998). "Vascular endothelial growth factor D (VEGF-D) is a ligand for the tyrosine kinases VEGF receptor 2 (Flk1) and VEGF receptor 3 (Flt4)." Proc Natl Acad Sci U S A 95(2): 548-553.

Adams, D. O. (1989). "Molecular interactions in macrophage activation." Immunol Today 10(2): 33-35.

Aharinejad, S., et al. (2009). "Targeting stromal-cancer cell interactions with siRNAs." Methods Mol Biol 487: 243-266.

Allavena, P., et al. (2008). "The Yin-Yang of tumor-associated macrophages in neoplastic progression and immune surveillance." Immunol. Rev. 222: 155-161.

Alon, T., et al. (1995). "Vascular endothelial growth factor acts as a survival factor for newly formed retinal vessels and has implications for retinopathy of prematurity." Nat Med 1(10): 1024-1028.

Amano, K., et al. (2004). "Mechanism for IL-1 beta-mediated neovascularization unmasked by IL-1 beta knock-out mice." J Mol Cell Cardiol 36(4): 469-480.

Amet, L. E., et al. (2001). "Enhanced hippocampal long-term potentiation in mice lacking heparin-binding growth-associated molecule." Mol Cell Neurosci 17(6): 1014-1024.

Ancelin, M., et al. (2004). "Vascular endothelial growth factor VEGF189 induces human neutrophil chemotaxis in extravascular tissue via an autocrine amplification mechanism." Lab. Invest. 84(4): 502-512.

Ancelin, M., et al. (2004). "Vascular endothelial growth factor VEGF189 induces human neutrophil chemotaxis in extravascular tissue via an autocrine amplification mechanism." Lab Invest 84(4): 502-512.

Aoki, Y., et al. (1999). "Angiogenesis and hematopoiesis induced by Kaposi's sarcoma-associated herpesvirus-encoded interleukin-6." Blood 93(12): 4034-4043.

Armstrong, D. A., et al. (2004). "Neutrophil chemoattractant genes KC and MIP-2 are expressed in different cell populations at sites of surgical injury." J Leukoc Biol 75(4): 641-648.

Astle, J. M., et al. (2008). "A VEGFR2 Antagonist and Other Peptoids Evade Immune Recognition." Int J Pept Res Ther 14: 223–227.

Balkwill, F. and A. Mantovani (2001). "Inflammation and cancer: back to Virchow?" Lancet 357(9255): 539-545.

Berardi, A. C., et al. (1995). "Basic fibroblast growth factor mediates its effects on committed myeloid progenitors by direct action and has no effect on hematopoietic stem cells." Blood 86(6): 2123-2129.

Bergers, G., et al. (2000). "Matrix metalloproteinase-9 triggers the angiogenic switch during carcinogenesis." Nat. Cell Biol. 2(10): 737-744.

Bilsland, J. G., et al. (2008). "Behavioral and neurochemical alterations in mice deficient in anaplastic lymphoma kinase suggest therapeutic potential for psychiatric indications." Neuropsychopharmacology 33(3): 685-700.

Bingle, L., et al. (2002). "The role of tumour-associated macrophages in tumour progression: implications for new anticancer therapies." J Pathol 196(3): 254-265.

Biswas, S. K., et al. (2006). "A distinct and unique transcriptional program expressed by tumor-associated macrophages (defective NF-kappaB and enhanced IRF-3/STAT1 activation)." Blood 107(5): 2112-2122.

Borowsky, A. D., et al. (2005). "Syngeneic mouse mammary carcinoma cell lines: two closely related cell lines with divergent metastatic behavior." Clin Exp Metastasis 22(1): 47-59.

Brekken, R. A., et al. (1998). "Vascular endothelial growth factor as a marker of tumor endothelium." Cancer Res 58(9): 1952-1959.

Brekken, R. A., et al. (2000). "Selective inhibition of vascular endothelial growth factor (VEGF) receptor 2 (KDR/Flk-1) activity by a monoclonal anti-VEGF antibody blocks tumor growth in mice." Cancer Res 60(18): 5117-5124.

Bunt, S. K., et al. (2006). "Inflammation induces myeloid-derived suppressor cells that facilitate tumor progression." J Immunol 176(1): 284-290.

Bunt, S. K., et al. (2007). "Reduced inflammation in the tumor microenvironment delays the accumulation of myeloid-derived suppressor cells and limits tumor progression." Cancer Res 67(20): 10019-10026.

Burger, J. A. and T. J. Kipps (2006). "CXCR4: a key receptor in the crosstalk between tumor cells and their microenvironment." Blood 107(5): 1761-1767.

Byrd, V. M., et al. (1999). "Fibroblast growth factor-1 (FGF-1) enhances IL-2 production and nuclear translocation of NF-kappaB in FGF receptor-bearing Jurkat T cells." J. Immunol. 162(10): 5853-5859.

Cao, Y., et al. (1998). "Vascular endothelial growth factor C induces angiogenesis in vivo." Proc Natl Acad Sci U S A 95(24): 14389-14394.

Carbon, J. G., Sullivan, L.A., Lynn, K.D., Brekken, R.A. (2007). "Unpulished Data."

Caruelle, D., et al. (2004). "Upregulation of HARP during in vitro myogenesis and rat soleus muscle regeneration." J. Muscle Res. Cell Motil. 25(1): 45-53.

Chambers, A. F., et al. (2002). "Dissemination and growth of cancer cells in metastatic sites." Nat Rev Cancer 2(8): 563-572.

Chang, N. C., et al. (2001). "A macrophage protein, Ym1, transiently expressed during inflammation is a novel mammalian lectin." J Biol Chem 276(20): 17497-17506.

Chang, Y., et al. (2007). "Secretion of pleiotrophin stimulates breast cancer progression through remodeling of the tumor microenvironment." Proc Natl Acad Sci U S A 104(26): 10888-10893.

Chang, Y., et al. (2007). "Secretion of pleiotrophin stimulates breast cancer progression through remodeling of the tumor microenvironment." Proc. Natl. Acad. Sci. U. S. A. 104(26): 10888-10893.

Chen, H., et al. (2009). "Pleiotrophin produced by multiple myeloma induces transdifferentiation of monocytes into vascular endothelial cells: a novel mechanism of tumor-induced vasculogenesis." Blood 113(9): 1992-2002.

Chen, X., et al. (2007). "Interaction of TNF with TNF receptor type 2 promotes expansion and function of mouse CD4+CD25+ T regulatory cells." J Immunol 179(1): 154-161.

Chikatsu, N., et al. (2003). "ALK+, CD30-, CD20- large B-cell lymphoma containing anaplastic lymphoma kinase (ALK) fused to clathrin heavy chain gene (CLTC)." Mod Pathol 16(8): 828-832.

Choudhuri, R., et al. (1997). "An angiogenic role for the neurokines midkine and pleiotrophin in tumorigenesis." Cancer Res 57(9): 1814-1819.

Choudhuri, R., et al. (1997). "An angiogenic role for the neurokines midkine and pleiotrophin in tumorigenesis." Cancer Res. 57(9): 1814-1819.

Christensen, J. G., et al. (2007). "Cytoreductive antitumor activity of PF-2341066, a novel inhibitor of anaplastic lymphoma kinase and c-Met, in experimental models of anaplastic large-cell lymphoma." Mol Cancer Ther 6(12 Pt 1): 3314-3322.

Clauss, M., et al. (1996). "The vascular endothelial growth factor receptor Flt-1 mediates biological activities. Implications for a functional role of placenta growth factor in monocyte activation and chemotaxis." J Biol Chem 271(30): 17629-17634.

Collino, F., et al. (2009). "Epithelial-mesenchymal transition of ovarian tumor cells induces an angiogenic monocyte cell population." Exp. Cell Res. 315(17): 2982-2994.

Courty, J., et al. (1991). "Mitogenic properties of a new endothelial cell growth factor related to pleiotrophin." Biochem. Biophys. Res. Commun. 180(1): 145-151.

Coussens, L. M. and Z. Werb (2002). "Inflammation and cancer." Nature 420(6917): 860-867.

Curiel, T. J., et al. (2004). "Specific recruitment of regulatory T cells in ovarian carcinoma fosters immune privilege and predicts reduced survival." Nat Med 10(9): 942-949.

de Groot, J. F., et al. (2010). "Tumor invasion after treatment of glioblastoma with bevacizumab: radiographic and pathologic correlation in humans and mice." Neuro Oncol 12(3): 233-242.

De Paepe, P., et al. (2003). "ALK activation by the CLTC-ALK fusion is a recurrent event in large B-cell lymphoma." Blood 102(7): 2638-2641.

De Palma, M., et al. (2005). "Tie2 identifies a hematopoietic lineage of proangiogenic monocytes required for tumor vessel formation and a

mesenchymal population of pericyte progenitors." Cancer Cell 8(3): 211-226.

Demetri, G. D., et al. (2006). "Efficacy and safety of sunitinib in patients with advanced gastrointestinal stromal tumour after failure of imatinib: a randomised controlled trial." Lancet 368(9544): 1329-1338.

DeNardo, D. G. and L. M. Coussens (2007). "Inflammation and breast cancer. Balancing immune response: crosstalk between adaptive and innate immune cells during breast cancer progression." Breast Cancer Res. 9(4): 212.

Deuel, T. F., et al. (2002). "Pleiotrophin: a cytokine with diverse functions and a novel signaling pathway." Arch Biochem Biophys 397(2): 162-171.

Dewals, B. G., et al. (2010). "IL-4Ralpha-independent expression of mannose receptor and Ym1 by macrophages depends on their IL-10 responsiveness." PLoS Negl Trop Dis 4(5): e689.

Dieckmann, D., et al. (2001). "Ex vivo isolation and characterization of CD4(+)CD25(+) T cells with regulatory properties from human blood." J. Exp. Med. 193(11): 1303-1310.

Dikov, M. M., et al. (2005). "Differential roles of vascular endothelial growth factor receptors 1 and 2 in dendritic cell differentiation." J Immunol. 174: 215-222.

Dineen, S. P., et al. (2008). "Vascular endothelial growth factor receptor 2 mediates macrophage infiltration into orthotopic pancreatic tumors in mice." Cancer Res 68(11): 4340-4346.

Dineen, S. P., et al. (2008). "Vascular endothelial growth factor receptor 2 mediates macrophage infiltration into orthotopic pancreatic tumors in mice." Cancer Res. 68(11): 4340-4346.

Dirks, W. G., et al. (2002). "Expression and functional analysis of the anaplastic lymphoma kinase (ALK) gene in tumor cell lines." Int J Cancer 100(1): 49-56.

Donovan, D., et al. (1997). "TGF beta-1 regulation of VEGF production by breast cancer cells." Ann. Surg. Oncol. 4(8): 621-627.

Du, X. L., et al. (2007). "Proteomic profiling of proteins dysregulted in Chinese esophageal squamous cell carcinoma." J Mol Med 85(8): 863-875.

DuPre, S. A. and K. W. Hunter, Jr. (2007). "Murine mammary carcinoma 4T1 induces a leukemoid reaction with splenomegaly: association with tumor-derived growth factors." Exp Mol Pathol 82(1): 12-24.

DuPre, S. A., et al. (2007). "The mouse mammary carcinoma 4T1: characterization of the cellular landscape of primary tumours and metastatic tumour foci." Int J Exp Pathol 88(5): 351-360.

Dvorak, H. F. (2002). "Vascular permeability factor/vascular endothelial growth factor: a critical cytokine in tumor angiogenesis and a potential target for diagnosis and therapy." J. Clin. Oncol. 20(21): 4368-4380.

Dvorak, H. F. (2002). "Vascular permeability factor/vascular endothelial growth factor: a critical cytokine in tumor angiogenesis and a potential target for diagnosis and therapy." J Clin Oncol 20(21): 4368-4380.

Ebos, J. M., et al. (2009). "Accelerated metastasis after short-term treatment with a potent inhibitor of tumor angiogenesis." Cancer Cell 15(3): 232-239.

Elliott, B. E., et al. (2002). "The role of hepatocyte growth factor (scatter factor) in epithelial-mesenchymal transition and breast cancer." Can J Physiol Pharmacol 80(2): 91-102.

Ellis, L. M. and D. J. Hicklin (2008). "Pathways mediating resistance to vascular endothelial growth factor-targeted therapy." Clin. Cancer Res. 14(20): 6371-6375.

Ellis, L. M. and D. J. Hicklin (2008). "VEGF-targeted therapy: mechanisms of anti-tumour activity." Nat Rev Cancer 8(8): 579-591.

Ezekowitz, R. A. (1985). "The role of growth factors and interferons in the induction of activated murine macrophages from bone marrow precursors." Immunol Lett 11(3-4): 135-140.

Ezekowitz, R. A. and S. Gordon (1984). "Alterations of surface properties by macrophage activation: expression of receptors for Fc and mannose-terminal glycoproteins and differentiation antigens." Contemp Top Immunobiol 13: 33-56.

Fang, W., et al. (1992). "Pleiotrophin stimulates fibroblasts and endothelial and epithelial cells and is expressed in human cancer." J. Biol. Chem. 267(36): 25889-25897.

Feng, D., et al. (2000). "Ultrastructural localization of the vascular permeability factor/vascular endothelial growth factor (VPF/VEGF) receptor-2 (FLK-1, KDR) in normal mouse kidney and in the hyperpermeable vessels induced by VPF/VEGF-expressing tumors and adenoviral vectors." J Histochem Cytochem 48(4): 545-556.

Feng, G., et al. (2008). "Interferon-gamma conditioning ex vivo generates CD25+CD62L+Foxp3+ regulatory T cells that prevent allograft rejection: potential avenues for cellular therapy." Transplantation 86(4): 578-589.

Ferrara, N. (2004). "Vascular endothelial growth factor: basic science and clinical progress." Endocr Rev 25(4): 581-611.

Ferrara, N. and W. J. Henzel (1989). "Pituitary follicular cells secrete a novel heparin-binding growth factor specific for vascular endothelial cells." Biochem Biophys Res Commun 161(2): 851-858.

Folkman, J. (1971). "Tumor angiogenesis: therapeutic implications." N. Engl. J. Med. 285(21): 1182-1186.

Folkman, J. (1995). "Angiogenesis in cancer, vascular, rheumatoid and other disease." Nat Med 1(1): 27-31.

Folkman, J. (2007). "Angiogenesis: an organizing principle for drug discovery?" Nat Rev Drug Discov 6(4): 273-286.

Fricke, I., et al. (2007). "Vascular endothelial growth factor-trap overcomes defects in dendritic cell differentiation but does not improve antigen-specific immune responses." Clin Cancer Res 13(16): 4840-4848.

Friedman, H. S., et al. (2009). "Bevacizumab alone and in combination with irinotecan in recurrent glioblastoma." J Clin Oncol 27(28): 4733-4740.

Gabrilovich, D. (2004). "Mechanisms and functional significance of tumour-induced dendritic-cell defects." Nat. Rev. Immunol. 4(12): 941-952.

Gabrilovich, D., et al. (1998). "Vascular endothelial growth factor inhibits the development of dendritic cells and dramatically affects the differentiation of multiple hematopoietic lineages in vivo." Blood 92(11): 4150-4166.

Gabrilovich, D. I., et al. (1996). "Production of vascular endothelial growth factor by human tumors inhibitis the functional maturation of dendritic cells." Nat Med 2: 1096-1103.

Gabrilovich, D. I., et al. (1998). "Vascular Endothelial Growth Factor Inhibits the Development of Dendritic Cells and Dramatically affects the Differentiation of Multiple Hematopoietic Lineages In Vivo." Blood 92: 4150-4166.

Gabrilovich, D. I. and S. Nagaraj (2009). "Myeloid-derived suppressor cells as regulators of the immune system." Nat Rev Immunol 9(3): 162-174.

Gabrilovich, D. I., et al. (2001). "Mechanism of immune dysfunction in cancer mediated by immature Gr-1+ myeloid cells." J Immunol 166(9): 5398-5406.

Galkin, A. V., et al. (2007). "Identification of NVP-TAE684, a potent, selective, and efficacious inhibitor of NPM-ALK." Proc Natl Acad Sci U S A 104(1): 270-275.

George, R. E., et al. (2007). "Genome-wide analysis of neuroblastomas using high-density single nucleotide polymorphism arrays." PLoS One 2(2): e255.

George, R. E., et al. (2008). "Activating mutations in ALK provide a therapeutic target in neuroblastoma." Nature 455(7215): 975-978.

Gerber, H. P., et al. (2002). "VEGF regulates haematopoietic stem cell survival by an internal autocrine loop mechanism." Nature 417(6892): 954-958.

Gerber, H. P., et al. (1998). "Vascular endothelial growth factor regulates endothelial cell survival through the phosphatidylinositol 3'-kinase/Akt signal transduction pathway. Requirement for Flk-1/KDR activation." J Biol Chem 273(46): 30336-30343.

Gerber, H. P., et al. (2007). "Mice expressing a humanized form of VEGF-A may provide insights into the safety and efficacy of anti-VEGF antibodies." Proc Natl Acad Sci U S A 104(9): 3478-3483.

Gordon, S. (2003). "Alternative activation of macrophages." Nat Rev Immunol 3(1): 23-35.

Gramage, E. and G. Herradon (2010). "Genetic deletion of pleiotrophin leads to disruption of spinal nociceptive transmission: evidence for pleiotrophin modulation of morphine-induced analgesia." Eur J Pharmacol 647(1-3): 97-102.

Gramage, E., et al. (2010). "The neurotrophic factor pleiotrophin modulates amphetamine-seeking behaviour and amphetamine-induced neurotoxic effects: evidence from pleiotrophin knockout mice." Addict Biol 15(4): 403-412.

Gramage, E., et al. (2010). "Genetic inactivation of pleiotrophin triggers amphetamine-induced cell loss in the substantia nigra and enhances amphetamine neurotoxicity in the striatum." Neuroscience 170(1): 308-316.

Grepin, R. and G. Pages (2010). "Molecular mechanisms of resistance to tumour anti-angiogenic strategies." J. Oncol. 2010: 835680.

Griffin, C. A., et al. (1999). "Recurrent involvement of 2p23 in inflammatory myofibroblastic tumors." Cancer Res 59(12): 2776-2780.

Grunewald, M., et al. (2006). "VEGF-induced adult neovascularization: recruitment, retention, and role of accessory cells." Cell 124(1): 175-189.

Grzelinski, M., et al. (2005). "Ribozyme-targeting reveals the rate-limiting role of pleiotrophin in glioblastoma." Int J Cancer 117(6): 942-951.

Gupta, S., et al. (2007). "Intratumoral FOXP3 expression in infiltrating breast carcinoma: Its association with clinicopathologic parameters and angiogenesis." Acta. Oncol. 46(6): 792-797.

Guy, C. T., et al. (1992). "Induction of mammary tumors by expression of polyomavirus middle T oncogene: a transgenic mouse model for metastatic disease." Mol Cell Biol 12(3): 954-961.

Hagemann, T., et al. (2005). "Macrophages induce invasiveness of epithelial cancer cells via NF-kappa B and JNK." J Immunol 175(2): 1197-1205.

Hanahan, D. and R. A. Weinberg (2000). "The hallmarks of cancer." Cell 100(1): 57-70.

Heiss, C., et al. (2008). "Pleiotrophin induces nitric oxide dependent migration of endothelial progenitor cells." J. Cell. Physiol. 215(2): 366-373.

Heng, D. Y., et al. (2009). "Prognostic factors for overall survival in patients with metastatic renal cell carcinoma treated with vascular endothelial growth factor-targeted agents: results from a large, multicenter study." J. Clin. Oncol. 27(34): 5794-5799.

Hesse, M., et al. (2001). "Differential regulation of nitric oxide synthase-2 and arginase-1 by type 1/type 2 cytokines in vivo: granulomatous pathology is shaped by the pattern of L-arginine metabolism." J Immunol 167(11): 6533-6544.

Hipp, M. M., et al. (2008). "Sorafenib, but not sunitinib, affects function of dendritic cells and induction of primary immune responses." Blood 111(12): 5610-5620.

Hoeben, A., et al. (2004). "Vascular endothelial growth factor and angiogenesis." Pharmacol Rev 56(4): 549-580.

Holloway, S. E., et al. (2006). "Selective blockade of vascular endothelial growth factor receptor 2 with an antibody against tumor-derived vascular endothelial growth factor controls the growth of human pancreatic adenocarcinoma xenografts." Ann Surg Oncol 13(8): 1145-1155.

Hooper, A. T., et al. (2009). "Engraftment and reconstitution of hematopoiesis is dependent on VEGFR2-mediated regeneration of sinusoidal endothelial cells." Cell Stem Cell 4(3): 263-274.

Huang, Y., et al. (2007). "Distinct roles of VEGFR-1 and VEGFR-2 in the abberant hematopoesis associated with elevated levels of VEGF." Blood 110: 624-631.

Huang, Y., et al. (2007). "Distinct roles of VEGFR-1 and VEGFR-2 in the aberrant hematopoiesis associated with elevated levels of VEGF." Blood 110(2): 624-631.

Hurwitz, H., et al. (2004). "Bevacizumab plus irinotecan, fluorouracil, and leucovorin for metastatic colorectal cancer." N Engl J Med 350(23): 2335-2342.

Imai, S., et al. (2009). "Osteocyte-derived HB-GAM (pleiotrophin) is associated with bone formation and mechanical loading." Bone 44(5): 785-794.

Inamura, K., et al. (2008). "EML4-ALK fusion is linked to histological characteristics in a subset of lung cancers." J Thorac Oncol 3(1): 13-17.

Iwahara, T., et al. (1997). "Molecular characterization of ALK, a receptor tyrosine kinase expressed specifically in the nervous system." Oncogene 14(4): 439-449.

Iwamoto, M., et al. (2003). "Prognostic value of tumor-infiltrating dendritic cells expressing CD83 in human breast carcinomas." Int J Cancer 104(1): 92-97.

Iwamoto, M., et al. (2003). "Prognostic value of tumor-infiltrating dendritic cells expressing CD83 in human breast carcinomas." Int J Cancer 104: 92-97.

Jazii, F. R., et al. (2006). "Identification of squamous cell carcinoma associated proteins by proteomics and loss of beta tropomyosin expression in esophageal cancer." World J Gastroenterol 12(44): 7104-7112.

Joyce, J. A. and J. W. Pollard (2009). "Microenvironmental regulation of metastasis." Nat Rev Cancer 9(4): 239-252.

Kaplan, R. N., et al. (2005). "VEGFR1-positive haematopoietic bone marrow progenitors initiate the pre-metastatic niche." Nature 438(7069): 820-827.

Karlen, Y., et al. (2007). "Statistical significance of quantitative PCR." BMC Bioinformatics 8(131): 1-16.

Keunen, O., et al. (2011). "Anti-VEGF treatment reduces blood supply and increases tumor cell invasion in glioblastoma." Proc Natl Acad Sci U S A 108(9): 3749-3754.

Kitayama, J., et al. (1994). "Suppressive effect of basic fibroblast growth factor on transendothelial emigration of CD4(+) T-lymphocyte." Cancer Res. 54(17): 4729-4733.

Ko, J. S., et al. (2009). "Sunitinib mediates reversal of myeloid-derived suppressor cell accumulation in renal cell carcinoma patients." Clin Cancer Res 15(6): 2148-2157.

Konecny, G. E., et al. (2004). "Association between HER-2/neu and vascular endothelial growth factor expression predicts clinical outcome in primary breast cancer patients." Clin Cancer Res 10(5): 1706-1716.

Kopp, H. G., et al. (2009). "Functional heterogeneity of the bone marrow vascular niche." Ann. N. Y. Acad. Sci. 1176: 47-54.

Kuang, D. M., et al. (2009). "Activated monocytes in peritumoral stroma of hepatocellular carcinoma foster immune privilege and disease progression through PD-L1." J Exp Med 206(6): 1327-1337.

Laaroubi, K., et al. (1994). "Mitogenic and in vitro angiogenic activity of human recombinant heparin affin regulatory peptide." Growth Factors 10(2): 89-98.

Lacouture, M. E., et al. (2008). "Evolving strategies for the management of hand-foot skin reaction associated with the multitargeted kinase inhibitors sorafenib and sunitinib." Oncologist 13(9): 1001-1011.

Lamant, L., et al. (2000). "Expression of the ALK tyrosine kinase gene in neuroblastoma." Am J Pathol 156(5): 1711-1721.

Le Beau, M. M., et al. (1989). "The t(2;5)(p23;q35): a recurring chromosomal abnormality in Ki-1-positive anaplastic large cell lymphoma." Leukemia 3(12): 866-870.

Lee, T. H., et al. (2007). "Vascular endothelial growth factor mediates intracrine survival in human breast carcinoma cells through internally expressed VEGFR1/FLT1." PLoS Med. 4(6): e186.

Lee, T. H., et al. (2007). "Vascular endothelial growth factor mediates intracrine survival in human breast carcinoma cells through internally expressed VEGFR1/FLT1." PLoS Med 4(6): e186.

Leek, R. D. and A. L. Harris (2002). "Tumor-associated macrophages in breast cancer." J. Mammary Gland Biol. Neoplasia 7(2): 177-189.

Leek, R. D., et al. (1996). "Association of macrophage infiltration with angiogenesis and prognosis in invasive breast carcinoma." Cancer Res. 56(20): 4625-4629.

Lewis, C. E., et al. (2007). "Tie2-expressing monocytes and tumor angiogenesis: regulation by hypoxia and angiopoietin-2." Cancer Res. 67(18): 8429-8432.

Lewis, C. E. and R. Hughes (2007). "Inflammation and breast cancer. Microenvironmental factors regulating macrophage function in breast tumours: hypoxia and angiopoietin-2." Breast Cancer Res. 9(3): 209.

Liang, Y., et al. (2006). "Vascular endothelial growth factor induces proliferation of breast cancer cells and inhibits the anti-proliferative activity of anti-hormones." Endocr Relat Cancer 13: 905-919.

Lin, E. Y., et al. (2003). "Progression to malignancy in the polyoma middle T oncoprotein mouse breast cancer model provides a reliable model for human diseases." Am J Pathol 163(5): 2113-2126.

Lin, E. Y., et al. (2007). "Vascular endothelial growth factor restores delayed tumor progression in tumors depleted of macrophages." Mol. Oncol. 1(3): 288-302.

Lin, E. Y., et al. (2006). "Macrophages regulate the angiogenic switch in a mouse model of breast cancer." Cancer Res. 66(23): 11238-11246.

Lin, E. Y., et al. (2001). "Colony-stimulating factor 1 promotes progression of mammary tumors to malignancy." J Exp Med 193(6): 727-740.

Lin, Y. L., et al. (2007). "Placental growth factor down-regulates type 1 T helper immune response by modulating the function of dendritic cells." J. Leukoc. Biol. 82(6): 1473-1480.

Linehan, D. C. and P. S. Goedegebuure (2005). "CD25+ CD4+ regulatory T-cells in cancer." Immunol Res 32(1-3): 155-168.

Liyanage, U. K., et al. (2002). "Prevalence of regulatory T cells is increased in peripheral blood and tumor microenvironment of patients with pancreas or breast adenocarcinoma." J Immunol 169(5): 2756-2761.

Lu, K. V., et al. (2005). "Differential induction of glioblastoma migration and growth by two forms of pleiotrophin." J Biol Chem 280(29): 26953-26964.

Lynn, K. D., Roland, C.L., Brekken, R.A. (2010). "VEGF and Pleiotrophin Modulate the Immune Profile of Breast Cancer." Cancers 2(2): 970-988.

Lynn, K. D., et al. (2010). "GU81, a VEGFR2 antagonist peptoid, enhances the anti-tumor activity of doxorubicin in the murine MMTV-PyMT transgenic model of breast cancer." BMC Cancer 10: 397.

Mantovani, A., et al. (1992). "Cytokine regulation of endothelial cell function." FASEB J 6(8): 2591-2599.

Mantovani, A., et al. (2002). "Macrophage polarization: tumor-associated macrophages as a paradigm for polarized M2 mononuclear phagocytes." Trends Immunol 23(11): 549-555.

Martinez, F. O., et al. (2008). "Macrophage activation and polarization." Front Biosci 13: 453-461.

Maruyama, K., et al. (1999). "Interleukin-1 beta upregulates cardiac expression of vascular endothelial growth factor and its receptor KDR/flk-1 via activation of protein tyrosine kinases." J Mol Cell Cardiol 31(3): 607-617.

Mason, D. Y., et al. (1990). "CD30-positive large cell lymphomas ('Ki-1 lymphoma') are associated with a chromosomal translocation involving 5q35." Br J Haematol 74(2): 161-168.

Meng, K., et al. (2000). "Pleiotrophin signals increased tyrosine phosphorylation of beta beta-catenin through inactivation of the intrinsic catalytic activity of the receptor-type protein tyrosine phosphatase beta/zeta." Proc Natl Acad Sci U S A 97(6): 2603-2608.

Miles, D. W., et al. (2010). "Phase III study of bevacizumab plus docetaxel compared with placebo plus docetaxel for the first-line treatment of human epidermal growth factor receptor 2-negative metastatic breast cancer." J Clin Oncol 28(20): 3239-3247.

Miller, K., et al. (2007). "Paclitaxel plus bevacizumab versus paclitaxel alone for metastatic breast cancer." N Engl J Med 357(26): 2666-2676.

Miller, K. D., et al. (2005). "Randomized phase III trial of capecitabine compared with bevacizumab plus capecitabine in patients with previously treated metastatic breast cancer." J Clin Oncol 23(4): 792-799.

Milner, P. G., et al. (1989). "A novel 17 kD heparin-binding growth factor (HBGF-8) in bovine uterus: purification and N-terminal amino acid sequence." Biochem. Biophys. Res. Commun. 165(3): 1096-1103.

Mimura, K., et al. (2007). "Vascular endothelial growth factor inhibits the function of human mature dendritic cells mediated by VEGF receptor-2." Cancer Immunol Immunother 56: 761-770.

Mitsiadis, T. A., et al. (1995). "Expression of the heparin-binding cytokines, midkine (MK) and HB-GAM (pleiotrophin) is associated with epithelial-mesenchymal interactions during fetal development and organogenesis." Development 121(1): 37-51.

Mokoena, T. and S. Gordon (1985). "Human macrophage activation. Modulation of mannosyl, fucosyl receptor activity in vitro by lymphokines, gamma and alpha interferons, and dexamethasone." J Clin Invest 75(2): 624-631.

Morris, S. W., et al. (1994). "Fusion of a kinase gene, ALK, to a nucleolar protein gene, NPM, in non-Hodgkin's lymphoma." Science 263(5151): 1281-1284.

Mosser, D. M. and E. Handman (1992). "Treatment of murine macrophages with interferon-gamma inhibits their ability to bind leishmania promastigotes." J Leukoc Biol 52(4): 369-376.

Motegi, A., et al. (2004). "ALK receptor tyrosine kinase promotes cell growth and neurite outgrowth." J Cell Sci 117(Pt 15): 3319-3329.

Motzer, R. J., et al. (2007). "Sunitinib efficacy against advanced renal cell carcinoma." J. Urol. 178(5): 1883-1887.

Murdoch, C., et al. (2008). "The role of myeloid cells in the promotion of tumour angiogenesis." Nat Rev Cancer 8(8): 618-631.

Nagaraj, S. and D. I. Gabrilovich (2008). "Tumor escape mechanism governed by myeloid-derived suppressor cells." Cancer Res. 68(8): 2561-2563.

Nair, M. G., et al. (2003). "Macrophages in chronic type 2 inflammation have a novel phenotype characterized by the abundant expression of Ym1 and Fizz1 that can be partly replicated in vitro." Immunol Lett 85(2): 173-180.

Nakao, S., et al. (2005). "Infiltration of COX-2-expressing macrophages is a prerequisite for IL-1 beta-induced neovascularization and tumor growth." J Clin Invest 115(11): 2979-2991.

Nakayama, T., et al. (2007). "Effect of fibroblast growth factor 2 on stromal cell-derived factor 1 production by bone marrow stromal cells and hematopoiesis." J. Natl. Cancer Inst. 99(3): 223-235.

Norden, A. D., et al. (2008). "Bevacizumab for recurrent malignant gliomas: efficacy, toxicity, and patterns of recurrence." Neurology 70(10): 779-787.

Nozawa, H., et al. (2006). "Infiltrating neutrophils mediate the initial angiogenic switch in a mouse model of multistage carcinogenesis." Proc. Natl. Acad. Sci. U. S. A. 103(33): 12493-12498.

O'Brien, J., et al. (2010). "Alternatively activated macrophages and collagen remodeling characterize the postpartum involuting mammary gland across species." Am J Pathol 176(3): 1241-1255.

Ochiai, K., et al. (2004). "The role of midkine and pleiotrophin in liver regeneration." Liver Int. 24(5): 484-491.

Ojalvo, L. S., et al. (2009). "High-density gene expression analysis of tumor-associated macrophages from mouse mammary tumors." Am J Pathol 174(3): 1048-1064.

Ojalvo, L. S., et al. (2010). "Gene expression analysis of macrophages that facilitate tumor invasion supports a role for Wnt-signaling in mediating their activity in primary mammary tumors." J Immunol 184(2): 702-712.

Onciu, M., et al. (2003). "ALK-positive plasmablastic B-cell lymphoma with expression of the NPM-ALK fusion transcript: report of 2 cases." Blood 102(7): 2642-2644.

Osada, T., et al. (2008). "The effect of anti-VEGF therapy on immature myeloid cell and dendritic cells in cancer patients." Cancer Immunol. Immunother. 57(8): 1115-1124.

Osada, T., et al. (2008). "The effect of anti-VEGF therapy on immature myeloid cell and dendritic cells in cancer patients." Cancer Immunol Immunother 57(8): 1115-1124.

Outtz, H. H., et al. (2010). "Notch1 deficiency results in decreased inflammation during wound healing and regulates vascular endothelial growth factor receptor-1 and inflammatory cytokine expression in macrophages." J Immunol 185(7): 4363-4373.

Oyama, T., et al. (1998). "Vascular endothelial growth factor affects dendritic cell maturation through inhibiton of nuclear factor-kB activation in hematopoetic progenitor cells." J Immunol 160: 1224-1232.

Ozao-Choy, J., et al. (2009). "The novel role of tyrosine kinase inhibitor in the reversal of immune suppression and modulation of tumor microenvironment for immune-based cancer therapies." Cancer Res 69(6): 2514-2522.

Paez-Ribes, M., et al. (2009). "Antiangiogenic therapy elicits malignant progression of tumors to increased local invasion and distant metastasis." Cancer Cell 15(3): 220-231.

Pahler, J. C., et al. (2008). "Plasticity in tumor-promoting inflammation: impairment of macrophage recruitment evokes a compensatory neutrophil response." Neoplasia 10(4): 329-340.

Palmer, R. H., et al. (2009). "Anaplastic lymphoma kinase: signalling in development and disease." Biochem J 420(3): 345-361.

Pariser, H., et al. (2005). "Fyn is a downstream target of the pleiotrophin/receptor protein tyrosine phosphatase beta/zeta-signaling pathway: regulation of tyrosine phosphorylation of Fyn by pleiotrophin." Biochem Biophys Res Commun 332(3): 664-669.

Pariser, H., et al. (2005). "Pleiotrophin regulates serine phosphorylation and the cellular distribution of beta-adducin through activation of protein kinase C." Proc Natl Acad Sci U S A 102(35): 12407-12412.

Pavlov, I., et al. (2002). "Role of heparin-binding growth-associated molecule (HB-GAM) in hippocampal LTP and spatial learning revealed by studies on overexpressing and knockout mice." Mol Cell Neurosci 20(2): 330-342.

Perez-Pinera, P., et al. (2006). "Pleiotrophin disrupts calcium-dependent homophilic cell-cell adhesion and initiates an epithelial-mesenchymal transition." Proc. Natl. Acad. Sci. U. S. A. 103(47): 17795-17800.

Perez-Pinera, P., et al. (2008). "Pleiotrophin, a multifunctional angiogenic factor: mechanisms and pathways in normal and pathological angiogenesis." Curr Opin Hematol 15(3): 210-214.

Perez-Pinera, P., et al. (2007). "Anaplastic lymphoma kinase is expressed in different subtypes of human breast cancer." Biochem Biophys Res Commun 358(2): 399-403.

Perez-Pinera, P., et al. (2007). "Pleiotrophin, a multifunctional tumor promoter through induction of tumor angiogenesis, remodeling of the tumor microenvironment, and activation of stromal fibroblasts." Cell Cycle 6(23): 2877-2883.

Perez-Pinera, P., et al. (2007). "The receptor protein tyrosine phosphatase (RPTP)beta/zeta is expressed in different subtypes of human breast cancer." Biochem Biophys Res Commun 362(1): 5-10.

Perruche, S., et al. (2008). "CD3-specific antibody-induced immune tolerance involves transforming growth factor-beta from phagocytes digesting apoptotic T cells." Nat. Med. 14(5): 528-535.

Pollard, J. W. (2004). "Tumour-educated macrophages promote tumour progression and metastasis." Nat Rev Cancer 4(1): 71-78.

Pollard, J. W. (2004). "Tumour-educated macrophages promote tumour progression and metastasis." Nat. Rev. Cancer. 4(1): 71-78.

Pollard, J. W. (2008). "Macrophages define the invasive microenvironment in breast cancer." J Leukoc Biol 84(3): 623-630.

Powers, C., et al. (2002). "Pleiotrophin signaling through anaplastic lymphoma kinase is rate-limiting for glioblastoma growth." J Biol Chem 277(16): 14153-14158.

Pradeep, C. R., et al. (2005). "Expression of vascular endothelial growth factor (VEGF) and VEGF receptors in tumor angiogenesis and malignancies." Integr. Cancer Ther. 4(4): 315-321.

Pukrop, T., et al. (2006). "Wnt 5a signaling is critical for macrophage-induced invasion of breast cancer cell lines." Proc Natl Acad Sci U S A 103(14): 5454-5459.

Qian, B., et al. (2009). "A distinct macrophage population mediates metastatic breast cancer cell extravasation, establishment and growth." PLoS One 4(8): e6562.

Qian, B. Z., et al. (2011). "CCL2 recruits inflammatory monocytes to facilitate breast-tumour metastasis." Nature.

Qian, B. Z. and J. W. Pollard (2010). "Macrophage diversity enhances tumor progression and metastasis." Cell 141(1): 39-51.

Qin, F. X. (2009). "Dynamic behavior and function of Foxp3+ regulatory T cells in tumor bearing host." Cell Mol. Immunol. 6(1): 3-13.

Raes, G., et al. (2002). "Differential expression of FIZZ1 and Ym1 in alternatively versus classically activated macrophages." J Leukoc Biol 71(4): 597-602.

Ran, S., et al. (2003). "Evaluation of novel antimouse VEGFR2 antibodies as potential antiangiogenic or vascular targeting agents for tumor therapy." Neoplasia. 5(4): 297-307.

Ranpura, V., et al. (2011). "Treatment-related mortality with bevacizumab in cancer patients: a meta-analysis." JAMA 305(5): 487-494.

Rauvala, H. (1989). "An 18-kd heparin-binding protein of developing brain that is distinct from fibroblast growth factors." EMBO. J. 8(10): 2933-2941.

Reichard, K. K., et al. (2007). "ALK-positive diffuse large B-cell lymphoma: report of four cases and review of the literature." Mod Pathol 20(3): 310-319.

Ribatti, D., et al. (1999). "Endogenous and exogenous fibroblast growth factor-2 modulate wound healing in the chick embryo chorioallantoic membrane." Angiogenesis 3(1): 89-95.

Riegel, A. T. and A. Wellstein (1994). "The potential role of the heparin-binding growth factor pleiotrophin in breast cancer." Breast Cancer Res. Treat. 31(2-3): 309-314.

Rikova, K., et al. (2007). "Global survey of phosphotyrosine signaling identifies oncogenic kinases in lung cancer." Cell 131(6): 1190-1203.

Rini, B. I., et al. (2008). "Bevacizumab plus interferon alfa compared with interferon alfa monotherapy in patients with metastatic renal cell carcinoma: CALGB 90206." J Clin Oncol 26(33): 5422-5428.

Robert, N. J., et al. (2011). "RIBBON-1: randomized, double-blind, placebo-controlled, phase III trial of chemotherapy with or without bevacizumab for first-line treatment of human epidermal growth factor receptor 2-negative, locally recurrent or metastatic breast cancer." J Clin Oncol 29(10): 1252-1260.

Robertson, S., et al. (1999). "Hematopoietic commitment during embryogenesis." Ann. N. Y. Acad. Sci. 872: 9-15; discussion 15-16.

Roger, J., et al. (2006). "Involvement of Pleiotrophin in CNTF-mediated differentiation of the late retinal progenitor cells." Dev. Biol. 298(2): 527-539.

Roland, C. L., et al. (2009). "Inhibition of vascular endothelial growth factor reduces angiogenesis and modulates immune cell infiltration of orthotopic breast cancer xenografts." Mol. Cancer Ther. 8(7): 1761-1771.

Roland, C. L., et al. (2009). "Cytokine levels correlate with immune cell infiltration after anti-VEGF therapy in preclinical mouse models of breast cancer." PLoS One 4(11): e7669.

Roland, C. L., et al. (2009). "Cytokine levels correlate with immune cell infiltration after anti-VEGF therapy in preclinical mouse models of breast cancer." PLoS One.

Rosenkilde, M. M. and T. W. Schwartz (2004). "The chemokine system -- a major regulator of angiogenesis in health and disease." APMIS 112(7-8): 481-495.

Roskoski, R., Jr. (2007). "Vascular endothelial growth factor (VEGF) signaling in tumor progression." Crit Rev Oncol Hematol 62(3): 179-213.

Salnikov, A. V., et al. (2006). "Inhibition of carcinoma cell-derived VEGF reduces inflammatory characteristics in xenograft carcinoma." Int J Cancer 119(12): 2795-2802.

Salnikov, A. V., et al. (2006). "Inhibition of carcinoma cell-derived VEGF reduces inflammatory characteristics in xenograft carcinoma." Int. J. Cancer 119(12): 2795-2802.

Sandler, A., et al. (2006). "Paclitaxel-carboplatin alone or with bevacizumab for non-small-cell lung cancer." N Engl J Med 355(24): 2542-2550.

Sawano, A., et al. (2001). "Flt-1, vascular endothelial growth factor receptor 1, is a novel cell surface marker for the lineage of monocyte-macrophages in humans." Blood 97(3): 785-791.

Scapini, P., et al. (2004). "CXCL1/macrophage inflammatory protein-2-induced angiogenesis in vivo is mediated by neutrophil-derived vascular endothelial growth factor-A." J. Immunol. 172(8): 5034-5040.

Schneider, B. P., et al. (2008). "Association of vascular endothelial growth factor and vascular endothelial growth factor receptor-2 genetic polymorphisms with outcome in a trial of paclitaxel compared with paclitaxel plus bevacizumab in advanced breast cancer: ECOG 2100." J Clin Oncol 26(28): 4672-4678.

Schreiber, S., et al. (1993). "Regulation of mouse bone marrow macrophage mannose receptor expression and activation by prostaglandin E and IFN-gamma." J Immunol 151(9): 4973-4981.

Schulz, C., et al. (2009). "Hematopoietic stem and progenitor cells: their mobilization and homing to bone marrow and peripheral tissue." Immunol. Res. 44(1-3): 160-168.

Selvaraj, S. K., et al. (2003). "Mechanism of monocyte activation and expression of proinflammatory cytochemokines by placenta growth factor." Blood 102(4): 1515-1524.

Senger, D. R., et al. (1990). "Purification and NH2-terminal amino acid sequence of guinea pig tumor-secreted vascular permeability factor." Cancer Res 50(6): 1774-1778.

Serafini, P., et al. (2004). "Derangement of immune responses by myeloid suppressor cells." Cancer Immunol Immunother 53(2): 64-72.

Sharifi, B. G., et al. (2006). "Pleiotrophin induces transdifferentiation of monocytes into functional endothelial cells." Arterioscler. Thromb. Vasc. Biol. 26(6): 1273-1280.

Shepherd, V. L., et al. (1997). "Ingestion of Candida albicans down-regulates mannose receptor expression on rat macrophages." Arch Biochem Biophys 344(2): 350-356.

Shin, J. Y., et al. (2009). "Vascular endothelial growth factor-induced chemotaxis and IL-10 from T cells." Cell Immunol 256(1-2): 72-78.

Shojaei, F., et al. (2007). "Tumor refractoriness to anti-VEGF treatment is mediated by CD11b+Gr1+ myeloid cells." Nat. Biotechnol. 25(8): 911-920.

Shojaei, F., et al. (2007). "Bv8 regulates myeloid-cell-dependent tumour angiogenesis." Nature 450(7171): 825-831.

Silos-Santiago, I., et al. (1996). "Localization of pleiotrophin and its mRNA in subpopulations of neurons and their corresponding axonal tracts suggests important roles in neural-glial interactions during development and in maturity." J. Neurobiol. 31(3): 283-296.

Soda, M., et al. (2007). "Identification of the transforming EML4-ALK fusion gene in non-small-cell lung cancer." Nature 448(7153): 561-566.

Stein, M., et al. (1992). "Interleukin 4 potently enhances murine macrophage mannose receptor activity: a marker of alternative immunologic macrophage activation." J Exp Med 176(1): 287-292.

Strieter, R. M., et al. (2005). "CXC chemokines in angiogenesis relevant to chronic fibroproliferation." Curr Drug Targets Inflamm Allergy 4(1): 23-26.

Strieter, R. M., et al. (2005). "CXC chemokines in angiogenesis." Cytokine Growth Factor Rev 16(6): 593-609.

Sullivan, L. A., et al. (2010). "r84, a novel therapeutic antibody against mouse and human VEGF with potent anti-tumor activity and limited toxicity induction." PLoS One 5(8): e12031.

Szekanecz, Z. and A. E. Koch (2001). "Chemokines and angiogenesis." Curr Opin Rheumatol 13(3): 202-208.

Takagi, S., et al. (2000). "Basic fibroblast growth factor modulates the surface expression of effector cell molecules and primes respiratory burst activity in human neutrophils." Acta. Haematol. 103(2): 78-83.

Tamura, H., et al. (2006). "Protein tyrosine phosphatase receptor type Z is involved in hippocampus-dependent memory formation through dephosphorylation at Y1105 on p190 RhoGAP." Neurosci Lett 399(1-2): 33-38.

Tare, R. S., et al. (2002). "Pleiotrophin/Osteoblast-stimulating factor 1: dissecting its diverse functions in bone formation." J. Bone Miner. Res. 17(11): 2009-2020.

Tsakiri, N., et al. (2008). "Differential effects of interleukin-1 alpha and beta on interleukin-6 and chemokine synthesis in neurones." Mol Cell Neurosci 38(2): 259-265.

Tuck, A. B., et al. (1996). "Coexpression of hepatocyte growth factor and receptor (Met) in human breast carcinoma." Am J Pathol 148(1): 225-232.

Tysnes, B. B. and R. Bjerkvig (2007). "Cancer initiation and progression: involvement of stem cells and the microenvironment." Biochim. Biophys. Acta. 1775(2): 283-297.

Udugamasooriya, D. G., et al. (2008). "A peptoid "antibody surrogate" that antagonizes VEGF receptor 2 activity." J Am Chem Soc 130(17): 5744-5752.

Udugamasooriya, D. G., et al. (2008). "The pharmacophore of a peptoid VEGF receptor 2 antagonist includes both side chain and main chain residues." Bioorg Med Chem Lett 18(22): 5892-5894.

Udugamasooriya, D. G., et al. (2008). "A peptoid antagonist of VEGF receptor 2 recognizes a 'hotspot' in the extracellular domain distinct from the hormone-binding site." Bioorg Med Chem 16(12): 6338-6343.

Vakkila, J. and M. T. Lotze (2004). "Inflammation and necrosis promote tumour growth." Nat Rev Immunol 4(8): 641-648.

van Cruijsen, H., et al. (2007). "Defective differentiation of myeloid and plasmacytoid dendritic cells in advanced cancer patients is not normalized by tyrosine kinase inhibition of the vascular endothelial growth factor receptor." Clin Dev Immunol 2007: 17315.

Vanderwinden, J. M., et al. (1992). "Cellular distribution of the new growth factor pleiotrophin (HB-GAM) mRNA in developing and adult rat tissues." Anat. Embryol. (Berl.) 186(4): 387-406.

Vazin, T., et al. (2009). "A novel combination of factors, termed SPIE, which promotes dopaminergic neuron differentiation from human embryonic stem cells." PLoS One 4(8): e6606.

Vroling, L., et al. (2007). "VEGFR2 expressing circulating (progenitor) cell populations in volunteers and cancer patients." Thromb. Haemost. 98(2): 440-450.

Wang, Y. C., et al. (2010). "Notch signaling determines the M1 versus M2 polarization of macrophages in antitumor immune responses." Cancer Res 70(12): 4840-4849.

Webb, T. R., et al. (2009). "Anaplastic lymphoma kinase: role in cancer pathogenesis and small-molecule inhibitor development for therapy." Expert Rev Anticancer Ther 9(3): 331-356.

Welch, J. S., et al. (2002). "TH2 cytokines and allergic challenge induce Ym1 expression in macrophages by a STAT6-dependent mechanism." J Biol Chem 277(45): 42821-42829.

Whitehurst, B., et al. (2007). "Anti-VEGF-A therapy reduces lymphatic vessel density and expression of VEGFR-3 in an orthotopic breast tumor model." Int J Cancer 121(10): 2181-2191.

Whitehurst, B., et al. (2007). "Anti-VEGF-A therapy reduces lymphatic vessel density and expression of VEGFR-3 in an orthotopic breast tumor model." Int. J. Cancer 121(10): 2181-2191.

Wilhelm, S. M., et al. (2008). "Preclinical overview of sorafenib, a multikinase inhibitor that targets both Raf and VEGF and PDGF receptor tyrosine kinase signaling." Mol Cancer Ther 7(10): 3129-3140.

Wyckoff, J., et al. (2004). "A paracrine loop between tumor cells and macrophages is required for tumor cell migration in mammary tumors." Cancer Res 64(19): 7022-7029.

Wyckoff, J. B., et al. (2007). "Direct visualization of macrophage-assisted tumor cell intravasation in mammary tumors." Cancer Res. 67(6): 2649-2656.

Yang, A. D., et al. (2006). "Vascular endothelial growth factor receptor-1 activation mediates epithelial to mesenchymal transition in human pancreatic carcinoma cells." Cancer Res. 66(1): 46-51.

Yang, L., et al. (2004). "Expansion of myeloid immune suppressor Gr+CD11b+ cells in tumor-bearing host directly promotes tumor angiogenesis." Cancer Cell 6(4): 409-421.

Yeh, H. J., et al. (1998). "Upregulation of pleiotrophin gene expression in developing microvasculature, macrophages, and astrocytes after acute ischemic brain injury." J. Neurosci. 18(10): 3699-3707.

Zabuawala, T., et al. (2010). "An ets2-driven transcriptional program in tumor-associated macrophages promotes tumor metastasis." Cancer Res 70(4): 1323-1333.

Zeisberger, S. M., et al. (2006). "Clodronate-liposome-mediated depletion of tumour-associated macrophages: a new and highly effective antiangiogenic therapy approach." Br. J. Cancer 95(3): 272-281.

Zhang, N., et al. (1997). "Human breast cancer growth inhibited in vivo by a dominant negative pleiotrophin mutant." J. Biol. Chem. 272(27): 16733-16736.

Zhang, W., et al. (2002). "A monoclonal antibody that blocks VEGF binding to VEGFR2 (KDR/Flk-1) inhibits vascular expression of Flk-1 and tumor growth in an orthotopic human breast cancer model." Angiogenesis 5(1-2): 35-44.

Zhao, X. M., et al. (1995). "Association of acidic fibroblast growth factor and untreated low grade rejection with cardiac allograft vasculopathy." Transplantation 59(7): 1005-1010.

Zheng, S. G., et al. (2007). "IL-2 is essential for TGF-beta to convert naive CD4+CD25- cells to CD25+Foxp3+ regulatory T cells and for expansion of these cells." J Immunol 178(4): 2018-2027.

Zou, H. Y., et al. (2007). "An orally available small-molecule inhibitor of c-Met, PF-2341066, exhibits cytoreductive antitumor efficacy through antiproliferative and antiangiogenic mechanisms." Cancer Res 67(9): 4408-4417.